UTILIZATION OF FLY ASH – PORTLAND CEMENT BINARY SYSTEMS TO
CONTROL ALKALI-SILICA REACTION

A THESIS SUBMITTED TO
THE GRADUATE SCHOOL OF NATURAL AND APPLIED SCIENCES
OF
MIDDLE EAST TECHNICAL UNIVERSITY

BY

AHMET ZİYA ÇELEN

IN PARTIAL FULFILLMENT OF THE REQUIREMENTS
FOR
THE DEGREE OF MASTER OF SCIENCE
IN
CIVIL ENGINEERING

SEPTEMBER 2019

Approval of the thesis:

**UTILIZATION OF FLY ASH – PORTLAND CEMENT BINARY SYSTEMS TO CONTROL ALKALI-SILICA REACTION**

submitted by **AHMET ZİYA ÇELEN** in partial fulfillment of the requirements for the degree of **Master of Science in Civil Engineering Department, Middle East Technical University** by,

Prof. Dr. Halil Kalıpçılar
Dean, Graduate School of **Natural and Applied Sciences**               _____

Prof. Dr. Ahmet Türer
Head of Department, **Civil Engineering**               _____

Assist. Prof. Dr. Çağla Meral Akgül
Supervisor, **Civil Engineering, METU**               _____

**Examining Committee Members:**

Prof. Dr. İsmail Özgür Yaman
Civil Engineering, METU               _____

Assist. Prof. Dr. Çağla Meral Akgül
Civil Engineering, METU               _____

Assist. Prof. Dr. Güzide Atasoy Özcan
Civil Engineering, METU               _____

Prof. Dr. Mustafa Şahmaran
Civil Engineering, Hacettepe University               _____

Assist. Prof. Dr. Fatma Toksoy Köksal
Geological Engineering, METU               _____

Date: 09.09.2019

**I hereby declare that all information in this document has been obtained and presented in accordance with academic rules and ethical conduct. I also declare that, as required by these rules and conduct, I have fully cited and referenced all material and results that are not original to this work.**

Name, Surname: Ahmet Ziya Çelen

Signature:

# ABSTRACT

## UTILIZATION OF FLY ASH-PORTLAND CEMENT BINARY SYSTEMS TO CONTROL ALKALI-SILICA REACTION

Çelen, Ahmet Ziya
Master of Science, Civil Engineering
Supervisor: Assist. Prof. Dr. Çağla Meral Akgül

September 2019, 124 pages

The highly alkaline pore solution of the portland cement concrete is not an ideal environment for certain reactive aggregates with poorly-crystalline or amorphous silica phases. In this environment, these aggregates partially or completely disintegrate resulting in formation of a hydrophilic, amorphous gel mainly composed of alkalis and water from the pore solution of the hydrated cement matrix and silica from the aggregates. The newly formed alkali-silica reaction (ASR) gel can expand by absorbing huge amounts of water irreversibly, becoming a significant problem if the gel is confined in a matrix such as hardened cement paste. Expansion of the gel can result in localized internal stresses that cannot be relieved by movement of the ASR gel into to the present voids of the matrix leading to extensive micro-cracks in the concrete. Eventually, ASR can cause critical loss of stiffness, impermeability and strength of concrete. The focus of this thesis is evaluating the ASR performance of portland cement/fly ash binary mortars. For this purpose, a total of 13 fly ashes with a wide range of chemical and mineralogical composition are selected from the leading thermal power plants in Turkey (Tunçbilek, Çatalağzı, Afşin Elbistan, İçdaş, Kemerköy, Yatağan and Yeniköy). The ASR performance of such a variety of Turkish fly ashes has not been investigated at this level before. An in-depth analysis of the

impact of chemical and mineralogical differences of the fly ashes on the ASR performance of binary Portland cement/fly ash mortars are also conducted.

Keywords: Alkali-Silica Reaction (ASR), Fly Ash, Chemical Composition, Portland Cement

# ÖZ

## ALKALİ-SİLİKA REAKSİYONUNUN KONTROLÜNDE UÇUCU KÜL – PORTLAND ÇİMENTOSU İKİLİ SİSTEM KULLANIMI

Çelen, Ahmet Ziya
Yüksek Lisans, İnşaat Mühendisliği
Tez Danışmanı: Dr. Öğr. Üyesi Çağla Meral Akgül

Eylül 2019, 124 sayfa

Portland çimentosu betonunun yüksek alkalin gözenek solüsyonu bazı amorf veya zayıf kristal silis fazlı reaktif agregalar için ideal bir ortam değildir ve agregaların dağılmasına yol açar. Bu reaksiyon agregadaki silisten ve hidrate olmuş çimento matrisinin gözenek solüsyonundaki alkaliler ve sudan oluşan amorf, hidrofilik bir jel ile sonuçlanır. Alkali – silika reaksiyonu (ASR) jeli geri dönülemez biçimde, büyük miktarda su emerek genişleyebilir. Bununla birlikte, jel, sertleşmiş çimento hamuru gibi bir matris içerisinde kısıtlanırsa önemli bir probleme dönüşebilir. Jelin hacimsel genişlemesi, boşluklara hareketi ile sönümlenemeyen bölgesel iç streslere yol açabilir ve bu durum, betonda yaygın mikro çatlaklara yol açabilir. İleri aşamalardaki ASR, beton sertliğinin, mukavemetinin ve geçirimsizliğinin kaybına neden olabilir.Bu tez, uçucu kül katkılı Portland çimentosu harçlarının alkali-silika reaksiyon performansının değerlendirilmesi konusuna geniş bir kimyasal ve mineralojik çeşitlilikteki uçucu küller kullanılarak odaklanmaktadır. Türkiye'nin önde gelen termik santralleri olan Tunçbilek, Çatalağzı, Afşin Elbistan, İçdaş, Kemerköy, Yatağan ve Yeniköy'den, toplam 13 uçucu kül seçilmiştir. Türkiye uçucu küllerinin ASR performansları sınıflandırılmıştır. Bu çeşitlilikte numunelerle bu seviyede bir araştırma Türkiye için daha önceden yapılmamıştır. Bunara ek olarak, uçucu küllerin

kimyasal ve mineralojik farklılıklarının, portland çimentosu / uçucu kül harcı ikili sistemlerinin ASR performansları üzerine olan etkisi detaylı olarak analiz edilmiştir.

Anahtar Kelimeler: Alkali-Silika Reaksiyonu (ASR), Uçucu Kül, Kimyasal Kompozisyon, Portland Çimentosu

To my mother.

# ACKNOWLEDGEMENTS

I would like to thank Prof. Dr. Çağla Meral Akgül for her guidance and supervision.

My thanks extends to Mr. Sepehr Seyedian Choubi for his support.

# TABLE OF CONTENTS

# LIST OF TABLES

# LIST OF FIGURES

# LIST OF ABBREVIATIONS

AEB: Afşin Elbistan

AMBT: Accelerated Mortar Bar Test

ASR: Alkali Silica reaction

BSE: Back Scattered Electron

CFA: Coal Fly Ash

Ç: Çatalağzı

IB: İçdaş Biga

K1: Kemerköy (Reactor 1)

K2: Kemerköy (Reactor 2)

K3: Kemerköy (Reactor 3)

SEM: Scanning Electron Microscopy

SCM: Supplementary cementitious materials

T3: Tunçbilek (Reactor 3)

T4: Tunçbilek (Reactor 4)

T5: Tunçbilek (Reactor 5)

XRD: X-Ray Diffractometry

XRF: X-ray fluorescence

Ya2: Yatağan (Reactor 2)

Ya3: Yatağan (Reactor 3)

Ye1: Yeniköy (Reactor 1)

Ye2: Yeniköy (Reactor 2)

# CHAPTER 1

# INTRODUCTION

## 1.1. General Information

## 1.1.1. Concrete

Concrete is the product of some of the most widespread raw materials found on Earth. It is basically a composite composed of aggregates, water and Portland cement. Portland cement, the hydraulic binder of concrete, is the combination of gypsum and Portland cement clinker while Portland cement clinker is manufactured from the controlled burning process of pulverized and mixed calcareous and clayey raw materials at rotary kilns.

As a result of its beneficial properties such as strength, durability, workability and inexpensiveness, reinforced concrete, combination of concrete with embedded steel members is still the favorite construction material all over the world. Since the invention of concrete, the most widely used construction material for the last decades, the problems encountered in its usage have not changed significantly. Although durability is an important advantage of this material, there are also several issues within deterioration. Degradation may occur as a result of physical and chemical causes some of which can be summarized as chemical attack, abrasion, corrosion, freeze-thaw effect, wetting-drying, sulphate attack, leaching and efflorescence, alkali-aggregate reactivity etc. Alkali-silica reaction has always been one of the most important issues of ancient and modern concrete as a result of the chemical compositions of its main constituents such as aggregates and cement. The map of aggregates which are identified to result in alkali-silica reaction in Turkey given in Figure 1.

1

At the present time, supplementary cementitious materials (SCM), formerly known as mineral admixtures, are very popular additives of concrete all over the world for not only reducing the costs and being nature friendly, but also improving the properties of fresh and hardened concrete at considerable levels. Extensively used supplementary cementitious materials can be classified (SCM) as fly ash (FA), ground granulated blast-furnace slag (GGBFS), silica fume (SF) and natural pozzolans (NP), all of which have different compositions and behaviors thus different effects on concrete. Effects of SCMs on concrete extend from workability to water requirement, bleeding and segregation, from setting time to strength and durability. In other words, use of mineral admixtures affect almost every characteristic of fresh and hardened concrete.

The trend of abundant usage of supplementary cementitious materials on concrete is also valid for Turkey. As a developing country, new constructions of buildings and infrastructures can be seen all over the region. It is definitely very important to reduce the costs and effects on nature and increase the properties of concrete at the same time. As a result, extensive use of supplementary cementitious materials is inevitable in the Turkey. Unsurprisingly, fly ash is the mostly preferred type of them as a result of the large number of largely scaled coal fired thermal power plants whose byproduct is the fly ash. For the sake of sustainability of natural resources, those byproducts are needed to be consumed. Moreover, replacement of the cement with fly ash has many beneficial effects such as increase in workability, lowered water demand and heat of hydration, increased final durability and strength. Since these beneficial effects are very favorable, fly ash is being used in concrete mixes increasingly.

*Figure 1.The locations of the aggregates which are identified to result in alkali-silica reaction in Turkey* [1]

### 1.1.2. Fly Ash

As the use of electricity became widespread, coal has become one of the most important resources of electricity production. As coal has been used in thermal power plants, the demand for this material have been increasing consistently. It can be predicted that this trend will not change in the next decades as well. Therefore, it is clear that not only the amount of raw materials of electricity production processes at thermal power plants, but also the byproducts will increase in the same manner inherently. This scenario does not progress differently in Turkey.

The annual fly ash output of the thermal power plants all over the world is greater than 800 million tons and increasing every year. The fly ash production of Turkey is scaling up in a much higher rate than the world average, as a result of the increasing usage of coal for electricity production. The number of leading thermal coal-fired power stations in the country is still increasing each year. The leading thermal coal power plants as can be seen in Figure 2.

3

*Figure 2.Leading thermal coal-fired power stations of Turkey*

Fly ash is the byproduct of the combustion process of coal in the coal-fired thermal power stations to produce electricity. When the pulverized coal is burnt in the boilers, dusty particles that are entrained in flue gases are collected by electrostatic or mechanical filters. This remnant, resulting from the combustion of coal, usually with pozzolanic properties, is called fly ash. The chemical constituents of fly ash vary significantly with respect to the composition and source of the coal being combusted, but all fly ashes comprise significant amount of CaO (calcium oxide), $SiO_2$ (silicon dioxide), $Al_2O_3$ (aluminum oxide) and unburnt carbon. In smaller quantities, chromium, beryllium, boron, chromium, cobalt, lead, arsenic, manganese, mercury etc. may exist depending on the coal type and composition used for the burning process.

Fly ashes can be classified into mainly two groups such as Class F Fly Ash and Class C Fly Ash. Firstly, class F fly ash, in other words low lime fly ash, is usually the byproduct of anthracite and bituminous coal burning process. It contains less than 10% CaO and generally has pozzolanic properties. Class F fly ash requires a cementitious material to have binding ability, such as Portland cement, quicklime, or hydrated lime. This type of fly ash is usually very beneficial by means of preventing alkali-silica reaction. Secondly, class C fly ash, i.e. high lime fly ash, is the byproduct of lignite or

4

subbituminous coal combustion operations. It usually contains more than 20% lime (CaO) and shows not only pozzolanic properties like class F fly ash, but also has self-cementing properties at some degree. This type of fly ash is usually not as beneficial as class F fly ash by means of preventing alkali-silica reaction. Thirdly, there are also fly ashes with lime content between class F and C fly ashes. Most useful fly ash type is low lime fly ashes by means of alkali-silica reaction reduction.

### 1.1.3. Alkali Silica Reaction

The problem focused on the study is mainly the alkali silica reaction in concrete. ASR is the outcome of the fact that the highly alkaline environment of the modern Portland cement concrete is not suitable for certain reactive aggregates with amorphous or poorly-crystalline silica phases, resulting in disintegration of them. The result of this reaction is an amorphous, hygroscopic gel called alkali-silica gel. The main consequence of this problem is the ASR gel being hygroscopic and able to irreversibly expand by imbibing large volumes of water. This can become an important issue if the gel is confined in a matrix like hardened cement paste.
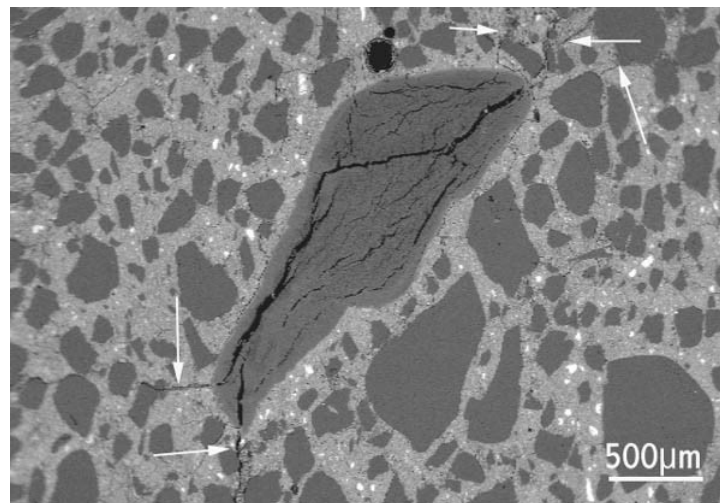


*Figure 3. SEM BSE image of concrete polished section: ASR cracks expanding from the aggregate*
[2]

5
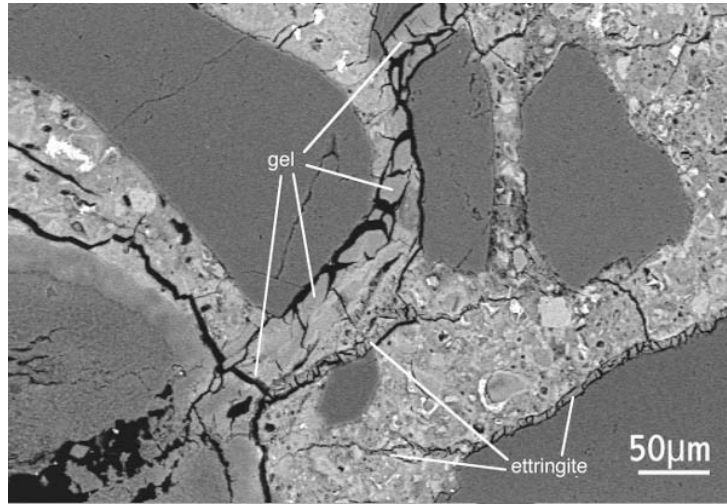
*Figure 4. SEM BSE Image of alkali silica gel spreading over the concrete* [2]

 The volumetric expansion of the gel can result in localized internal stresses that cannot be dissipated by movement of the gel into to the voids and this might lead to extensive micro-cracking in the concrete [3]on as can be seen in Figure 3 and Figure 4. This phenomenon is significant since ASR lead to strength and durability loss of concrete. As the ambient temperature of the concrete increases, so may the rate of expansion [4].  ASR damaged structural members are shown in Figure 5 and Figure 6.



*Figure 5. ASR damage on the drying concrete surface of bridge pylon* [5]

6

*Figure 6.* ASR damaged concrete photographs [6]

In order to prevent ASR, several measures are taken which can be summarized as; using non-alkali cement and non-reactive aggregates, controlling the moisture and external alkali supplies, reducing water/cement ratio, air entrainment, decreasing cement amount and using mineral admixtures. Mineral admixtures, used as cement replacements materials to prevent ASR, are natural or artificial materials and byproducts such as silica fume, natural pozzolans, ground granulated blast furnace slag and fly ash.

Fly ash is one of the most important mineral admixtures used to reduce ASR. Moreover, since it is a byproduct of the electricity production processes, using the fly ash at concrete mixture not only decreases the costs, but also is favorable by means of environmental issues.

## 1.2. Objective and Scope

The main goal of this thesis is to evaluate the ASR performance of binary portland cement/fly ash mortars prepared with a wide range of fly ashes with varying chemical and mineralogical compositions. The main objectives of this study are:

- Identifying the chemical and mineralogical compositions of the raw materials, namely fly ashes, aggregates and portland cement that are used in the experiments;
- Evaluating the ASR performance of the binary portland cement/fly ash mortars through expansion tests;
- Investigating the ASR damaged mortar bars through scanning electron microscopy to identify the chemical and morphological properties of the ASR products;
- Exploring possible relationships between the constituents of the fly ash and the ASR performance of the binary mortar.

# CHAPTER 2

# LITERATURE REVIEW

## 2.1. Alkali-Silica Reaction

## 2.1.1. General Information

Alkali silica reaction occurs in presence of several factors such as alkalis from mostly cement, reactive silica from the aggregates and moisture from the environment (Figure 7). It has been one of the most significant problems of the modern reinforced concrete structures all over the world for the last decades since it causes serious strength and durability issues.
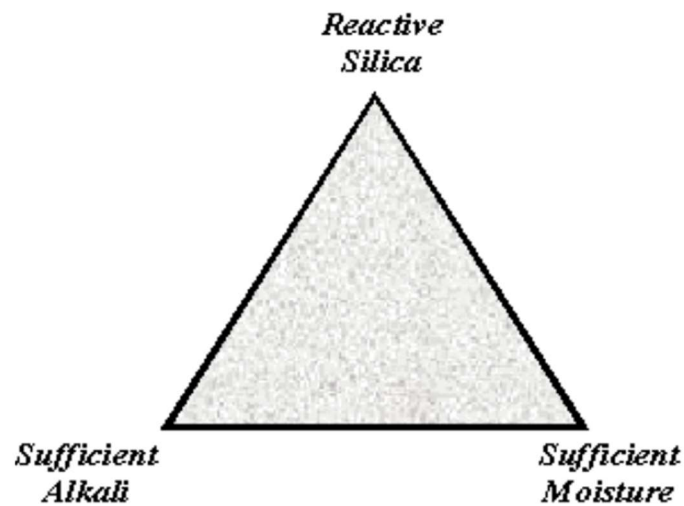


*Figure 7. Three necessary components for ASR-induced damage in concrete* [7]

After the formation of the gel, it absorbs large amount of water, resulting in a considerable increase in its volume. Such volume instabilities after the hardening of concrete is highly undesirable because of triggering cracks. Thus, as the final outcome of this process is the disintegration of the concrete structure in several years of duration, it is very important to prevent such mechanisms before taking place. When

at least one of the components of the alkali silica reaction is eliminated (Figure 7), the reaction is totally restrained [7].

Firstly, reactive silica is present in reactive aggregates. Such kind of aggregates are prone to degradation after being exposed to alkaline solutions. After being subject to the alkaline pore solution of the cement, it reacts with alkali-hydroxides resulting in the formation of the alkali silica gel.

Secondly, alkalis are mostly found in Portland cement. However, there are also other sources such as mineral and chemical admixtures, aggregates, materials entering through environment, water etc. The total alkalis of the concrete mix affect the expansion due to alkali silica reaction severely (Figure 8).
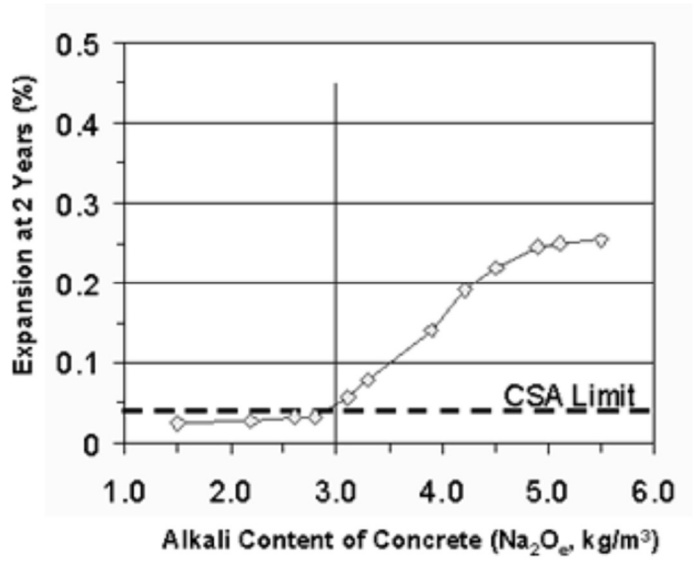


*Figure 8. ASTM C1293 experiment results for alkali content effects* [8] *(CSA: Canadian Standards Association)*

Lastly, water, which is also an ingredient of concrete and also found in the environment at large amount, is the third cause of alkali silica reaction. The water causing alkali silica reaction usually penetrates the concrete from the environment.

### 2.1.2. Expansion Mechanism

As stated before, the main reason of occurrence of alkali silica reaction is the existence of the three factors in the concrete at the same time, namely alkalis (potassium oxide ($K_2O$) and sodium oxide ($Na_2O$)), reactive silicates and water. When these three ingredients are all found in the concrete, the alkalis, namely sodium and potassium dissolved in the solution causes rise in OH- ion concentration, which leads to increase in PH levels. This highly alkaline medium induces the dissolving of the reactive silicates of the aggregates. Afterwards, this dissolved silicates cause alkali silica gel formation.

Within the far going literature and many scientists working on the subject, the expansion mechanism of the ASR is investigated in-depth by Glasser and Kataoka [9]. It is indicated that, when the alkalis attack the well or dense crystallized silica, the output of the reaction occurs insignificantly at the surface (Figure 9). On the other hand, hydrous silica in poorly crystalline form facing a solution high in alkalinity, results in entrance of sodium-potassium and hydroxyl ions inside the material and a severe acid base reaction occurs. This reaction ends up with ASR gel formation, imbibing water and swelling of the matter. When the swelling occurs sufficiently, causing enough internal pressure, this process results in deterioration of concrete in the form of expansive cracks.

In the reaction, after the mixing of sodium hydroxide with poorly crystalline silica, the hydroxyl ions attack the silica, resulting in dissolving of the silica[9]. The higher the sodium and potassium alkalis in the concrete, the more hydroxyl ions in the pore fluid, which means more alkaline pore solution (higher PH). As the pore fluid gets more and more alkaline, the reactive silica is attacked more. In other words, the alkalinity of the solution controls the solubility of the silica and the reaction speed [10]. Moreover, the size of the silica particle plays an important role on the reactivity. The result of the silica reacting with alkalis is alkali silica gel. This reaction starts at the contact area of the cement paste and the reactive aggregate. The chemical formulas of the reaction are given in Equation 1.
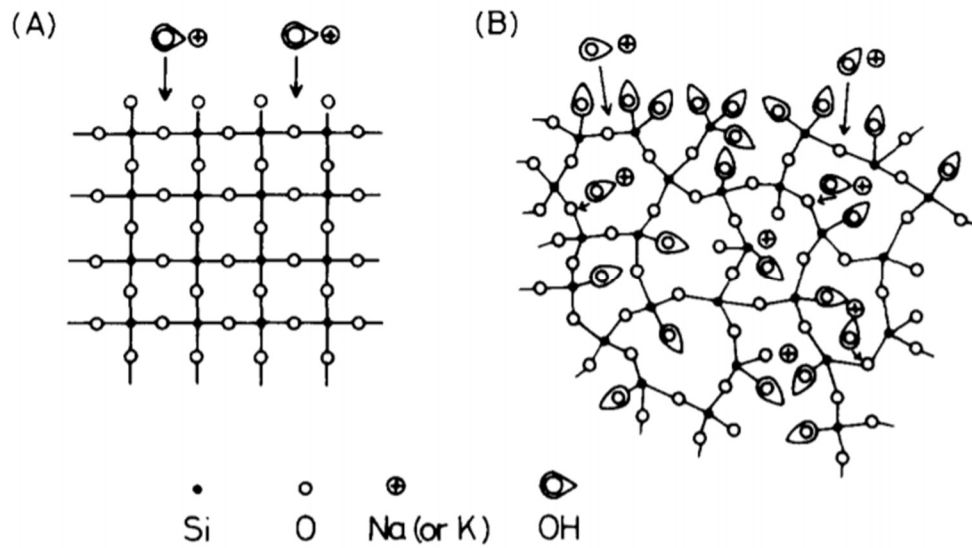
*Figure 9. Diagrammatic illustrations of attacked A) well crystallized silica B) Hydrous silica in poorly-crystalline form* [9]
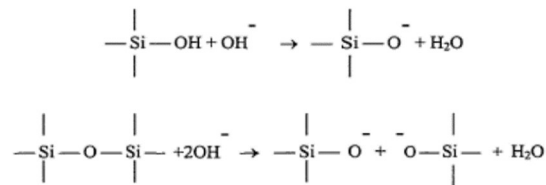


*Equation 1. Alkali-silica gel formulations* [11]

### 2.1.3. Symptoms of Alkali Silica Reaction

Alkali-silica reaction has several indicators. Visually determined issues can be summarized as crack occurrences (Figure 10), deformative expansions, displacement and movement of members with respect to each other, regional crushing, problems of joints, pop-outs, discoloration and gel exudations at the surfaces [6]. Moreover, by means of material mechanical properties, ASR occurance significantly affects the compressive and tensile strengths and the Young's modulus of the concrete[12].
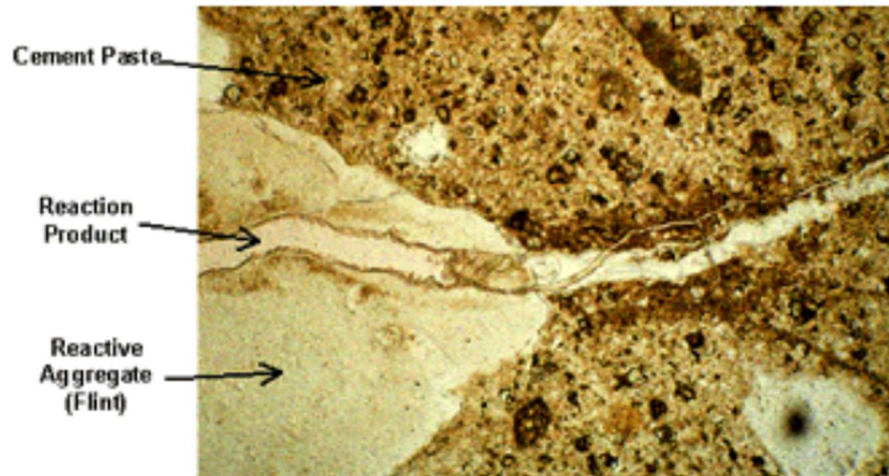
*Figure 10. ASR damaged concrete thin section* [7]

Firstly, map cracking (pattern cracking) occurrences (Figure 11) are the most common symptoms of ASR[6]. These random cracks usually move in every direction, sometimes with discoloration as a result of the gel exudation. Most of the time, the expansion of the concrete is prevented in some directions because of prestressing, post stressing, confinement or exterior loading resulting in increase in expansion in the unrestrained direction. As a result, the cracks' directions become nearly the same.



*Figure 11.  Concrete airfield pavement map cracks with discoloration* [13]

13

Secondly, deformative expansions, displacement and movement of members with respect to each other (Figure 12) are other problems associated with ASR.



*Figure 12. Movement of concrete members because of ASR* [6]

Thirdly, regional crushing is another symptom of ASR as can be seen in Figure 13. This phenomenon occurs as a result of the fact that incompressible members gets stuck on joints, leading to increase in stress concentrations.



*Figure 13. Cracks in joint of concrete members as a result of the high stress concentration occurrence because of ASR* [6]

Problems related with joint squeezing, especially popping out of the joint sealing materials (Figure 14), is again one of the problems related with ASR.



*Figure 14. Popped out sealing material at the pavement joint* [6]

Next issue associated with ASR is a surface problem. The surface of the concrete members pop out as a result of the expansions near the surface (Figure 15).



*Figure 15. Pop outs in concrete* [6]

The last visually determined problem related with ASR is discoloration and gel exudations at the surfaces as seen in Figure 16. These regions look like wet concrete. The gel exudations reach through the cracks formed on the surface of the concrete and form in the domain of these cracks.



*Figure 16. ASR gel exudation and discoloration on the surface of concrete* [6]

Lastly, ASR affects the mechanical properties concrete by means of compressive and tensile strengths and the Young's modulus [12]. Many scientists have agreed on the fact that the Young's modulus is decreased 50-60% but, there is no consistent result in tensile and compressive stresses [14–19]. This is probably as a result of the fact that they use different ingredients for the mortar and different circumstances for the environment, and the ingredients of the solutions are extremely reactive.

## 2.1.4. Laboratory Test Methods for Assessing Alkali Silica Reaction

A broad range of experiments exist for assesing the ASR. The list of the most common tests are given below in Figure 17 where they are divided into ones investigating the aggregates and the combinations of the cement and aggregate. Modifications to these

test methods are also applied such as variations in temperature, the alkali levels and duration.
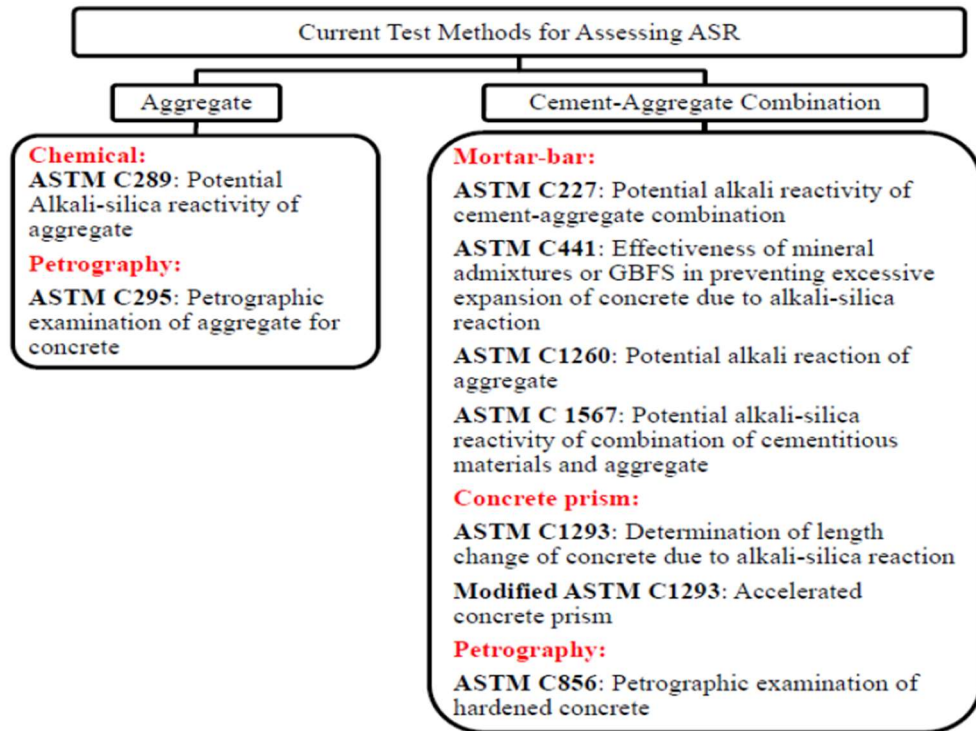


*Figure 17. Available tests for measuring the alkali silica reaction* [20]

Accelerated mortar bar tests (AMBT), as the name implies, are designed for testing the materials in short periods. They have very aggressive test environments. Since the specimens are kept in a highly alkaline solution, the pH of the pore solution is high, the ASR occurrence is severe and the completion of the reaction is fast [21]. ASTM C1260 [22] is the one chosen in this thesis for the assessment of the ASR reactivity since this method gives quick results. Although the standard specifies a testing period of 16 days, this duration is extended to 75 days to see the ASR reactivity in a wider view.

The available ASR tests are given below in Table 1 with the advantages and disadvantages summarized.

*Table 1. ASR tests available* [7]

| | |
|---|---|
| ASTM C 227 (Mortar Bar Method): Standard Test Method for Potential Alkali Reactivity of Cement-Aggregate Combinations | Main purpose is testing combinations of cement/aggregates High-humidity containers are used for storage at 38 °C. Problems such as too much alkali leaching samples are reported. |
| ASTM C 289 (Chemical Method): Standard Test Method for Potential Alkali-Silica Reactivity of Aggregates | Test for aggregates where the specimen is crushed and stored in 1 molar sodium hydroxide solution for 1 day. Then, alkalinity and dissolved silica are investigated. Not reliable. Several problems: Silica dissolution may be affected by the other phases the aggregate contains Too severe testing environment which may lead to failure of good aggregates also. Loss of some reactive phases may ocur at processing of pretest. |
| ASTM C 295: Standard Guide for Petrographic Examination of Aggregates for Concrete | Several potentially reactive potentially reactive constituents of the aggregates are identified. Petrographer's skills and experience are important for the success of the results. Approval or refusal of the aggregates can not be taken solely depending on this experiment, it should be used with other experiments such as ASTM C 1293 and/or ASTM C 1260 [22]. |
| ASTM C 856: Practice for Petrographic Analysis of Hardened Concrete | Helpful for the analysis of concrete specimens from field or lab and determination of the ASR reaction products or aggregates with reactive properties. Petrographer's skills and experience are important for the success of the results. Vital test for finding the relationship of the field performance and the activity of the aggregates. |

*Table 1. ASR tests available* [7] *(continued)*

| | |
|---|---|
| ASTM C441: Standard Test Method for Effectiveness of Mineral Admixtures or Ground Blast Furnace Slag in Preventing Excessive Expansion of Concrete Due to the Alkali-Silica Reaction | Mortar bar test used for evaluation of the performance of SCMs in mitigation of expansions caused by ASR. PyrexTM glass and high alkali cement are used. As a result of the sensitivity of the PyrexTM glass to test conditions and containment of alkalies of the material itself, reliability issues occur. Moreover, the correlation of the data for concretes which contains natural aggregates, is weak. [23] |
| ASTM C 1260 (Mortar Bar Method): Standard Test Method for Potential Alkali Reactivity of Aggregates | Essentially developed for measurement of reactivity of aggregates 1 molar sodium hydroxide solution is used to keep the bars in for two weeks. Appropriate rapid test for eliminating but not to be used by itself for denial of an aggregate since the test is very severe. When both ASTM C 1293 and ASTM C 1260 tests are applied, the governing test should be ASTM C 1293. For the examination of lithium compounds and SCMs, the test seems good. For lithium tests, sodium hydroxide solution needs modification. |
| ASTM C 1293: Standard Test Method for Concrete Aggregates by Determination of Length Change of Concrete Due to Alkali-Silica Reaction | Conducted at high humidity environment (nearly 100%) and 38 °C ,usually seen as best indicator concrete prism test for assesment of ASR reactivity of aggregates. High-alkali cement (raised to 1.25% Na20e) is used. Has purpose of testing the ASR reactivity of aggregates where nonreactive coarse aggregates are used for testing the fine aggregates and vice versa. 1 year duration is needed for the test. If the test is used for assessing the performance of lithium compounds and SCMs, the duration is doubled. The test is accepted to a large extend for ASR assesment but the duration is the most important problem. |

19

## 2.1.5. ASTM C1260

990 grams total of graded fine aggregates, 440 grams of binder and 206,8 grams of tap water are mixed by a mixer according to the ASTM C305−14 Standard Practice for Mechanical Mixing of Hydraulic Cement Pastes and Mortars of Plastic Consistency [24].

Then, the mixture (mortar) is placed in mortar bar molds in two equal layers and compacted with a tamper according to the standard. Nuts are placed at each end of the bars to measure the lengths changes. For each specimen, 3 mortar bar samples are prepared. After the first day, molds are removed, the length of the mortar bars are measured. Afterwards, the specimens are put in boxes filled with water, and the boxes are put on steam oven at $80\pm 2$°C for 1 day. After the next day, the mortar bars are removed from the oven and the lengths are measured again (zero reading). After the zero reading, the specimens are put on Sodium hydroxide (NaOH) solution. After that, the bars are again put in steam oven at $80\pm2$°C. Afterwards, the lengths of the bars are measured at least 3 times in the next 2 weeks. When the test is going to be performed longer, at least 1 measurement is required for each week.

According to the ASTM C1260 − 14 [22] test method, the classification of ASR is performed as follows:

- When the expansion less than 0.10 % after 16 days of testing, the aggregates are probably harmless;
- When the expansion is over 0.20 % after 16 days of testing, the aggregates are probably deleterious;
- When the expansion is between 0.10 and 0.20 % after 16 days of testing, the aggregates may be harmless or deleterious.

## 2.1.6. ASR Prevention Methods

As stated before in the introduction of this thesis, ASR occurrence needs three components such as water (moisture), alkalis and reactive silicates. If one of these

three ingredients can be prevented, ASR is reduced or prevented at all [25–27]. In other words, limiting the moisture (water), changing the kind and amount of aggregates with reactive siliceous constituents and decreasing the alkalinity (pH) of the pore fluid to lower the solubility of the silica are the fundamental ways of preventing ASR.

Firstly, moisture is available in the environment, moreover concrete structures in contact with the ground are usually wet enough internally to promote ASR reaction [28]. Moreover, the formed gel imbibes water and swell, causing expansive crack in the concrete. In order to prevent such problems, water should be kept away from the structure. To achieve this, permeability of the concrete can be decreased by lowering the water/cement ratio. Moreover, curing process can be performed adequately. On the other hand, reduced water/cement ratio may lead to several problems such as increase in alkalinity of the pore solution. Also, reduced pore amount in the matrix may result in internal stresses as a result of the expansion of the ASR gel [29][30]. As a result, best way of preventing entrance of water inside concrete is using mineral admixtures. Moreover, coating the concrete is another way of water prevention [25][29].

Secondly, selecting aggregates with little or no reactive siliceous constituents[31] is a prevention method. The material information papers of the aggregates should be checked or ASR assessment experiments shall be done to achieve this goal. In addition, petrographic examination can be performed. If the aggregates have reactive siliceous constituents, blending it with aggregates with nonreactive constituents is a method to reduce the reactivity[26]. Moreover, washing the aggregates may be beneficial in reducing reactivity.

Thirdly, reducing the alkali content of the concrete is a method of preventing ASR. In other words, the hydroxyl ion concentration and pH of the pore solution is lowered. Small fragments of hydroxyl ions may be originated from slag or pozzolans. In fact, the main alkali content contributor of the concrete mixture is the Portland cement[25][26]. Some fly ash, sea water, some aggregate types may also provide significant amount of alkalis to the solution. Lastly, alkalis may enter the concrete from environment such as deicing salts form and marine. Precautions should be taken in

such environments. Most importantly, Portland cement with low alkali content (less than 0.60 percent Na2Oe) is recommended to be used with reactive aggregates[32].

Lastly, ASR can be reduced by replacing some amount of cement with supplementary cementitious materials such as pozzolans, slag and fly ash [7][16,25][29]. Replacement with SCM's with low alkali content, reduces the total alkalis in the pore solution. Moreover, $CaO:SiO_2$ ratio decreases, resulting in entrapment of alkalis and decrease in pH [4]. Moreover, reactions with pozzolans and slag consume calcium hydroxide. In addition, the cement paste gets denser as a result of the decrease in the calcium hydroxide amount and thus more C-S-H gel forms.


## 2.2. Alkali Silica Reaction Performance of Fly Ash – Portland Cement Binary Systems

Fly ash, the byproduct of thermal power plants burning coal, is a SCM being used all over the world not only to enhance the properties of concrete, but also reduce the costs. Replacement of cement with fly ash in different ratios, which is also the subject of the thesis, is one of the most feasible ways to prevent ASR.

Fly ashes, according to their composition, can be classified into two groups such as Class F and Class C according to ASTM C 618 [33]. Class F fly ash is the byproduct of bituminous coal and anthracite combustion. Its CaO content is usually less than 5%. On the other hand, Class C fly ash is the byproduct of subbituminous coal and lignite burning. It usually contains 10-40 % CaO. Class F fly ashes are generally much more effective in controlling ASR than Class C ashes.

Efficiency of the fly ash on controlling the ASR depends on several factors such as cement replacement ratio, composition of the fly ash (such as CaO and $Na_2Oeq$ contents), aggregate silicate reactivity level and alkali content of the concrete mix [7].

There is a wide literature available on the utilization of fly ashes as a SCM in portland cement concrete [34–36], and [8]. These studies not only focus on the effect of the physical, chemical and mineralogical properties of fly ashes, but also on different mix ratios and curing procedures. These are review papers written on this subject

summarizing previous studies as [5]. In fact, complex relationships with the material properties and ASR have been studied in papers such as [37–39]. Even new relationships are studied at [40,41] for coal fly ashes. Moreover, different supplementary cementitious materials are studied together with fly ashes in [42].

Among the huge literature on the effect of coal fly ashes on mitigation of ASR expansions, [40] and [41] have been found the most relevant for this study. Firstly, Malvar has studied a detailed investigation on the subject by determining the effect of every constituent of the binary mixes providing and inhibiting ASR one by one and tried to find approximations for the behavior of the ASR expansions with respect to the quantity of these constituents[41]. Afterwards, the study focused on finding new correlations with combining these contents and ended up with reasonable results. Moreover, formulas of the minimum replacement levels of coal fly ash specimens for the mitigation of the reaction are also investigated. Secondly, Kizhakkumodom has investigated the mitigation performance of the coal fly ashes in more detail in [40]. The study firstly focused different aggregates and different coal fly ashes (namely low lime, intermediate lime and high lime) combinations and their results on ASR expansions. Then, individual oxide contents of the fly ashes and their impact on ASR are investigated. Afterwards, the combinations of these oxide contents are also studied. Moreover, immersion period of the specimens in extremely alkaline environments are searched. Additionally, a deep research has been done on particle size distributions of the fly ashes and their impact on the ASR expansions. To sum up, both studies [40], [41] have come up with good findings and reasonable relationships on fly ash properties and their ASR mitigation performances. In this thesis study, these studies are investigated in detail and their results are used for comparison purposes.

However, a comprehensive study on the fly ash samples from the power plants in Turkey has not been conducted. There is a need to perform tests on the fly ashes collected from the leading thermal power plants in Turkey and conduct an in-depth analysis of the impact of chemical and mineralogical differences of the fly ashes on the ASR performance of binary portland cement/fly ash mortars.

# CHAPTER 3

# MATERIALS AND METHODS

Experiments are conducted to define the fly ash, aggregates and cement used in the mortar bars and ASR performance of the fly ash specimens, in order to be able to find correlations of the properties of the fly ashes with respect to alkali-silica reaction performance. An in-depth analysis of the impact of chemical and mineralogical differences of the fly ashes on the ASR performance of binary portland cement/fly ash mortars are conducted. Different statistical methods are used for this purpose.

ASR performance of the fly ashes are determined by conducting experiments with the mortar bars prepared by the aggregates, cement, fly ash and tap water. The experiments are performed to define the properties of the fly ash, aggregates and cement. Details of the experiments are explained in the methodology section of the thesis.

## 3.1. Raw Materials

The materials used in this thesis are listed below:

### 3.1.1. Fly Ash

13 different samples of collected fly ashes in the materials of construction laboratory (Figure 18) are selected from leading thermal power plants in Turkey. These samples are taken from Tunçbilek reactor 3, 4, 5 (T3, T4, T5), Çatalağzı (Ç), Afşin Elbistan (AEB), İçdaş (İB), Kemerköy reactor 1, 2, 3 (K1, K2, K3), Yatağan reactor 2, 3 (Ya2,Ya3) and Yeniköy reactor 1, 2 (Ye1,Ye2) thermal power plants.

These coal fly ash specimens are sieved through standard sieve no:120 (125-micron sieve) in order to get rid of the coarser particles and to increase the reactivity of the fly ashes for the mitigation of the ASR.
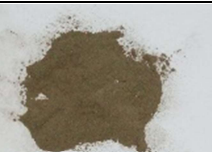
*Figure 18. Fly ash specimens, located at the materials of construction laboratory*

*Table 2. Fly Ash Specimens After Sieving (a)* Low-Ca CFAs (b) Intermediate-Ca CFAs (c) High-Ca
CFAs

*(a)*

| Low-Ca CFAs | | | |
|---|---|---|---|
| **(Ç)** | **(T3)** | **(T4)** | **(T5)** |
|  |  |  |  |

(b)

| Intermediate-Ca CFAs | | |
|---|---|---|
| **(IB)** | **(Ya2)** | **(Ya3)** |
|  |  |  |

(c)

| High-Ca CFAs | | |
|---|---|---|
| **(AEB)** | **(K1)** | **(K2)** |
|  |  |  |
| **(K3)** | **(Ye1)** | **(Ye2)** |
|  |  |  |

After sieving, the color differences between the fly ash samples were apparent as can be seen. The fly ash specimens with high iron content usually have darker color whereas the ones with higher calcium and/or gypsum content are mostly lighter in color. The images of coal fly as (CFA) specimens are given at Table 2 below:

All of the fly ash samples unscreened, sieved and retained on sieve are collected in separate bags. Only the sieved specimens are used at the experiments of this thesis. The fly ashes retained on sieve may be used for further studies.

### 3.1.2. Cement

CEM-I 42,5 R type portland cement (TS EN 197-1) which is provided from Baştaş Cement Factory, is used in the project for the mortar bar preparation. Since the material was fresh and ready to be used, sieving process is not performed. This cement, which is an ordinary type, has no extra alkaline characteristics.

Although the type of the cement used in the experiments is known, namely CEM-I 42,5 R type Portland cement (TS EN 197-1), the exact composition was not certain as a result of the fact that cements with similar properties can be provided with different blends which also means different compositions. As a result, characterization experiments, XRD and XRF are conducted to have the certain composition of the cement.

### 3.1.3. Aggregates

Aggregates which are present in the storage of the Materials of Construction Laboratory of the Civil Engineering Department in Middle East Technical University (Figure 19), is used for the mortar bar preparation of the experiments conducted. Unfortunately, there was no information (source, chemistry, mineralogy, …) available on the aggregates, therefore several experiments are conducted in order to get information on them.

*Figure 19. Aggregates located in front of the materials of construction laboratory*

The material is oven dried, then sieved (Figure 20 and Figure 21) according to the gradation requirements stated in the ASTM C-1260 standard given in Table 3.



*Figure 20 Graded aggregate spcimens*

In order to increase the possibility of having the ASR aggressively, aggregates are not washed.

*Table 3. Grading Requirements according to ASTM C1260* [22]

| Sieve size | | Mass, % |
|---|---|---|
| Passing | Retained on | |
| 4.75 mm (No. 4) | 2.36 mm (No. 8) | 10 |
| 2.36 mm (No. 8) | 1.18 mm (No. 16) | 25 |
| 1.18 mm (No. 16) | 600 μm (No. 30) | 25 |
| 600 μm (No. 30) | 300 μm (No. 50) | 25 |
| 300 μm (No. 50) | | 15 |

*Figure 21. The aggregate samples arranged according to the experiment requirements*

### 3.1.4. Alkaline Solution

Alkaline solution is prepared (Figure 22) by mixing 40 grams of sodium hydroxide (NaOH) with enough amount of distilled water to end up with 1 liter of solution according to the requirements stated in the ASTM C-1260 standard.



*Figure 22. Distilled water, NaOH salt and pouring the mixed solution into the box containing the mortar bars.*

## 3.2. Experimental Procedures

### 3.2.1. Characterization of the Raw Materials

The raw materials are characterized by x-ray diffraction (XRD), x-ray fluorescence (XRF), scanning electron microscope (SEM), laser particle size and petrographic analysis. The characterization methods are briefly explained below.

### 3.2.1.1. X-Ray Diffraction

Investigation of the mineralogical properties of the raw materials are conducted through XRD method. XRD measurements on the portland cement and the aggregate are conducted on the XRD device located at the Middle East Technical University Central Lab. Portland cement is already in very fine powder form; hence, XRD measurements are conducted without any sample preparation. The aggregate specimen prepared according to the ASTM C-1260 gradation requirements is much coarser. Therefore, in order to conduct XRD measurements, the aggregate specimen is pulverized by hammering it in to a very fine, homogenous powder. XRD measurements on the sieved fly ashes are conducted at a XRD device located at Turkish Cement Manufacturers Association (TÇMB) [43]. The results of the XRD analysis are interpreted through Highscore Plus software and available literature on the existing measurements [43].

### 3.2.1.2. X-Ray Fluorescence

The chemical composition of the portland cement and aggregate specimens are analyzed utilizing a XRF device located at the Middle East Technical University Central Laboratory. Since the portland cement is already in powdered form, there is no need to do any further sample preparation. The sample is pressed into a cylinder cup at the laboratory and the XRF measurement are conducted right away. The much coarser aggregate sample is pulverized at the central laboratory by a special crusher,

the pulverized material is pressed in a cylinder cup and then, the XRF measurement were conducted.

The results of these XRF measurements are taken from [43]. The chemical compositions of the sieved fly ash specimens are determined by an XRF device located at TÇMB. The sieved fly ashes samples were already in fine powder form; therefore, no additional sample preparation was necessary. The samples were pressed into a cylindrical cup and measured.

### 3.2.1.3. Laser Particle Size Distribution

Particle sizes of the fly ash specimens were determined by laser diffraction method. In this method, laser beam is scattered on the particles of the material being tested. The device collects the scattered beams by its detectors and uses the correlation between the beam's scattering angle to the particle sizes of the materials, which are inversely proportional. A computer program is used to turn this data into volumetric particle size distributions of the specimens [44]. The laser particle size distributions of the fly ash specimens are determined by an XRF device located at TÇMB [43].

### 3.2.1.4. Petrographic Analysis

Petrographic analysis is performed only on the aggregates in order to understand the aggregates, more thoroughly. Firstly, thin-section of the aggregates is prepared at METU Geological Engineering Department. To prepare the thin sections, the aggregate sample was mixed with resin and set into a small block. Once the block hardens, it is treated as a rock and thin sectioned in the same way. Obtained thin section is examined at optical microscopy. Finally, the prepared thin section specimen is interpreted by the help of an expert from Department of Geological Engineering.

### 3.2.1.5. Scanning Electron Microscope

The morphological properties of the portland cement and sieved fly ash specimens are examined by the SEM device located at the Middle East Technical University Central Lab. The powder specimens are placed on carbon tapes which are put on metal holders. Afterwards, the specimens are coated with gold-palladium mixture as a conductive layer.

### 3.2.2. Alkali – Silica Reaction Tests

### 3.2.2.1. ASTM C-1260

The accelerated mortar bar test is conducted in accordance with the ASTM C1260 standard[22]. 13 selected fly ashes are mixed at 3 replacement ratios with cement; 15wt%, 25wt% and 50%, for a total of 440 grams of binder (cement + fly ash) for each casting. For every fly ash replacement ratio and control group, three mortar bars are prepared according to the ASTM C1260 specifications. Moreover, for every replacement ratio, one set (three mortar bars) of control specimens are also prepared. The discussed results are the average of these three mortar bars for every fly ash replaced mortar bar and control specimens.

Secondly, 990 grams total of graded fine aggregates, 440 grams of cement + fly ash mix and 206.8 grams of tap water are mixed by a mixer according to the ASTM C305−14 Standard Practice for Mechanical Mixing of Hydraulic Cement Pastes and Mortars of Plastic Consistency [9].

Thirdly, the mixture (mortar) is placed in mortar bar molds in two equal layers and compacted with a tamper (Figure 23 and Figure 24) according to the ASTM C1260−14 [8]. Nuts are placed at each end of the bars to be able to measure the lengths precisely. For each trial, 3 mortar bar samples are cast.

*Figure 23 Preparation of the mold, hand tools used and the mixing process*



*Figure 24. Filling the mold with the fresh mortar*

After 1 day, molds are removed and the length of the mortar bars are measured (initial measuring). Then, the specimens are put in boxes filled with municipal water, and the boxes are put on steam oven at 80±2°C for 1 day. After 1 more day, the specimens are taken out of the oven and the lengths are measured (Figure 26) again (zero reading). Subsequent to the zero reading, the specimens are put on alkaline solution, in other words sodium hydroxide (NaOH) solution (Figure 25). Then, the boxes are again put in steam oven at 80± 2°C. Subsequently, the lengths of the bars are measured at least 3 times in the next 14 days. If the test is to be continued afterwards, at least 1 measurement is required each week.

*Figure 25. Mortar bars in the NaOH solution and outside*



*Figure 26. The standard rod used for the comparison of the measurements and the measurement process*

According to the ASTM C1260 − 14 test method, the classification of ASR is performed as follows [8]:

− If the expansion is less than 0.10 % at the end of the 16 days (2 days of preparation and 14 days of measurement) of test duration, the aggregates are probably harmless by means of ASR expansion;

- If the expansion is over 0.20 % at the end of the 16 days of test duration, the aggregates are probably deleterious by means of ASR expansion;
- If the expansion is between 0.10 and 0.20 % at the end of the 16 days of test duration, the aggregates may be deleterious or harmless.

At the first control experiment which was performed without fly ash, the aggregates were determined to be highly deleterious by means of alkali silica reaction with much more than the 0.20% limit. The elongation of the mortar bar specimens with fly ash replacement are compared with the control experiments every week as specified in the standards, to understand their effect on ASR occurrence.

### 3.2.2.2. SEM Examinations on the Mortar Bars with Alkali–Silica Reaction Damage

The morphological and chemical variations on the mortar bar specimens with aggressive alkali – silica reactivity, are examined by scanning electron microscope (SEM) device located at the Middle East Technical University Central Lab for determining whether ASR gel is present in the sample and analyzing the damage to the specimens caused by ASR in the concrete mixture, Moreover sieved fly ash specimens are also investigated by means of sizes and shapes of the grains and their general condition. In addition, backscattered electrons (BSE) method is also used to investigate the chemical differences within the samples. Furthermore, an EDX mapping trial is performed to determine the chemical condition of an aggregate particle exposed to ASR in detail. Only control, Ç, T3, IB and K1 samples were investigated because of the limitations of duration and finance. For the measurements, roughly one-year-old samples stored at the steam room, were used. The specimens were broken into smaller pieces for easier sample preparation (Figure 27). Secondly, polished sections of these pieces are prepared at the MTA laboratory. The broken pieces were first embedded in epoxy resin and then polished to achieve a smooth surface. Afterwards, the polished samples are coated with a conductive material (carbon). Polished specimens prepared for measurements can be seen in Figure 28. Then the

widths of the sections are painted with conductive ink and the metal holders are attached to the specimens as can be seen in Figure 29.



*Figure 27. Broken mortar bar specimens for the preparation of the polished sections*



*Figure 28.  Polished sections prepared for examination through SEM*

*Figure 29. Preparation of the specimens for SEM examination*

# CHAPTER 4

# DISCUSSIONS AND RESULTS

## 4.1. Characterization of the Raw Materials

Properties of the raw materials are investigated by XRD, XRF, laser particle size distribution test, SEM and petrographic analysis for chemical and mineralogical properties, particle size distribution and morphology. All the provided chemical, mineralogical and physical data on fly ashes are taken from [43].

## 4.1.1. Chemical Analysis

XRF experiment results for the cement and aggregate samples used are given in Table 4 below:

*Table 4 XRF results of the cement and aggregates*

| Oxide (wt%) | Cement | Aggregate |
|---|---|---|
| $SiO_2$ | 17.5 | 60.2 |
| $Al_2O_3$ | 4.34 | 12.5 |
| $CO_2$ | - | 8.19 |
| CaO | 66.5 | 6.01 |
| $Fe_2O_3$ | 3.41 | 4.32 |
| $Na_2O$ | 0.585 | 2.69 |
| $K_2O$ | 1.05 | 2.45 |
| MgO | 1.35 | 2.40 |
| $TiO_2$ | 0.233 | 0.646 |
| $P_2O_5$ | 0.0638 | 0.454 |
| $SO_3$ | 4.94 | 0.0856 |

XRF experiment results for the fly ash samples are provided in Table 5. According to their CaO content, fly ash samples are classified into three groups such as high-Ca fly ash (CaO > 20%), intermediate-Ca fly ash (CaO 8–20%) and low-Ca fly ash (CaO < 8%). Moreover, Yeniköy (reactor 1) and Yeniköy (reactor 2) fly ashes are also

classified as high free CaO fly ashes because of their very high free CaO content (9,19% and 10,76 % respectively) and its negative effects on ASR expansion.

R.SiO$_2$ (reactive SiO$_2$ content): From the total SiO$_2$ content of the fly ash specimens, the insoluble residue SiO$_2$ content is subtracted according to EN197-1.

R.CaO (reactive CaO content): Calcium-aluminate-hydrates or calcium-silicate-hydrates forming CaO fragment. Calculated by subtracting the calcium carbonate (CaCO3) and calcium sulfate (CaSO$_4$) parts from the total CaO content according to EN197-1.

Free CaO: Titration method was used for the determination according to EN451-1 [43].

The formula of the Na$_2$O equivalent (total alkalis) is given in Equation 2.

*Equation 2.* Na$_2$O eq = (K$_2$O×0.658)+ Na$_2$O

*Table 5. XRF results of CFAs* [43]

| Oxide (wt%) | Low-Ca | | | | Intermediate-Ca | | |
|---|---|---|---|---|---|---|---|
| | Ç | Ç | T3 | T4 | IB | Ya2 | Ya3 |
| SiO$_2$ | 56.44 | 56.44 | 52.98 | 58.85 | 45.39 | 47.44 | 49.24 |
| Al$_2$O$_3$ | 25.26 | 25.26 | 19.38 | 18.94 | 18.25 | 19.62 | 18.81 |
| Fe$_2$O$_3$ | 5.90 | 5.90 | 13.38 | 9.97 | 10.15 | 6.82 | 7.38 |
| CaO | 1.72 | 1.72 | 1.30 | 3.12 | 14.20 | 15.93 | 14.34 |
| MgO | 2.22 | 2.22 | 3.92 | 4.41 | 4.48 | 3.06 | 2.75 |
| SO$_3$ | 0.08 | 0.08 | 0.49 | 0.45 | 3.10 | 1.96 | 1.98 |
| Na$_2$O | 0.40 | 0.40 | 0.04 | 0.11 | 0.35 | 0.76 | 0.71 |
| K$_2$O | 3.90 | 3.90 | 1.36 | 1.96 | 1.65 | 2.09 | 2.72 |
| Na$_2$O eq | 2.97 | 2.97 | 0.93 | 1.40 | 1.44 | 2.14 | 2.50 |
| TiO$_2$ | 1.12 | 1.12 | 1.08 | 0.83 | 0.57 | 0.72 | 0.78 |
| LOI | 2.65 | 2.65 | 4.93 | 0.66 | 0.55 | 0.73 | 0.53 |
| Free CaO | 0.03 | 0.03 | 0.02 | 0.01 | 1.5 | 2.34 | 1.7 |
| R.CaO | 0.97 | 0.97 | 0.79 | 2.77 | 11.97 | 13.82 | 12.52 |
| R.SiO$_2$ | 42.31 | 42.31 | 36.43 | 43.24 | 36.33 | 31.28 | 33.91 |

Table 5. XRF results of CFAs [43] (continued)

| Oxide (wt%) | High-Ca | | | | High F.CaO | |
|---|---|---|---|---|---|---|
| | AEB | K1 | K2 | K3 | Ye1 | Ye2 |
| $SiO_2$ | 39.79 | 38.57 | 36.10 | 31.23 | 25.93 | 25.93 |
| $Al_2O_3$ | 16.26 | 18.76 | 18.95 | 15.57 | 11.40 | 12.07 |
| $Fe_2O_3$ | 7.11 | 7.41 | 7.92 | 7.41 | 4.85 | 5.05 |
| CaO | 21.13 | 24.41 | 26.30 | 32.77 | 40.52 | 40.61 |
| MgO | 2.26 | 2.20 | 2.28 | 1.79 | 1.93 | 2.02 |
| $SO_3$ | 6.85 | 4.12 | 4.42 | 6.84 | 8.97 | 8.18 |
| $Na_2O$ | 0.33 | 0.63 | 0.52 | 0.44 | 0.78 | 0.29 |
| $K_2O$ | 1.40 | 2.01 | 1.92 | 1.59 | 1.40 | 1.04 |
| $Na_2O$ eq | 1.25 | 1.95 | 1.78 | 1.49 | 1.70 | 0.97 |
| $TiO_2$ | 0.75 | 0.77 | 0.78 | 0.63 | 0.51 | 0.49 |
| LOI | 2.88 | 0.54 | 0.37 | 0.75 | 2.53 | 3.11 |
| Free CaO | 3.11 | 2.28 | 3.46 | 4.71 | 9.59 | 10.76 |
| R.CaO | 13.45 | 20.98 | 23.05 | 27.03 | 31.71 | 31.59 |
| $R.SiO_2$ | 31.97 | 31.97 | 29.29 | 26.78 | 20.84 | 20.45 |

## 4.1.2. Mineralogical Analysis

The results of the XRD measurements are interpreted through Highscore Plus software. Quartz, calcite and plagioclase minerals are identified in the aggregate sample which are also identified by petrographical analysis. Among these minerals, quartz is known to be prone to ASR damage and plagioclase may also contribute to the reaction at lower levels. For the portland cement sample, $C_3S$, $C_2S$, brownmillerite and gypsum are identified. The XRD diffractograms are given in Figure 30.
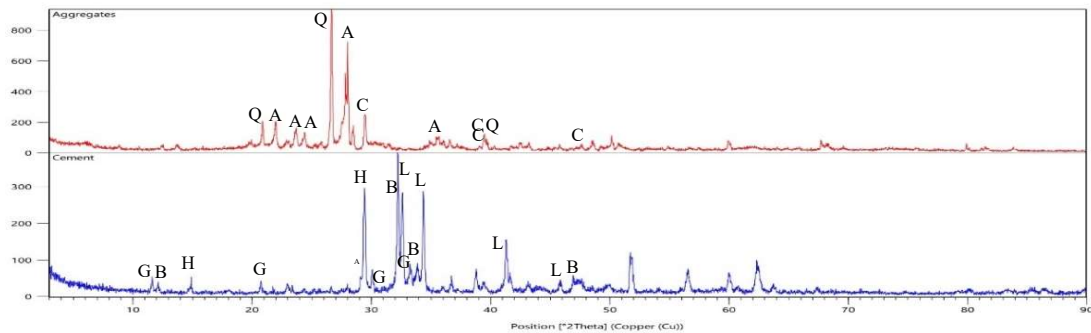


A: Anorhtite Sodian (plagioclase); C: Calcite; Q: Quartz; H: $C_3S$; L: $C_2S$; B: Brownmillerite; G:Gypsum

*Figure 30. XRD diffractograms of aggregates and cement*

41

The XRD diffractograms of all fly ash specimens are given in Figure 31.
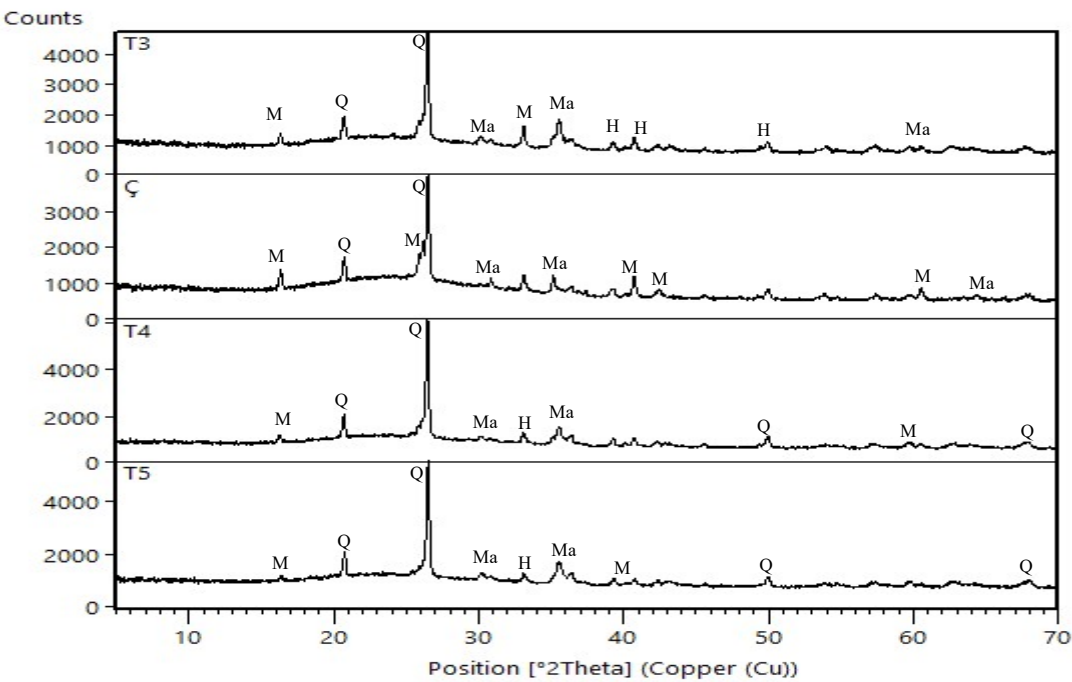


*(a) Low-Ca*
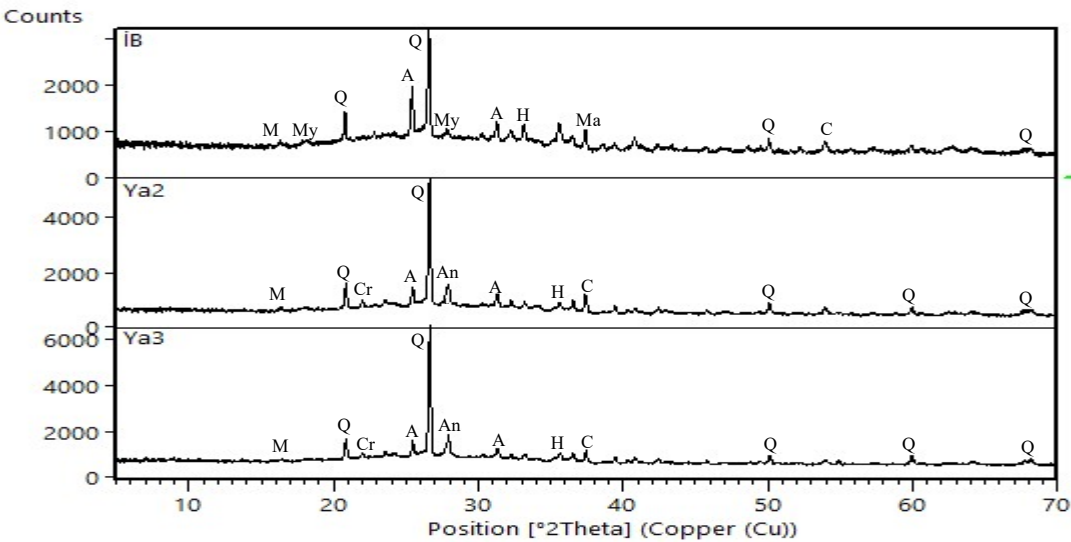


*(b) Intermediate-Ca*
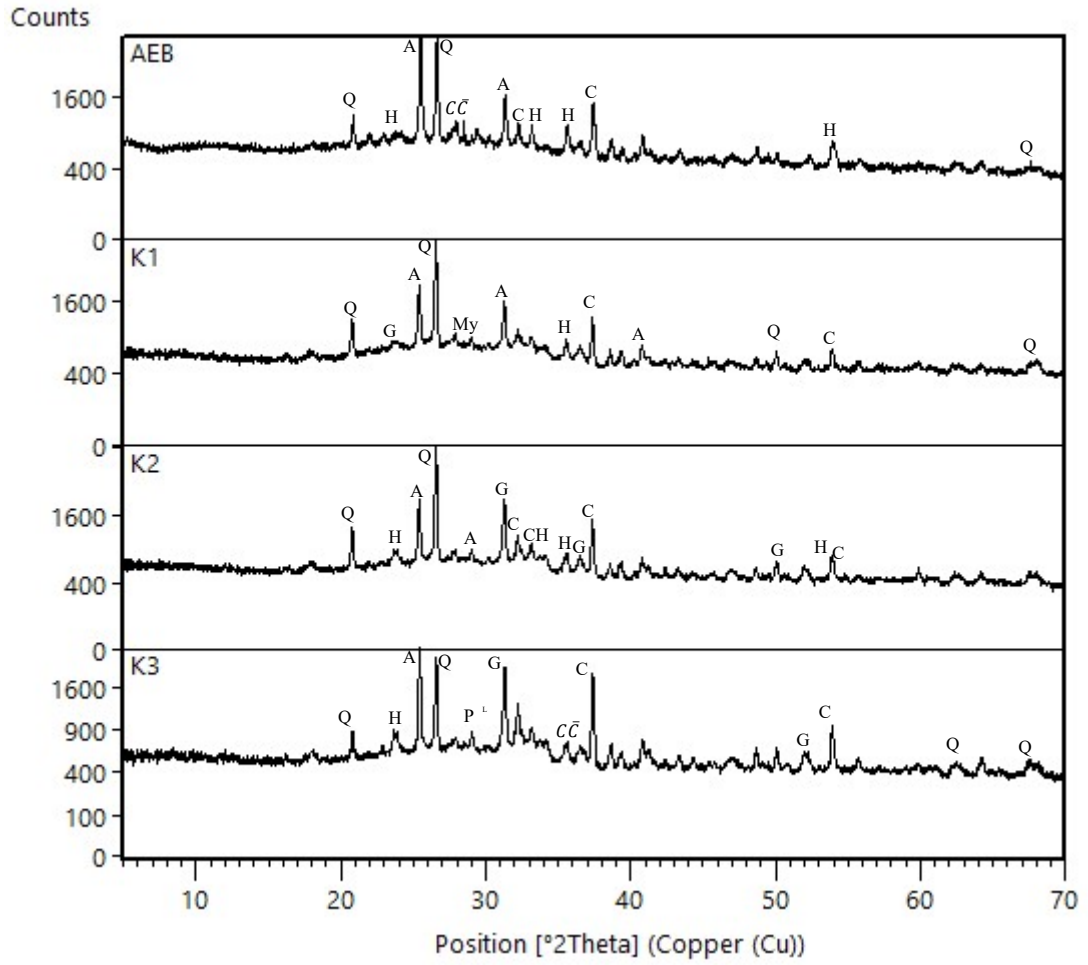
*(c) High-Ca*
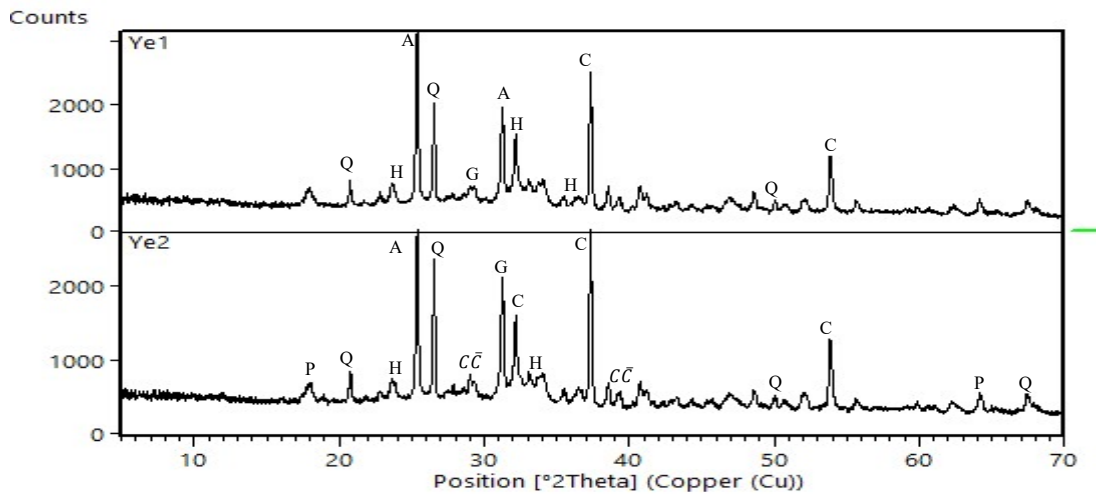


*(d) High F.CaO*

*A: Anhydrite, C: Calcium oxide, C$\bar{C}$:Calcite, Cr: Cristobalite, G: Gehlenite, H: Hematite, M: Mullite, Ma: Magnetite, My: Mayenite , P: Portlandite, Q:Quartz,*

*Figure 31. (a-d) XRD diffractograms of fly ash specimens* [43]

43

The XRD analysis results are summarized below[43]:

- Ç fly ash appears to have a composition of glassy structure and crystalline phase in small quantity. The crystalline phases are quartz ($SiO_2$), mullite ($3Al_2O_3$ $2SiO_2$) and magnetite ($Fe_3O_4$). The glassy phase is maximized between 22-27°2θ. This build up is the result of the fact that the glassy phase is in the form of alumina-silicate composition which is rich in silica [43].

- IB fly ash is generally composed of crystalline phases and glassy structure. Crystalline phases are quartz, calcium oxide (CaO), anhydrite ($CaSO_4$), hematite ($Fe_2O_3$), mullite, mayenite ($12CaO.7Al_2O_3$) and magnetite ($Fe_3O_4$) [43].

- K1 fly ash broadly has crystalline phases and glassy structure. Crystalline phases are quartz, calcium oxide, anhydrite, hematite, gehlenite ($Ca_2Al[AlSiO_7]$) and mayenite [43].

- K2 fly ash appears to have mostly crystalline phases and glassy structure. Crystalline phases are quartz, calcium oxide , anhydrite, hematite and gehlenite [43].

- K3 fly ash is composed of generally crystalline and glassy phases. Crystalline phases are quartz, calcium oxide , anhydrite , hematite, gehlenite, calcite ($CaCO_3$) and portlandite ($Ca(OH)_2$) [43].

- T3 fly ash has broadly crystalline and glassy phases. Crystalline phases are quartz, , magnetite, hematite and mullite. The glassy phase appears to be maximized between 22-28°2θ in the x-ray diffractogram [43].

- T4 fly ash generally has crystalline and glassy phases. Crystalline phases are quartz, mullite, hematite and magnetite [43].

- T5 fly ash is broadly composed of crystalline and glassy phases. Crystalline phases are quartz, mullite, hematite and magnetite [43].

- Ya2 fly ash appears to have generally crystalline and glassy phases. Crystalline phases are quartz, calcium oxide , magnetite, hematite, anhydrite  and cristobalite ($SiO_2$) [43].

- Ya3 fly ash has generally crystalline and glassy phases. Crystalline phases are quartz, calcium oxide, anhydrite, cristobalite, hematite, mullite and anorthite (($Ca,Na)(Al,Si)_4O_8$) [43].

- Ye1 fly ash is generally composed of crystalline and glassy phases. Crystalline phases are quartz, calcium oxide, gehlenite, hematite  and anhydrite [43].
- Ye2 fly ash is broadly in crystalline and glassy phases. Crystalline phases are quartz, calcium oxide, gehlenite, hematite, anhydrite, portlandite and calcite [43].

### 4.1.3. Particle Size Distribution

The particle size distributions of the fly ash samples classified according to their CaO content, are given in Figure 32.

– When the graph for the low-Ca coal fly ashes is analyzed, it is seen that T4 is the finest specimen whereas T5 is the coarsest one. T3 and Ç samples have average gradations. Although they are byproducts of different power plants, T5 and Ç are the most similar fly ashes by means of gradation values.

– As can be seen in the intermediate-Ca diagram, these three coal fly ash specimens have closer gradations than the low-Ca samples. IB is the finest sample, Ya2 is the coarsest and Ya3 is the median. Ya2 and Ya3 are very similar, almost identical at the fine and coarse gradation regions.

– Lastly, high-Ca CFA coal fly ash specimens also have very close gradation values like the intermediate-Ca fly ashes. Except for the Ye1 and AEB specimens which are the finest and coarsest among this category, it is not easy to notice the difference between the samples with average gradations such as K1, K2, K3 and Ye2 from the graph.
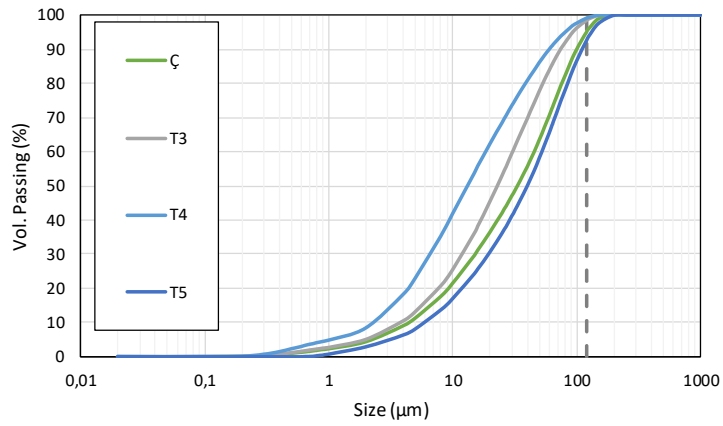
(a)
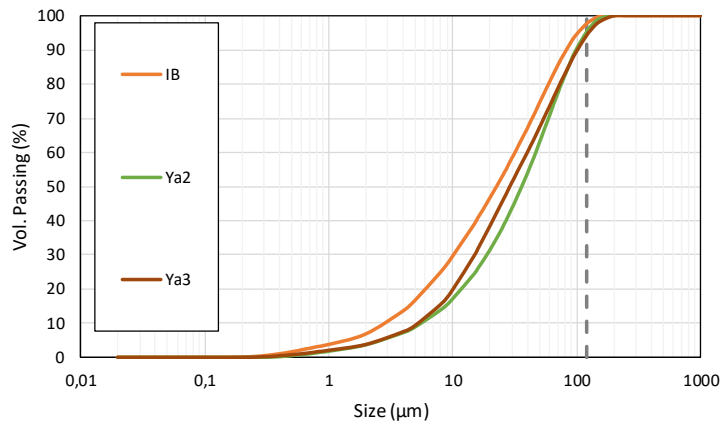


(b)
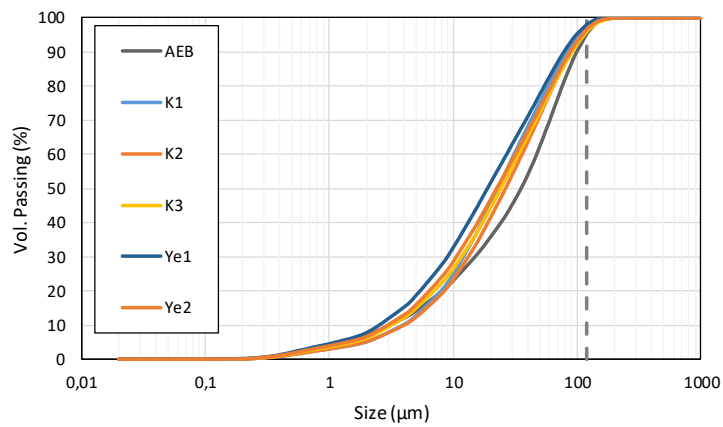


(c)

*Figure 32. Particle size distributions of (a) low-Ca, (b) intermediate-Ca and (c) high-Ca CFAs* [43]

D10, D50 and D90 are the diameters at which 10%, 50% and 90% of the material volume is composed of particles smaller than these values. These values of the fly ash samples are summarized in Table 6. IB specimen which has D10 value of 2.9 has the finest 10% portion by volume whereas T5 with D10 value of 6 has the least fine 10% portion. In other words, IB sample has the most dust-like particles whereas T5 has the least. Likewise, when the D90 values are analyzed, it is seen that T5 has the largest value of 110.6 whereas T3 has the smallest value of 74.2, which means that the coarsest 10% grains of T5 are the largest whereas T3 has smallest. Lastly, when the D50 values, in other words the average particle sizes are investigated, Ye1 specimen seems to have the smallest value with 19 and T5 has largest with 40. This condition also holds with the fact that T5 was the coarsest specimen according to the Figure 32 as stated in the discussions above. Other specimens' cases are parallel with their D10, D50 and D90 values.

*Table 6. D10, D50 and D90 values of the fly ash samples* [43]

|  | AEB | Ç | IB | K1 | K2 | K3 | T3 | T4 | T5 | Ya2 | Ya3 | Ye1 | Ye2 |
|---|---|---|---|---|---|---|---|---|---|---|---|---|---|
| D10 | 3.1 | 4.4 | 2.9 | 4 | 4.0 | 3.3 | 3.8 | 5.3 | 6 | 5.7 | 5.3 | 2.6 | 3.1 |
| D50 | 35.4 | 33.5 | 22.6 | 23.1 | 26.6 | 24.3 | 22.9 | 31.7 | 40 | 36.3 | 29 | 19 | 22.5 |
| D90 | 99.5 | 100.7 | 82.5 | 83.4 | 89.0 | 91.3 | 74.2 | 101.4 | 110.6 | 99.5 | 101.7 | 78.9 | 88.1 |

### 4.1.4. Petrographical Analysis

A detailed petrographic analysis on the aggregate sample was conducted at Department of Geological Engineering with the supervision of Assist. Prof. Dr. Fatma Köksal (Figure 33). The sandy gravel sample, which is grayish macroscopically, is composed of loose silt to gravel sized grains, where the grains are mostly subrounded to subangular. High composition variability is determined in these grains such as basalt, microgabbro, iddingtized dunite, dacite, phyllite, quartzite, sandstone, limestone, free quartz, clinopyroxene, plagioclase, where the roundness varies from angular to round depending on grain composition. Iron oxide staining is a common property in the grains:

- Basalt grains, which are ~45% in abundance, are subangular to angular in shape. These grains are composed of plagioclase, clinopyroxene both as phenocryst and as matrix material. In matrix, opaque minerals with magmatic origin are also exit. Moreover, glass is identified as interstial component in the matrix. There is another basalt variety in which rather than clinopyroxene olivine is present as mafic mineral. Olivine is completely iddingtized due to alteration.

- Sandstone grains, which are ~15% in abundance, are angular to subangular. They are composed of variable sized quartz and rock fragments.

- Dacite grains, which are ~8% in abundance, are subrounded. Dacite is fine grained and contains plagioclase phenocryst and microlites in a glassy matrix. Biotite is also present but its amount is less %6. Microliths display flow texture. Dacite graines are generalIy stained by iron oxide due to surface alteration.

- Limestone grains, ~10% in abundance and generally rounded, are composed of micritic calcite.

- Microgabbro grains which are subangular, are low in amount (<3%). They are composed of olivine, plagioclase and opague phases. Microgabbro grains are stained by iron oxide due to alteration. Olivine crystals are iddingtized.

- In the sample, rounded metamorphic rock grains, phyllite and quartzite are determined in abundance of ~6%. Phyllite has variable amount of mica and quartz with slaty foliation. Quartzite is characterized mortar texture and andulatory extinction in quartz crystals due to pressure.

- The grains of dunite, complete iddingtized, are also present in abundance of ~3%, which are re rounded.

- As free mineral grains, quartz, plagioclase, clinopyroxene are also present with abundance of ~10%. All the free mineral grains are subangular to angular in shape.
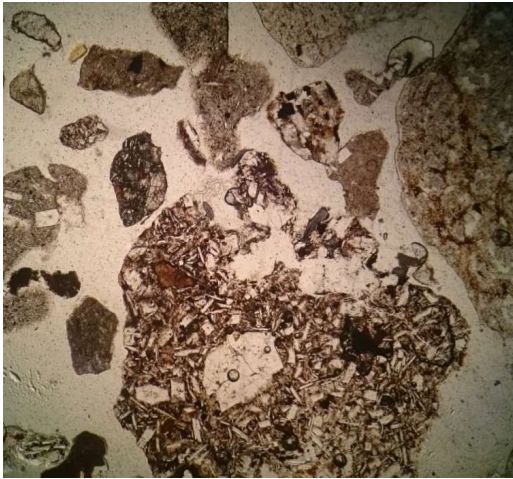
(a)
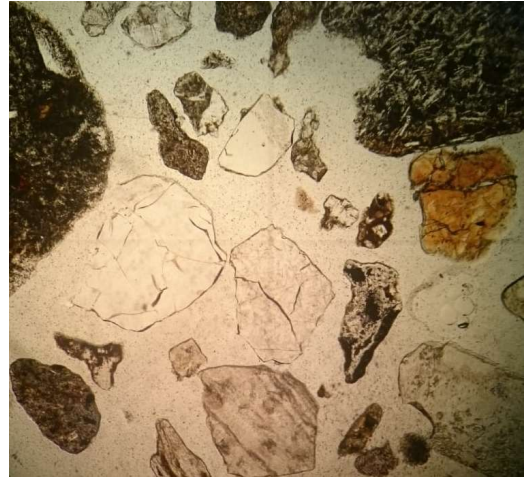
(b)
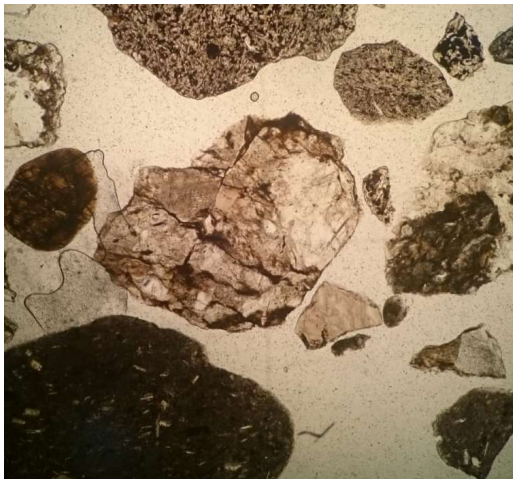
(c)

(d)
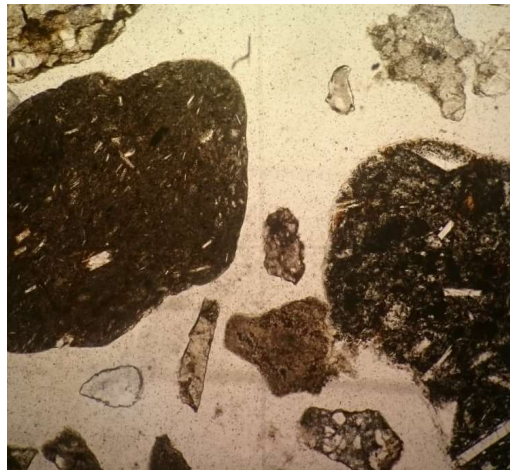
(e)

*Figure 33. (a-e) Images of the aggregate specimen for petrographical analysis*

### 4.1.5. Scanning Electron Microscope Analysis

### 4.1.5.1. Cement

General view SEM micrographs taken from the cement specimen at 250, 500 and 1000 magnification levels are given in Figure 34.  The particle shapes are irregular where there have been some coagulations of them. Particle sizes are variable whereas the maximum particle size is ~50 microns.
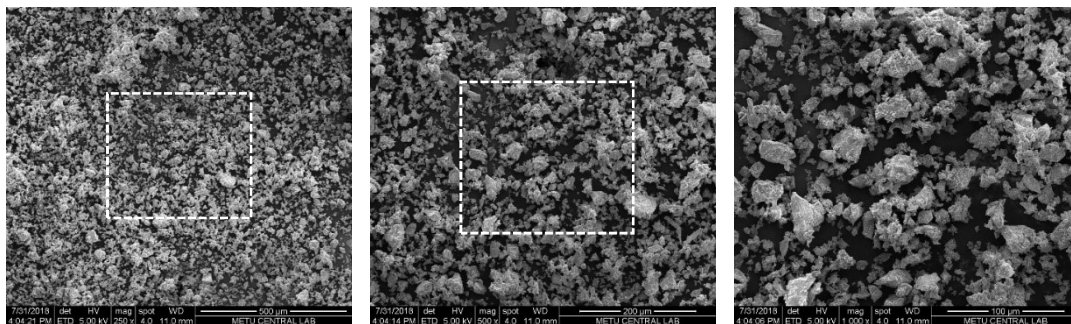


*Figure 34. SEM BSE images of portland cement specimen*

### 4.1.5.2. Fly Ash Specimens

General view SEM micrographs taken from all the coal fly ash specimens are discussed in this chapter. Since the samples are sieved before the examination, the bigger particles are eliminated. Please note that the hole-like black appearances are caused by the tape used to contain the specimens.

### 4.1.5.2.1. Low-Ca Fly Ash Specimens

General view SEM micrographs taken from the low-Ca fly ash specimens at 250, 500 and 1000 magnification levels are given at Figure 35:
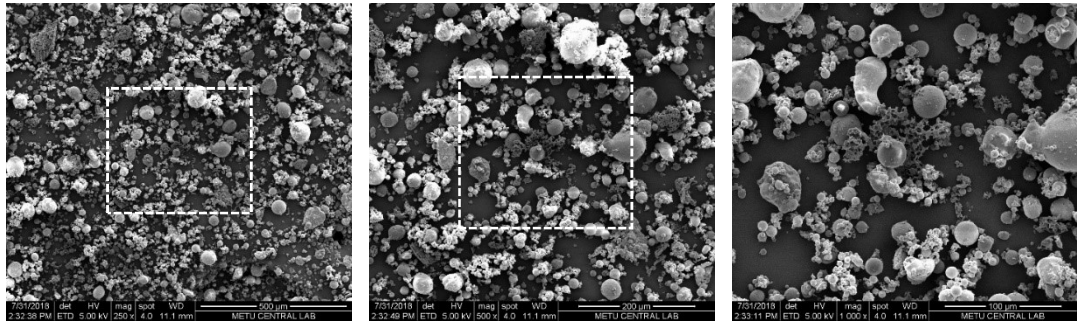
*(a) Ç*
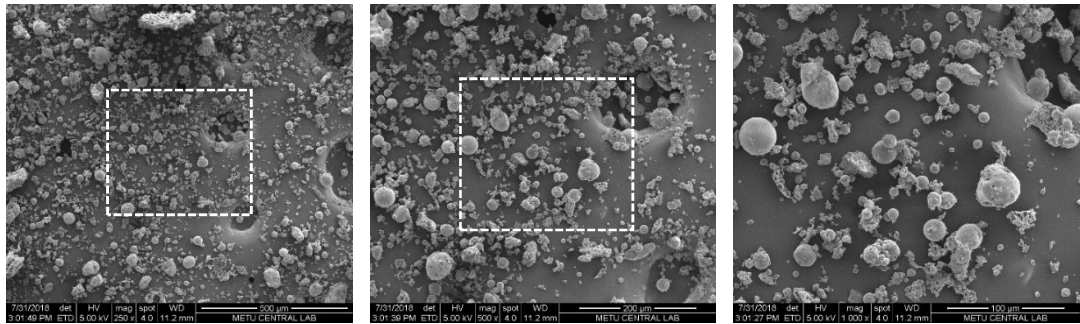


*(b) T3*
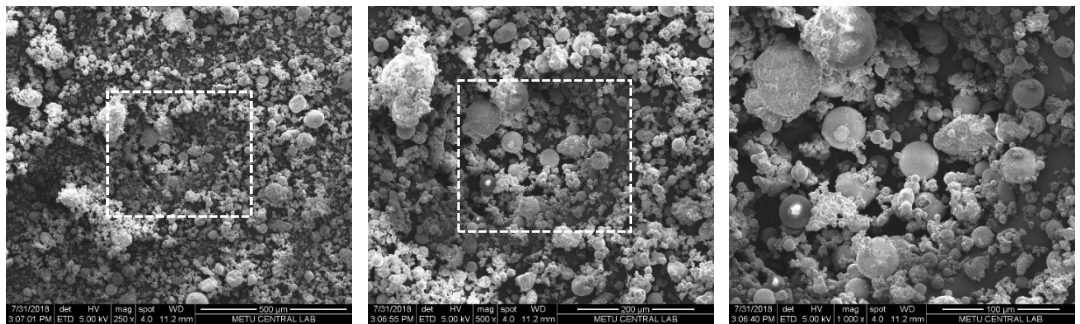


*(c) T4*
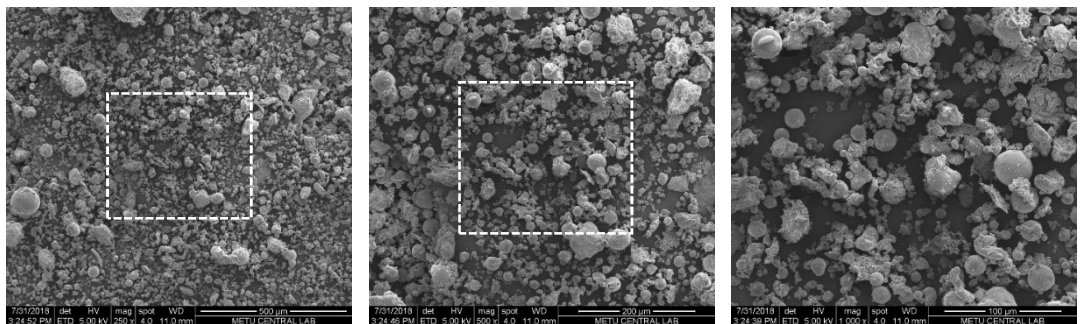


*(d) T5*

*Figure 35. (a-d) SEM BSE images of low-Ca fly ash specimens*

- When the figure of Ç specimen is analyzed, it is seen that the particle size and shapes are variable. Particle size range extends to ~70 microns whereas their shapes are mostly spherical, some grains are also irregular. There are also porous structures.

- As can be seen in the images of T3, there is diversity in both size and shape of the materials. There are both spherical irregular shaped particles. The visible maximum particle size is ~50 microns.

- The next images show that T4 sample has more spherical particles than T3, and it also contains weird shaped ones. The maximum particle size is ~70 microns.

- Lastly, T5 sample images are similar to T3 by means of diversity of size and shapes of the particles. The maximum particle size is also ~50 microns.


## 4.1.5.2.2. Intermediate-Ca Fly Ash Specimens

General view SEM micrographs taken from the intermediate-Ca fly ash specimens at 250, 500 and 1000 magnification levels are given at Figure 36.

- As can be seen in the images of IB, the particles are mostly spherical. The maximum particle size is ~50 microns whereas there are variety of particle sizes.

- Next, Ya2 specimen images have spherical and irregular shaped materials. There are also coagulated smaller particles. Moreover, are porous structures are also seen. There is diversity by means of sizes. The maximum particle size determined in the images is ~60 microns.

- Ya3 samples are similar to Ya2 according to the SEM images. There are both spherical and irregular particles. Also coagulated ones and porous structures are also observed. The largest particle is ~70 microns.
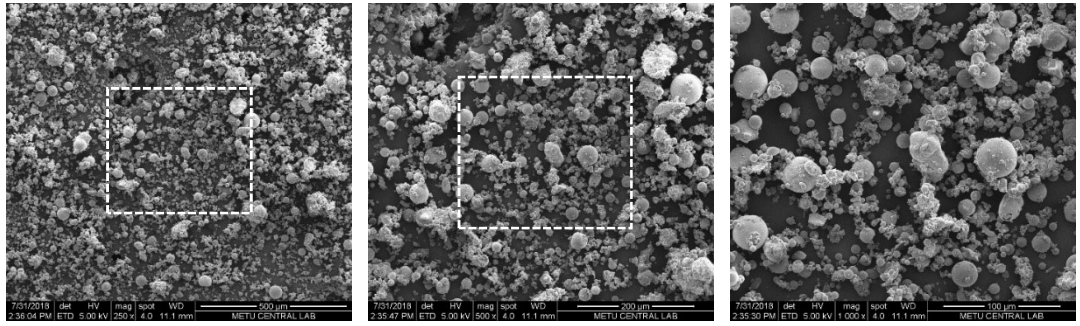
*(a) IB*
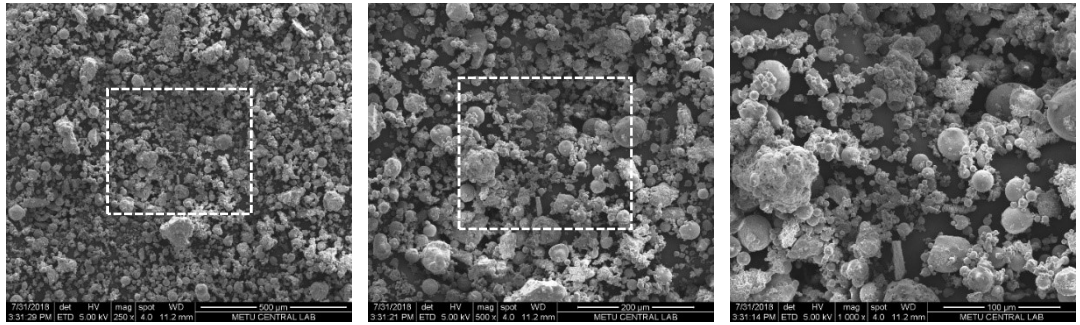


*(b) Ya2*
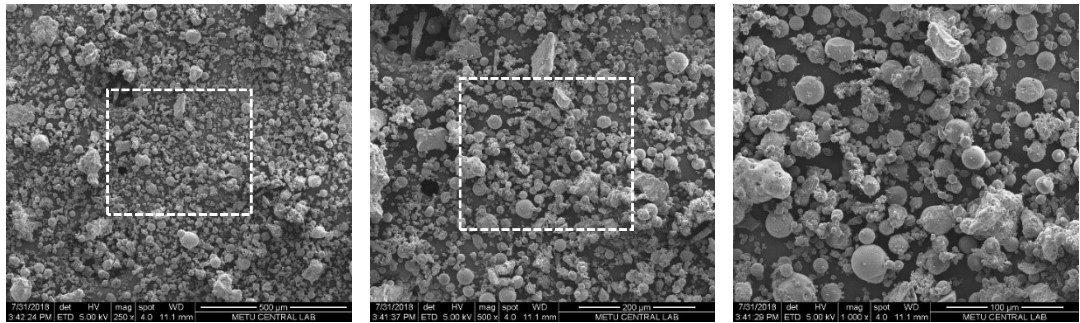


*(c) Ya3*

*Figure 36. (a-c) SEM BSE images of intermediate-Ca fly ash samples*

### 4.1.5.2.3. High-Ca Fly Ash Specimens

General view SEM micrographs taken from the intermediate-Ca fly ash specimens at 250, 500 and 1000 magnification levels are given at Figure 37. These images are different than the images of low-Ca and intermediate-Ca samples:

*(a) AEB*



*(b) K1*



*(c) K2*



*(d)  K3*

54

*(e) Ye1*



*(f) Ye2*
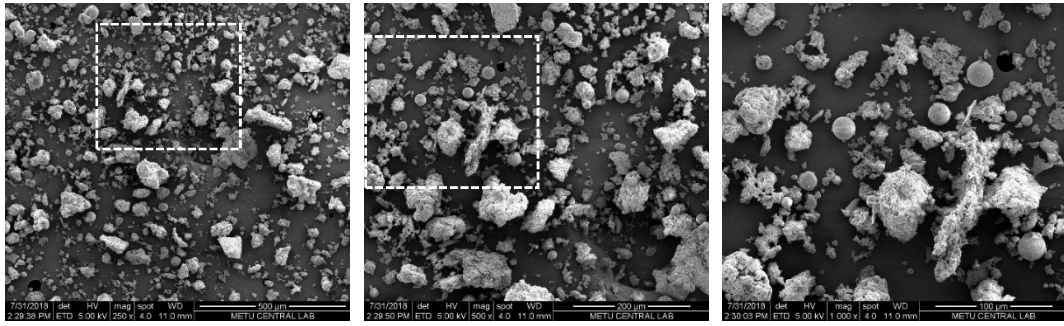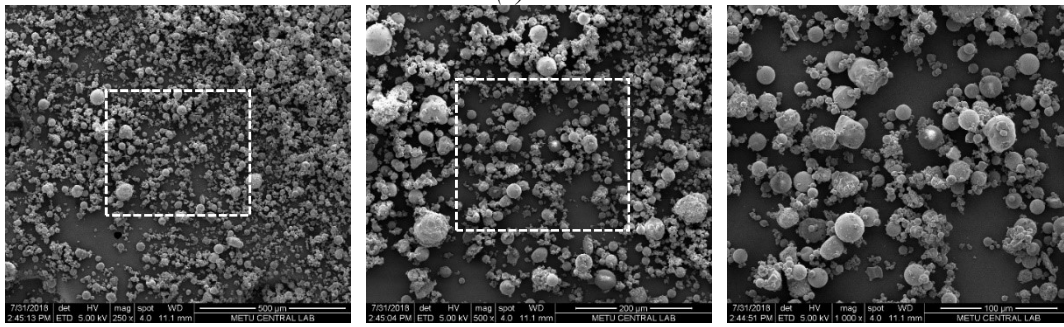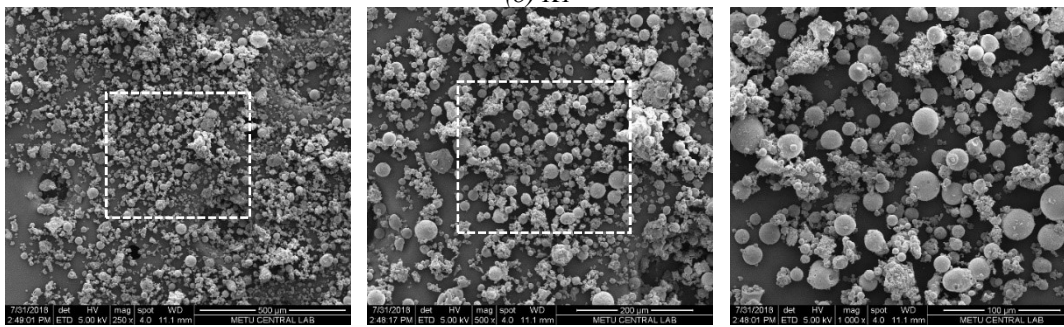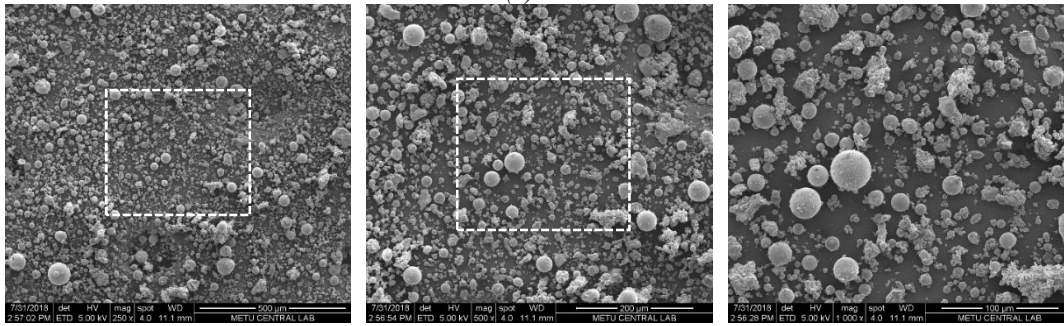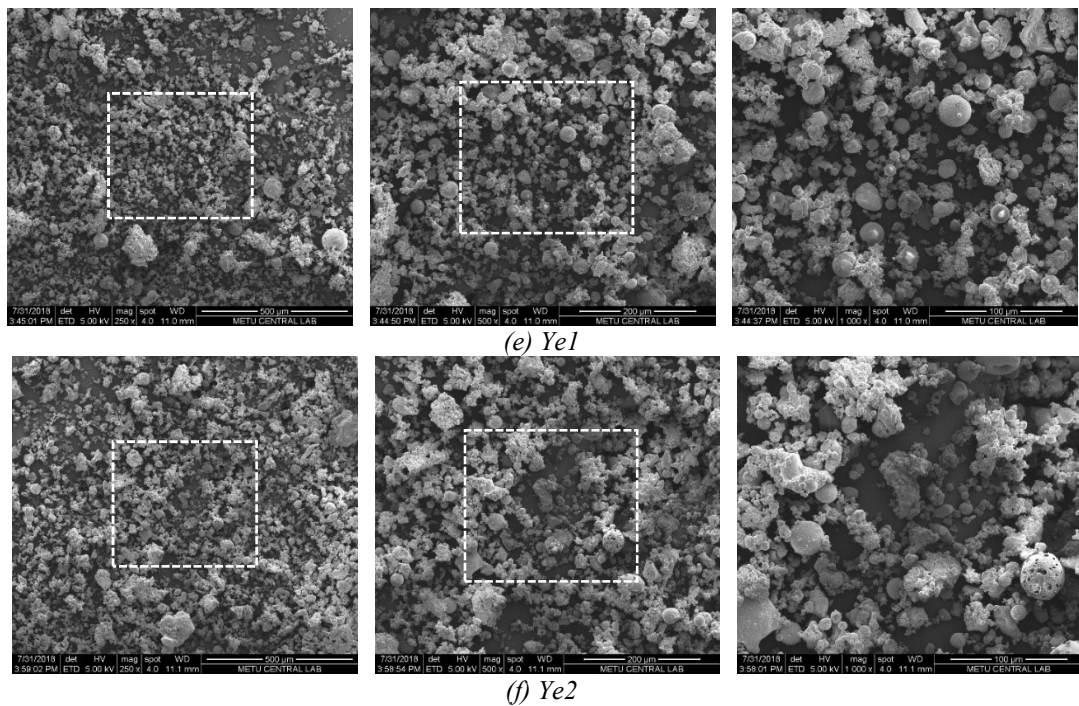
*Figure 37. (a-f) SEM BSE images of high-Ca fly ash specimens*

- AEB specimen is mostly composed of irregular shaped particles and porous ones. Moreover, there have been also spherical shaped objects determined. There are more larger particles, and the maximum particle size seen in the images is ~80 microns.

- K1 and K2 images are similar. They are mostly composed of spherical particles. There is diversity in particle sizes where the smaller ones usually coagulated. Maximum particle size determined from the images is ~50 microns.

- K3 specimen is also mostly composed of spherical particles. The particle size distribution seems to be different than K1 and K2 where bigger and smaller sized materials are more than middle sized ones. There are also coagulated small particles. The maximum size is ~50 microns.

- As can be seen in the next images, Ye1 and Ye2 specimens are also similar. They are mostly composed of irregular shaped particles. There are also spherical materials. Coagulations and porous particles are also observed. The particle size is diversified where the observed maximum particle size is ~70 microns.

**4.2. ASTM 1260 – Accelerated Mortar Bar Test Expansion Results**

The accelerated expansion results for the control mortars and the 15wt%, 25wt% and 50wt% replacement mortars – a total of 40 mortar mixes - are given in Figure 38. Generally, increase of the replacement level of cement with coal fly ash has positive effect on mitigation of the ASR on the mortar bars except for the Ye1 and Ye2 specimens. Especially at 50wt% replacement level, all of the 11 samples seems to have satisfactory results on the mitigation of ASR. For 15wt%, 25wt% levels, the outcomes depend on the coal fly ash type and composition which are discussed in detail in next sections.

The 14-day and 75-day expansion results for 40 mortar mixes are reported in Table 7. It is clearly seen that the specimens with lower Ca levels have given better performance for the mitigation of the ASR expansions. Samples with higher Ca levels (except for the high free CaO samples) have also given reasonable results in prevention of ASR. Even high-Ca fly ashes were satisfactory by means of controlling ASR at 50% replacement level.

14-day and 75-day expansions are linearly proportional except for the control specimen and high F.CaO (Ye1 and Ye2) specimens (Figure 39). The ASR expansions are more severe for these specimens at the early stages of the experiment.

+
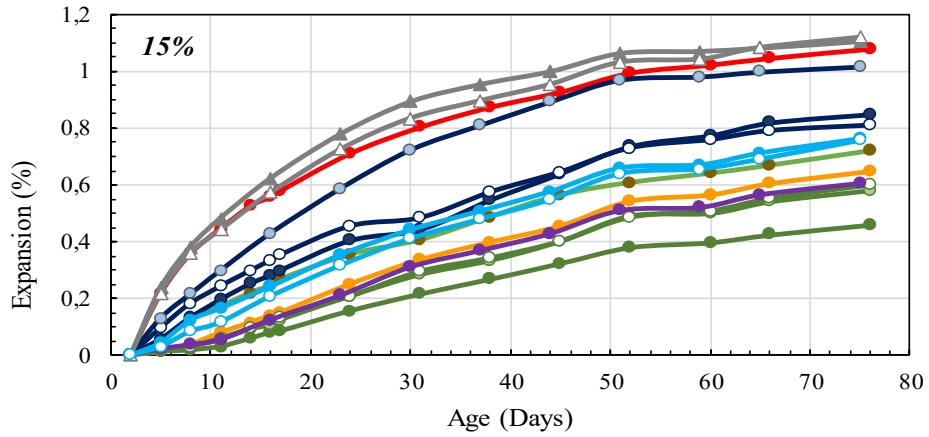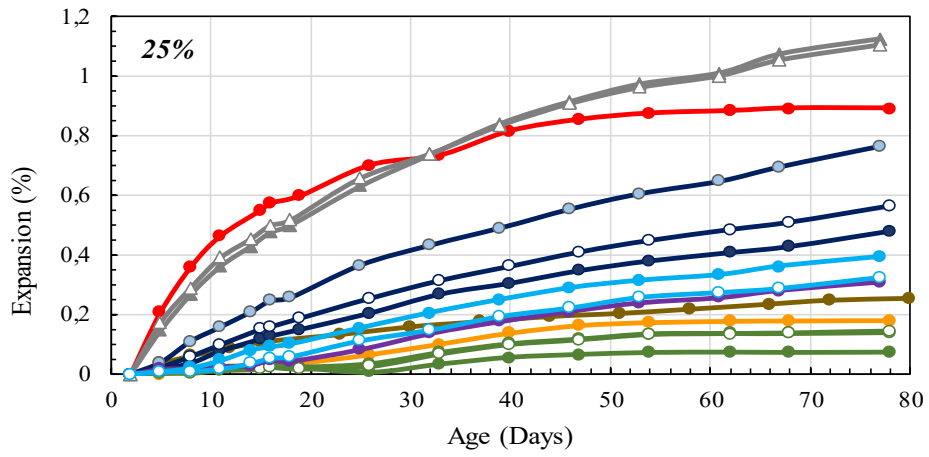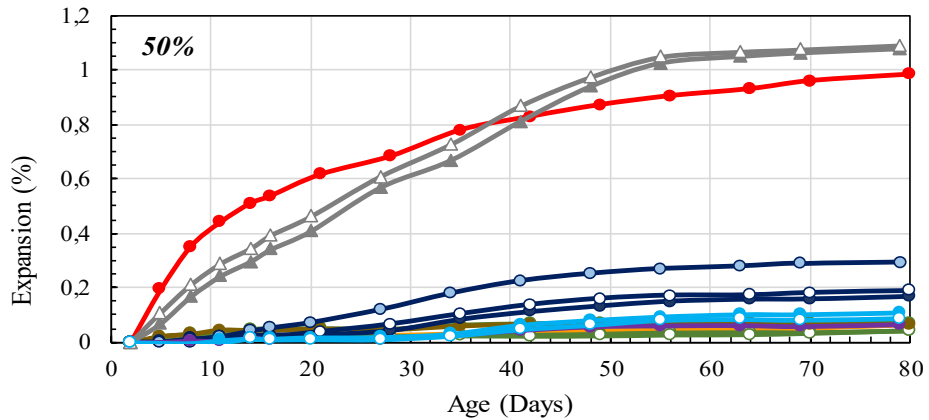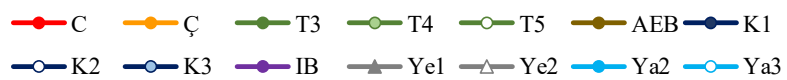
*Figure 38. ASTM C1260 expansion test results for (a) 15%, (b) 25% and (c) 50% CFA mortar mixes*

*Table 7. Expansion of mortar bars at 14-days and 75 days with respect to (a) the zero reading (%) and (b) the control sample expansion at the measurement day (%)*

(a)

| Expansion of mortar bars | | After 14-days (%) | | | | After 75-days (%) | | | |
|---|---|---|---|---|---|---|---|---|---|
| Coal fly ash | | Replacement level | | | | Replacement level | | | |
| Type | Source | 0% | 15% | 25% | 50% | 0% | 15% | 25% | 50% |
| Control* | C (average) | 0.521 | | | | 0.979 | | | |
| Low-Ca | Ç | | 0.115 | 0.027 | 0.024 | | 0.642 | 0.179 | 0.060 |
| Low-Ca | T3 | | 0.059 | 0.021 | 0.048 | | 0.457 | 0.071 | 0.071 |
| Low-Ca | T4 | | 0.092 | 0.025 | 0.017 | | 0.576 | 0.139 | 0.039 |
| Low-Ca | T5 | | 0.095 | 0.015 | 0.016 | | 0.595 | 0.141 | 0.038 |
| Int-Ca | IB | | 0.096 | 0.030 | 0.014 | | 0.605 | 0.304 | 0.060 |
| Int-Ca | Ya2 | | 0.211 | 0.081 | 0.012 | | 0.761 | 0.386 | 0.105 |
| Int-Ca | Ya3 | | 0.171 | 0.036 | 0.013 | | 0.756 | 0.319 | 0.086 |
| High-Ca | AEB | | 0.220 | 0.101 | 0.044 | | 0.714 | 0.251 | 0.065 |
| High-Ca | K1 | | 0.252 | 0.108 | 0.025 | | 0.845 | 0.463 | 0.162 |
| High-Ca | K2 | | 0.298 | 0.138 | 0.018 | | 0.806 | 0.549 | 0.185 |
| High-Ca | K3 | | 0.377 | 0.209 | 0.041 | | 1.016 | 0.751 | 0.291 |
| HF.CaO | Ye1 | | 0.567 | 0.430 | 0.295 | | 1.104 | 1.117 | 1.072 |
| HF.CaO | Ye2 | | 0.519 | 0.454 | 0.344 | | 1.118 | 1.096 | 1.085 |

* For each replacement level, a separate set of control specimens were prepared.

(b)

| Expansion of mortar bars | | After 14-days (%) | | | | After 75-days (%) | | | |
|---|---|---|---|---|---|---|---|---|---|
| Coal fly ash | | Replacement level | | | | Replacement level | | | |
| Type | Source | 0% | 15% | 25% | 50% | 0% | 15% | 25% | 50% |
| Control* | C *15% (average) | 100 | | | | 100 | | | |
| Low-Ca | Ç | | 22 | 5 | 5 | | 60 | 20 | 6 |
| Low-Ca | T3 | | 11 | 4 | 9 | | 42 | 8 | 7 |
| Low-Ca | T4 | | 17 | 5 | 3 | | 54 | 16 | 4 |
| Low-Ca | T5 | | 18 | 3 | 3 | | 55 | 16 | 4 |
| Int-Ca | IB | | 18 | 6 | 3 | | 56 | 34 | 6 |
| Int-Ca | Ya2 | | 40 | 15 | 2 | | 71 | 43 | 11 |
| Int-Ca | Ya3 | | 32 | 7 | 2 | | 70 | 36 | 9 |
| High-Ca | AEB | | 42 | 19 | 9 | | 66 | 28 | 7 |
| High-Ca | K1 | | 48 | 20 | 5 | | 79 | 52 | 17 |
| High-Ca | K2 | | 57 | 26 | 4 | | 75 | 62 | 19 |
| High-Ca | K3 | | 72 | 40 | 8 | | 94 | 84 | 30 |
| HF.CaO | Ye1 | | 108 | 81 | 58 | | 103 | 125 | 110 |
| HF.CaO | Ye2 | | 99 | 86 | 67 | | 104 | 123 | 112 |

* For each replacement level, a separate set of control specimens were prepared.
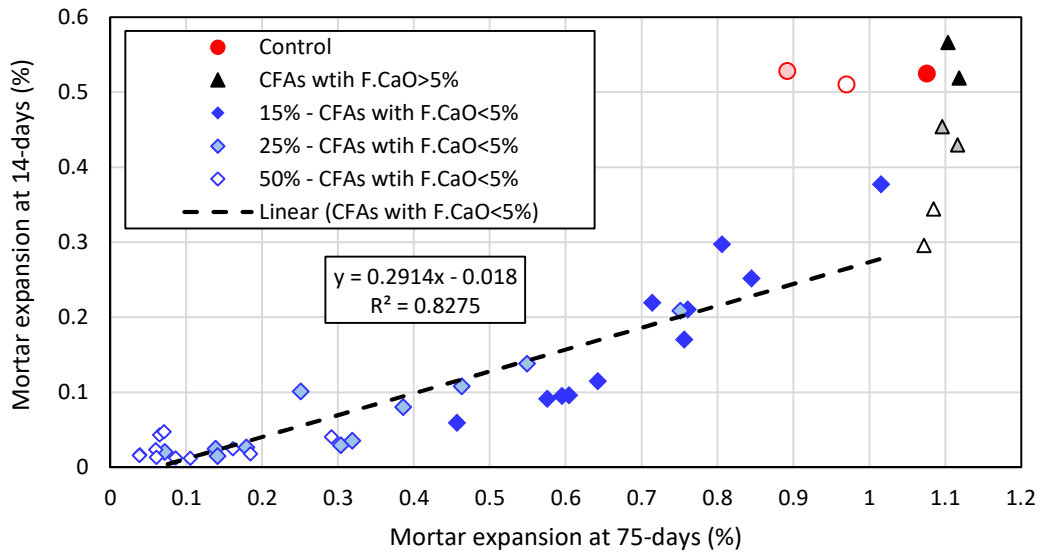
*Figure 39. The relationship between ASTM C1260 expansion test results at 14-days and 75-days*

## 4.3. Effect of Replacement Levels of Coal Fly Ashes on Preventing Alkali Silica Reaction Expansions

### 4.3.1. Low Ca Fly Ashes

The 75-day expansion results of the mortar specimens prepared with low-Ca fly ashes are given in Figure 40. All low-Ca CFAs have significantly decreased the ASR expansion amount at 15%, 25% and 50% replacement ratios. Their average mitigation performance is over 50% even in the 15% replacement level, which is the minimum replacement option chosen for this study.

It is clear that 25% replacement level is also suitable for the mitigation of ASR expansions for all of the low-Ca CFAs. All of the low Ca fly ash samples have decreased the ASR expansion level to almost zero level 50% replacement level. Although 50% replacement level has given the best performance for the mitigation of ASR expansions for all the low Ca fly ash samples, because of the workability issues, it is not convenient to replace the cement with fly ash at this level, 25% ratio is the best option.

### 4.3.2. Intermediate Ca Fly Ashes

As can be seen from Figure 41, all of the specimens have shown a tendency to decrease the ASR expansions at 15%, 25% and 50% replacement level. The mitigation ratio is less than that of the low Ca fly ashes but still at favorable levels. At even 15% replacement level, the mitigation performance is almost half of the control specimen. When the replacement level is increased to 25%, the ASR expansions decrease to almost 1/3 of the control specimen. Although not as good as the low Ca fly ash samples, all the intermediate Ca fly ash specimens have shown enough performance for the mitigation of ASR expansion at 25% replacement level. Finally, at 50% level, the ASR expansions almost vanish as in the example of the low Ca fly ash specimens. Just like the low Ca fly ashes, since the workability is a significant issue at 50% replacement level, it is not convenient to use this replacement ratio, so most feasible choice is 25% for intermediate Ca fly ashes.

### 4.3.3. High-Ca Fly Ashes

When the next three graphs are analyzed at Figure 42, it can be seen that high Ca fly ash samples' performance is not as good as the low Ca and intermediate Ca fly ash samples. Especially at 15% replacement level, the mitigation performance drops to less than 50% which does not seem to be enough to prevent the ASR related problems within structures. 25% replacement ratio has given fair results but most of them are not acceptable according to the ASTM C1260 specifications, 0.1% limit. At 50% ratio, the elongations related with ASR decreases to almost half of the control specimens on average. The best performance is AEB whereas the worst one is K3. AEB might be used at 25% for preventing ASR but the other fly ashes' performance seems to be not enough. At 50% replacement level, just like the low and intermediate Ca fly ashes, the ASR expansions decrease at considerable amount. The mitigation level is less than the other two alternatives but enough for prevention of the unwanted effects of ASR. On the other hand, again this replacement level is not suitable because of the workability problems at this replacement level just as in the case of low and intermediate Ca coal fly ashes.

### 4.3.4. High F.CaO Fly Ashes

Lastly, the two specimens which are named high free Cao fly ashes in this study (Ye1 and Ye2), have even increased the ASR expansion at every stage of the experiment at %15 replacement level (Figure 43). Although at 50% and 25% replacement levels they seemed to decrease ASR expansions at some level, after 2 weeks their effect became negative. At all replacement levels, the ultimate ASR expansion was more than that of control specimens with no fly ash replacement. This situation is probably caused by the free CaO content of these two specimens, resulting in $Ca(OH)_2$ (abbreviation of CH is used in cement chemistry) formation. For this reason, performance of Ye1 and Ye2 are investigated in separate graphs as high free CaO fly ashes.
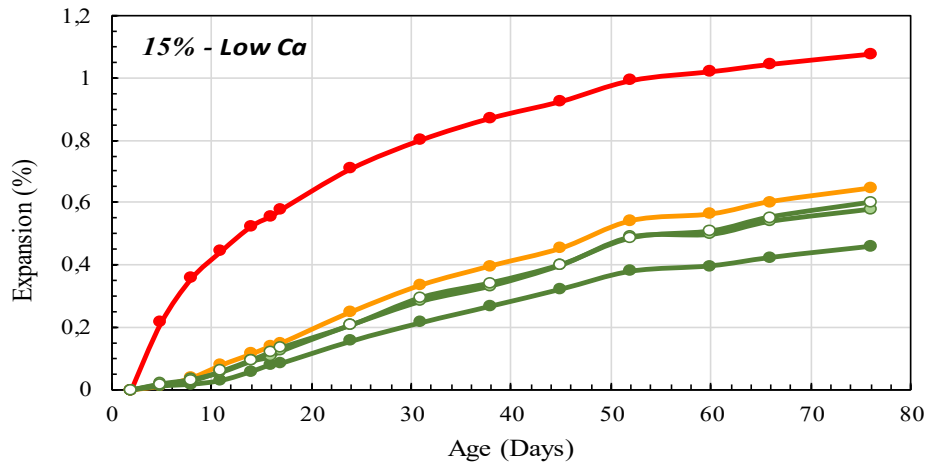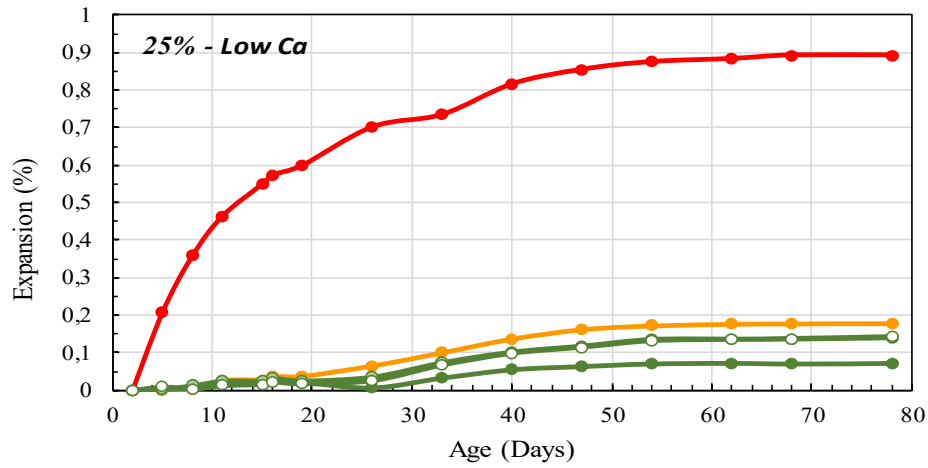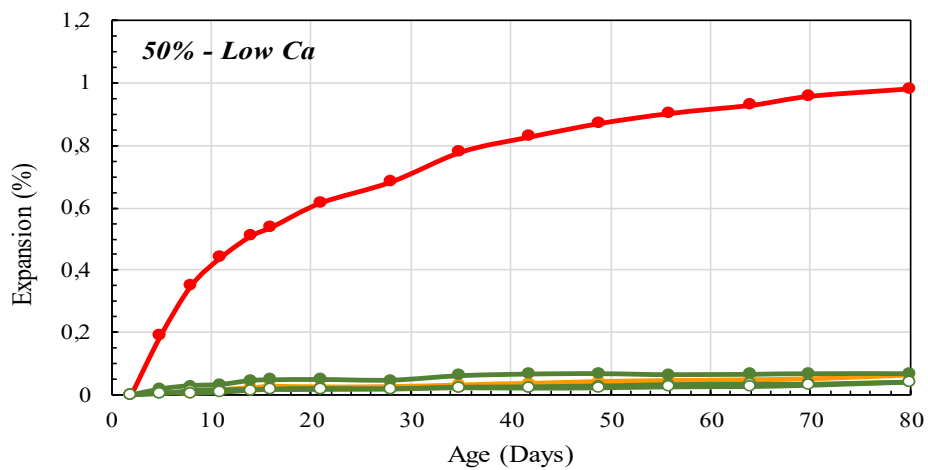
*Figure 40. ASTM C1260 expansion test results for (a) 15%, (b) 25% and (c) 50% low-Ca CFA mortar mixes*
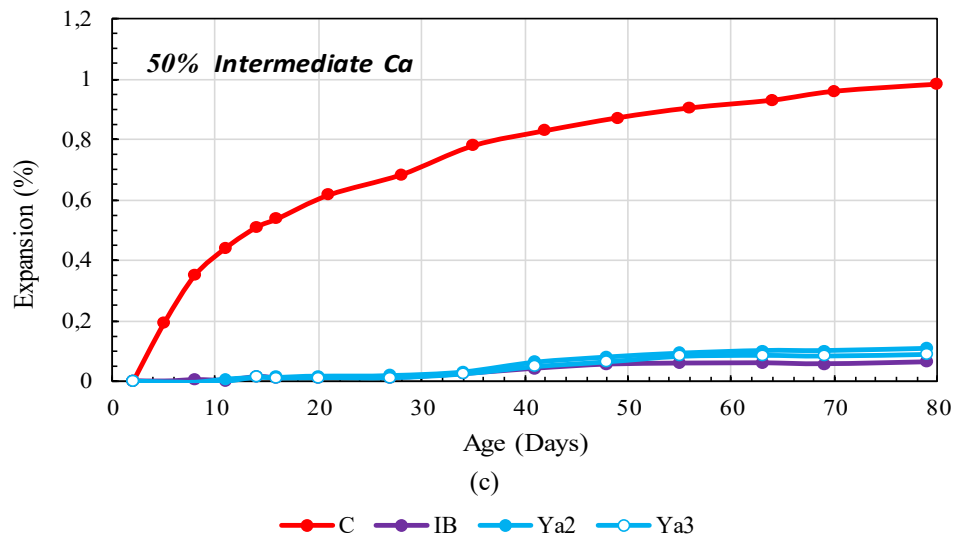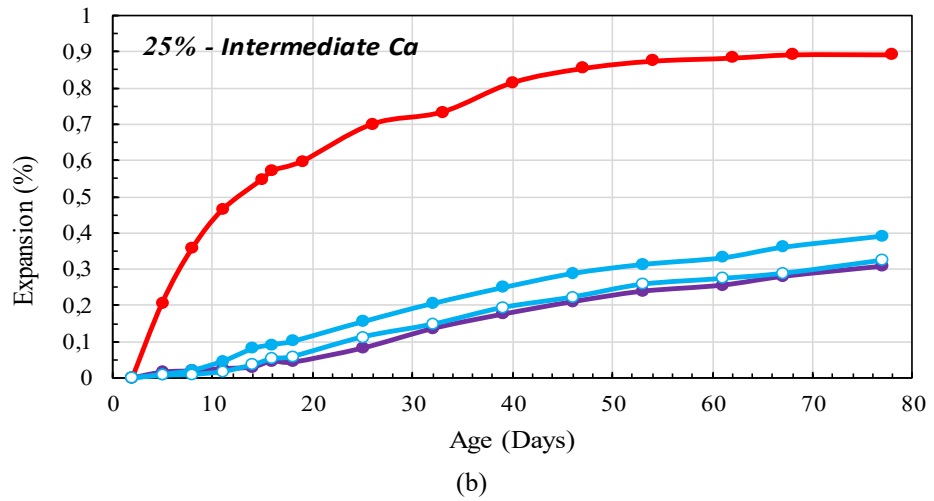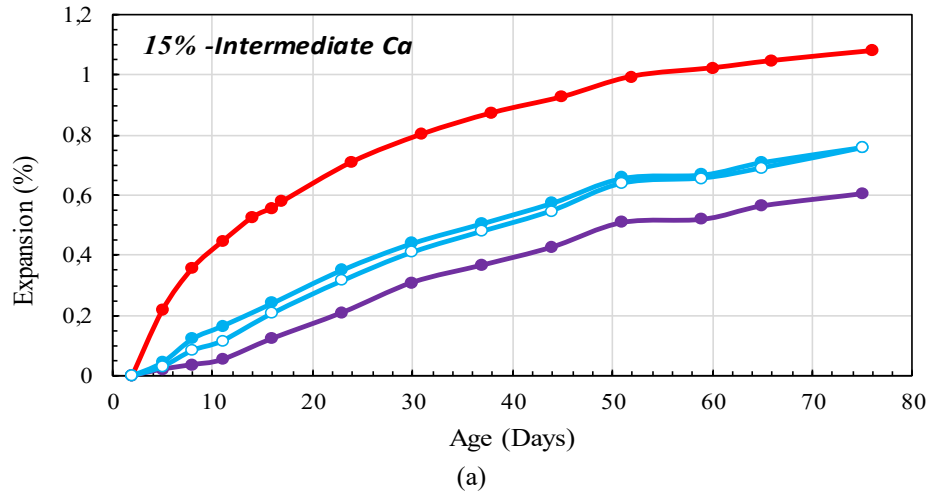
*Figure 41. ASTM C1260 expansion test results for (a) 15%, (b) 25% and (c) 50% intermediate-Ca CFA mortar mixes*
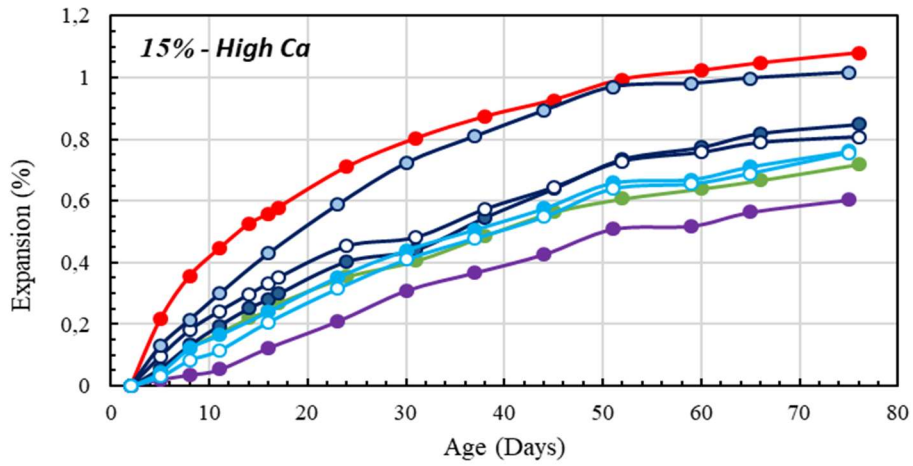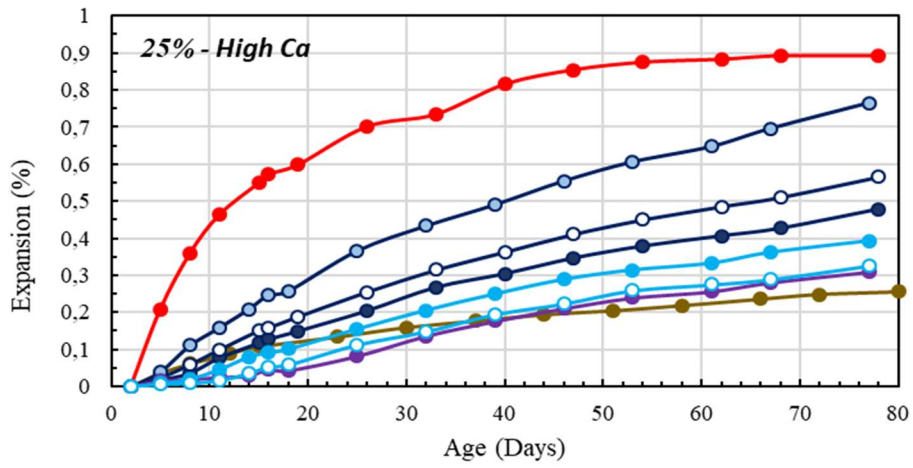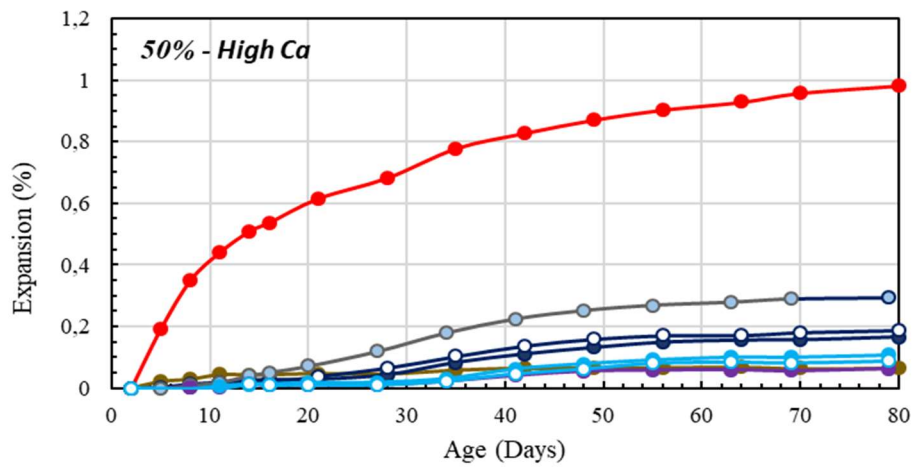
*Figure 42. ASTM C1260 expansion test results for (a) 15%, (b) 25% and (c) 50% high-Ca CFA mortar mixes*
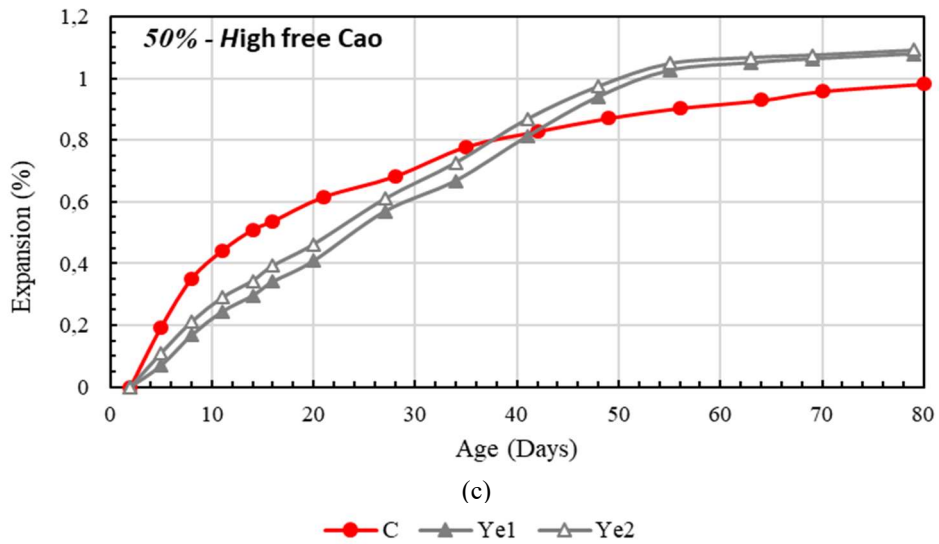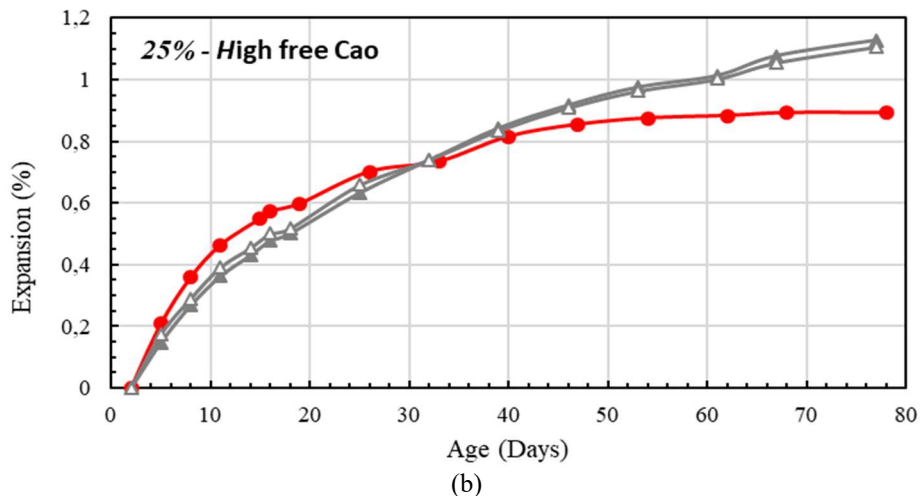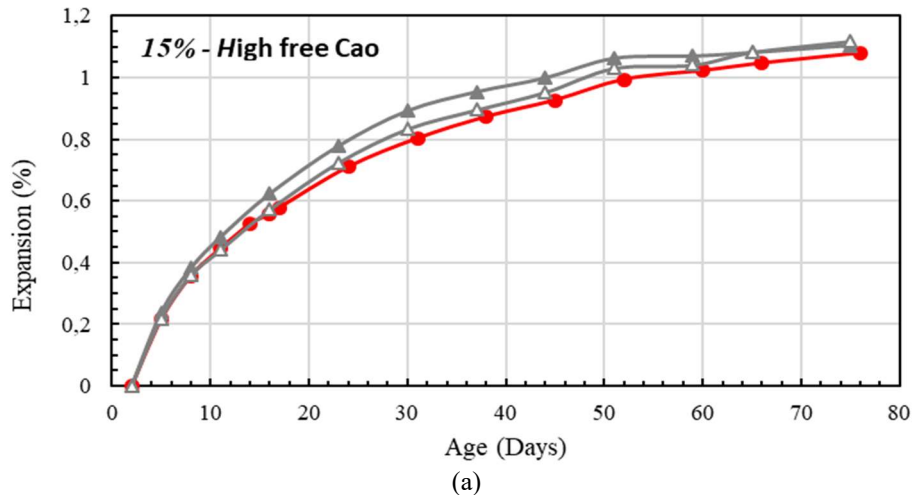
*Figure 43. ASTM C1260 expansion test results for (a) 15%, (b) 25% and (c) 50% high free Cao CFA mortar mixes.*

## 4.3.5. Relationships Between Replacement Level of Coal Fly Ashes and Accelerated Mortar Bar Expansions

The relationship of ASR performance of high-, low- and intermediate-Ca fly ash samples with respect to their replacement levels are discussed below. Ye1 and Ye2 fly ashes are considered in a separated group due to their high free CaO contents resulting in CH formation leading to considerable expansions, even more than that of the control specimens.

For each group the expansion data is fitted to an exponential function in the form of:

$$\text{Equation 3. } y = \alpha e^{-\beta x}$$

where $\alpha$ and $\beta$ are constants depending on the cement, aggregate, fly ash type and replacement levels. This exponential function form is selected after several trials to best fit to the experiment result data.

As can be seen from Figure 44, the 14 days expansion of the mortar bars decrease with the increased replacement of low-Ca coal fly ash samples. It can be said that, 25% replacement level is suitable for these fly ash samples, meeting the below 0.10 % expansion requirement of the ASTM C1260 standard. After that point, increasing the cement replacement level to 50% does not have significant effect on the expansions. Even 15% replacement level is satisfactory for T3, T4 and T5 specimens. In the 75 days graph, the effect of 50% replacement ratio becomes visible. In addition to exponential function for each fly ash, an overall exponential is also investigated in the graph. Please note that, %50 replacement data for T3-50% is omitted in the exponential trendline fits, as there might be possible experimental errors in that particular measurement. When the 75 days expansion graph is analyzed, the same conditions are seen. In addition to exponential function for each fly ash, an overall exponential trendline is also investigated in the graphs. The R-squared value of 14 days expansion is fairly well for the 14 days expansion, on the other hand the 75 days expansion's R-squared value of 0.8937 is much better by means of reliability.

66

$y = 0.5211e^{-0.085x}$
$R^2 = 0.6872$

$y = 0.5211e^{-0.075x}$
$R^2 = 0.7147$

$y = 0.5211e^{-0.133x}$
$R^2 = 0.9922$

$y = 0.5211e^{-0.081x}$
$R^2 = 0.7607$

$y = 0.5211e^{-0.086x}$
$R^2 = 0.6765$

(a)

$y = 0.9793e^{-0.062x}$
$R^2 = 0.8937$

$y = 0.9793e^{-0.056x}$
$R^2 = 0.9453$

$y = 0.9793e^{-0.062x}$
$R^2 = 0.7389$

$y = 0.9793e^{-0.065x}$
$R^2 = 0.9519$

$y = 0.9793e^{-0.065x}$
$R^2 = 0.9497$
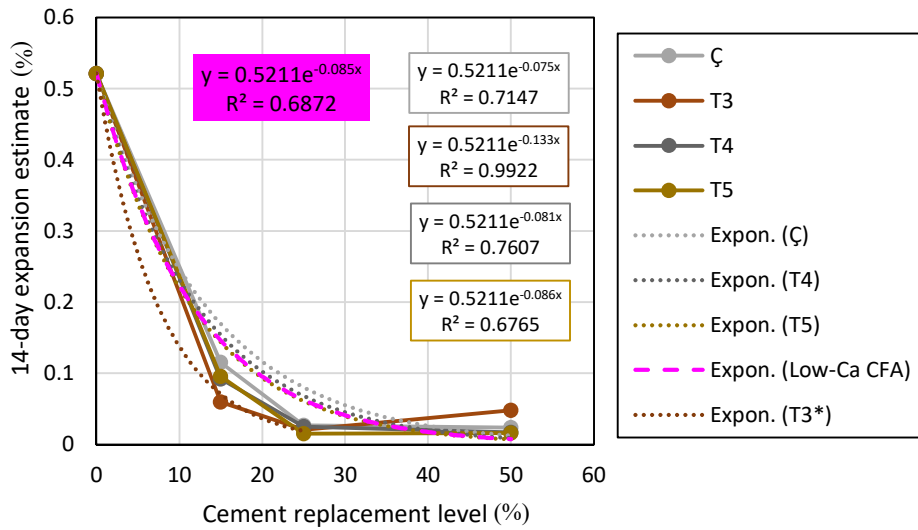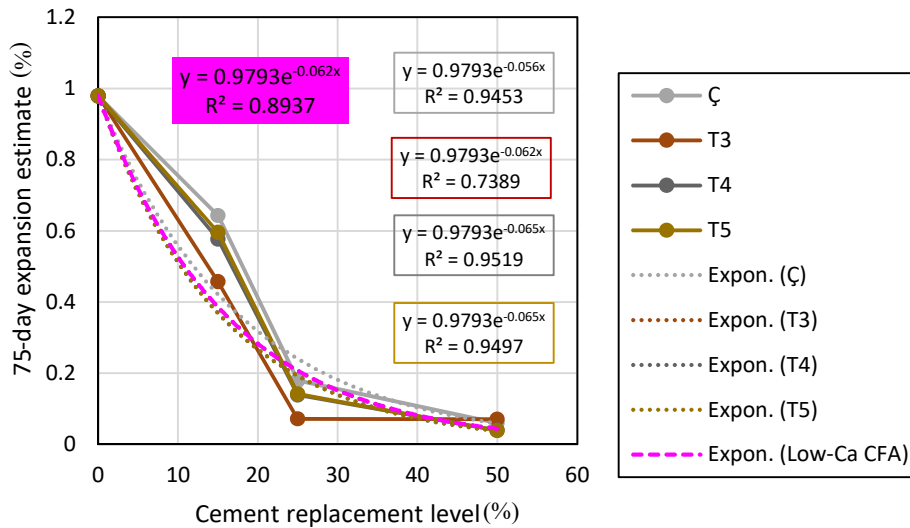
(b)

*Figure 44 Expansion-cement replacement level graphs for the low-Ca fly ashes for (a) 14 days, (b) 75 days*

When the next graphs are analyzed at Figure 45, it is seen that the 14 days expansion of the mortar bars decrease with the increased replacement of intermediate-Ca coal fly ash samples. Although expansion level is not as low as the low-Ca fly ash samples, it can again be said that, 25wt% replacement level is suitable for the intermediate Ca fly ashes, meeting the below 0.10 % expansion requirement of the ASTM C1260 standard. Contrary to the results of low-Ca fly ash samples, increasing the cement replacement level to 50wt% has some more positive effect on the expansions. In addition to

67

exponential function for each fly ash, an overall exponential trendline is also investigated in the graph. The R-squared value of 0,9229, which shows reliability of the trendline with the given data, is much better than the low-Ca fly ash trendline. In the case of 75 days expansion, the mitigation performance becomes much more visible between 25%wt and 50wt% replacement levels. Moreover, the R-squared value of 0,9352 is also more reliable.
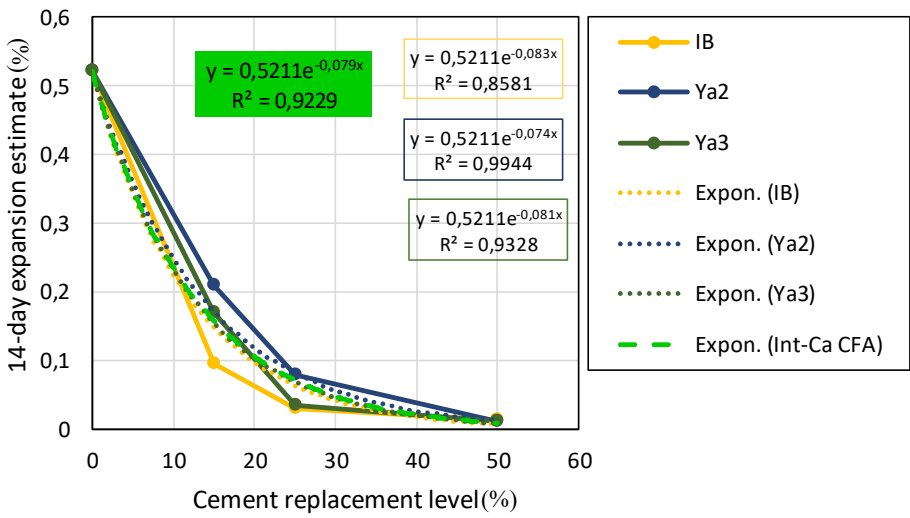


(a)
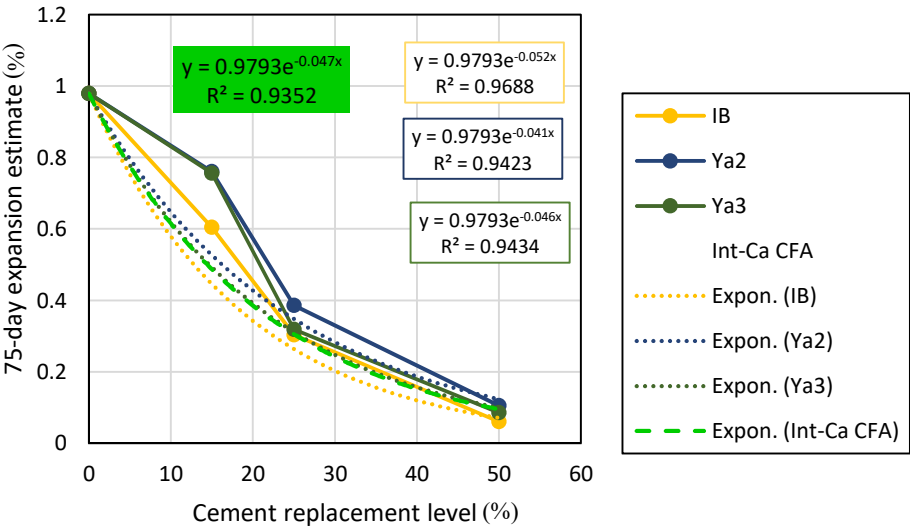


(b)

*Figure 45. Expansion-cement replacement level graphs for the intermediate Ca fly ashes for (a) 14 days, (b) 75 days*

As can be seen from the next graphs at Figure 46, the 14-day expansion of the mortar bars decrease with the increased replacement of high-Ca fly ash samples. The expansion reduction level is not as low as the low and intermediate Ca fly ash specimens.



(a)
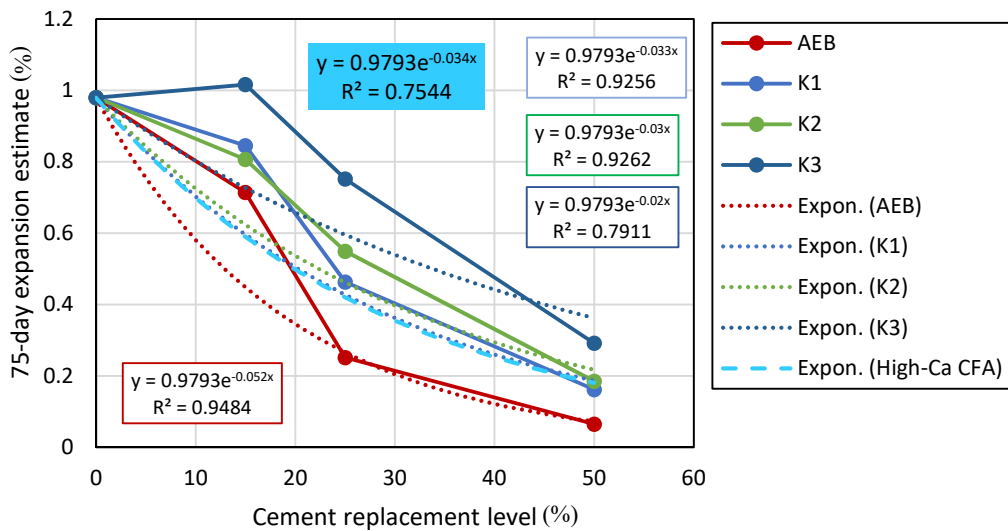


(b)

*Figure 46. Expansion-cement replacement level graphs for the high Ca fly ashes for (a) 14 days, (b) 75 days*

It can be interpreted that, 50% replacement level is necessary for the high Ca fly ashes, meeting the below 0.10 % expansion requirement of the ASTM C1260 standard. In addition to exponential function for each fly ash, an overall exponential trendline is also investigated in the graph. The R-squared value of 0.937 is better than the low and intermediate-Ca fly ash trendlines in 14 days graphs. At the 75 days graph, this value drops to 0.7544 which is a fair value.

As can be seen from the next graphs of Figure 47, the 14 days expansion of the mortar bars decrease (except 15% replacement level) with the increased replacement of high free CaO coal fly ash samples. The expansion level is not as low as any other fly ash samples. It can be said that, even 50% replacement level is not enough for the high free Cao fly ashes to meet the below 0.10 % expansion requirement of the ASTM C1260 standard. In addition to exponential function for each fly ash, an overall exponential trendline is also investigated in the graph. The R-squared value of 0.7656, which shows reliability of the trendline with the given data, is not as good as the other fly ash trendlines. At the 75 days graph, the situation even gets worse because of increased ASR expansions with increased fly ash replacement levels. The reason for this failure of the high free CaO fly ash samples, is the fact that the free CaO content results in CH formation, as discussed before. It is apparent that exponential fit is not a suitable option for this fly ash type especially for the 75 days case with the negative R-squared value.
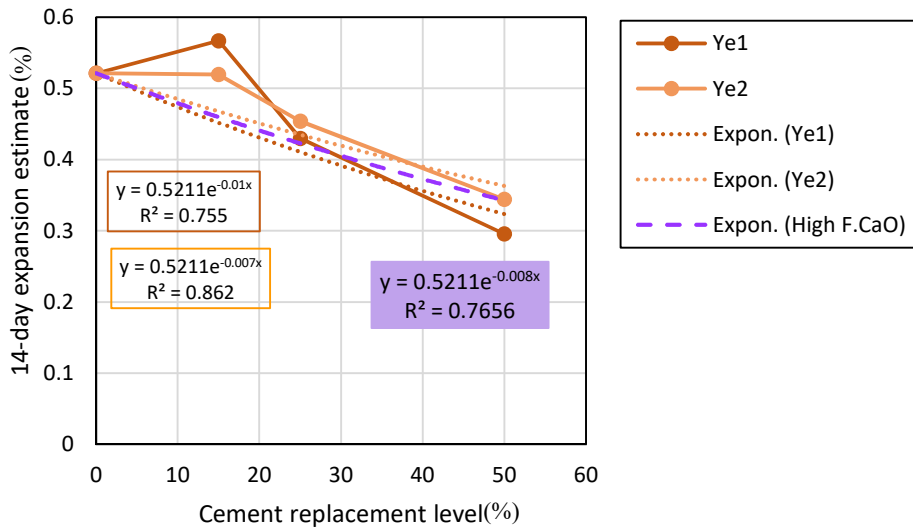
(a)
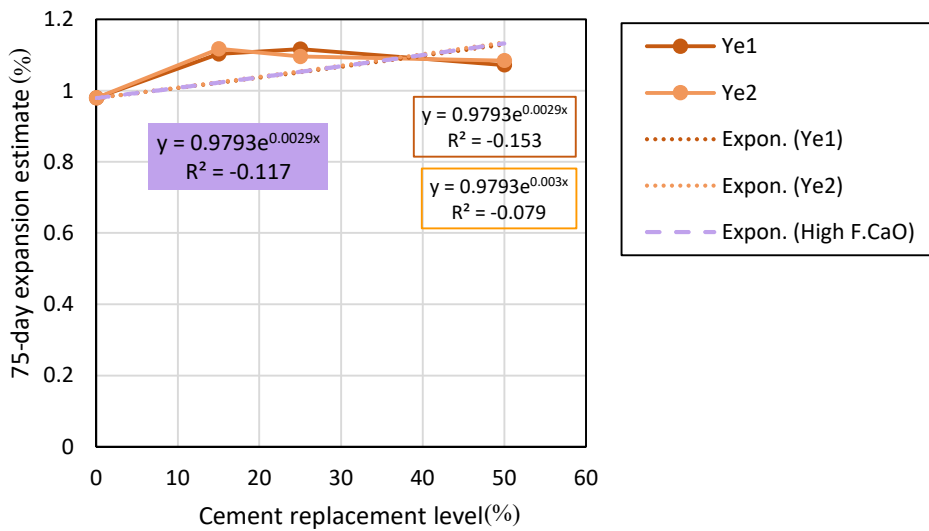


(b)

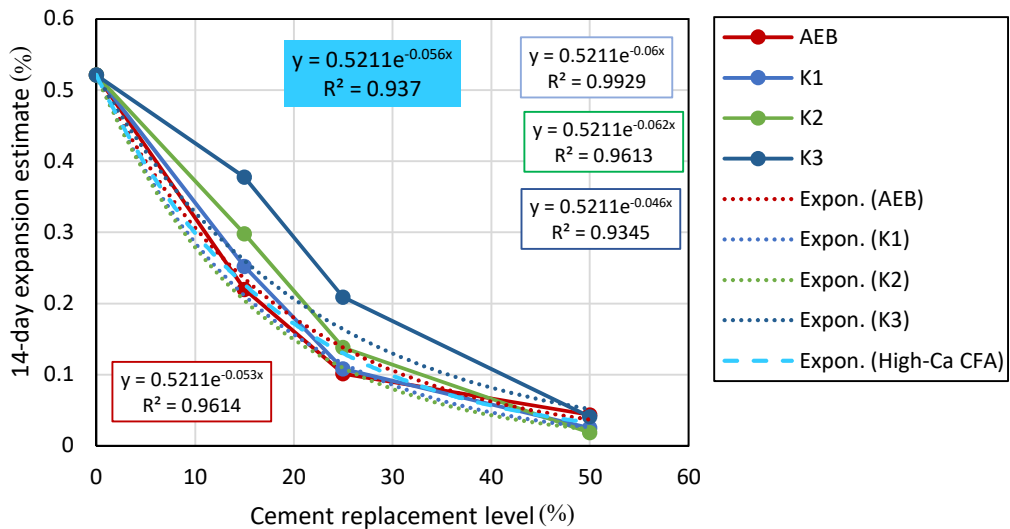*Figure 47. Expansion-cement replacement level graphs for the high free CaO fly ashes for (a) 14 days, (b) 75 days*

The α, β and R2 values for the exponential fits for 14-days values are summarized at Table 8. The most suitable specimens for the exponential fitting seem to be AEB, K1, K2, K3, T3 Ya2 and Ya3 with R squared values greater than 0.9, meaning that these

fits are reliable and can be used for estimation purpose. The other samples also have reasonable results all of which are more than 0.67.

*Table 8. Constants for the exponential fit for 14-day expansion and replacement level (a) all CFAs and (b) CFAs grouped according to their Ca contents*

(a)

|  | AEB | Ç | IB | K1 | K2 | K3 | T3 | T4 | T5 | Ya2 | Ya3 | Ye1 | Ye2 |
|---|---|---|---|---|---|---|---|---|---|---|---|---|---|
| α | 0.521 | 0.521 | 0.521 | 0.521 | 0.521 | 0.521 | 0.521 | 0.521 | 0.521 | 0.521 | 0.521 | 0.521 | 0.521 |
| β | 0.053 | 0.075 | 0.083 | 0.060 | 0.062 | 0.046 | 0.133 | 0.081 | 0.086 | 0.074 | 0.081 | 0.010 | 0.007 |
| $R^2$ | 0.961 | 0.715 | 0.858 | 0.993 | 0.961 | 0.934 | 0.992 | 0.761 | 0.676 | 0.994 | 0.933 | 0.755 | 0.862 |

(b)

|  | Low-Ca | Int-Ca | High-Ca | High F.CaO |
|---|---|---|---|---|
| α | 0.521 | 0.521 | 0.521 | 0.521 |
| β | 0.085 | 0.079 | 0.056 | 0.008 |
| $R^2$ | 0.687 | 0.923 | 0.937 | 0.766 |

The α, β and R2 values for the exponential fits for 75 days values are summarized at Table 9. The most suitable specimens for the exponential fitting seems to be AEB, Ç, IB, K1,K2, T4, T5, Ya2 and Ya3 with R squared values greater than 0.9, meaning that these fits are also dependable. The samples of K3 and T3also have reasonable results all of which are more than 0.73. It is apparent that Ye1 and Ye2 coal fly ashes do not fit exponentially for the data with negative R squared values. This is probably caused by their negative effect on the ASR expansions of the mortar bars, which is incompatible with the other specimens' behavior and the logic of the exponential fitting. It should be also noted that, the reliance factor of low-ca fly ashes increases drastically when the test duration is increased from 14 days to 75 days. The reason for this rise is probably the fact that the low-ca fly ashes show their effect to a large extent at 75 days, which almost completes the exponential behavior of the replacement levels.

*Table 9. Constants for the exponential fit for 75-day expansion values (a) all CFAs and (b) CFAs grouped according to their Ca contents*

(a)

|  | AEB | Ç | IB | K1 | K2 | K3 | T3 | T4 | T5 | Ya2 | Ya3 | Ye1 | Ye2 |
|---|---|---|---|---|---|---|---|---|---|---|---|---|---|
| α | 0.979 | 0.979 | 0.979 | 0.979 | 0.979 | 0.979 | 0.979 | 0.979 | 0.979 | 0.979 | 0.979 | 0.979 | 0.979 |
| β | 0.052 | 0.056 | 0.052 | 0.033 | 0.030 | 0.020 | 0.062 | 0.065 | 0.065 | 0.041 | 0.046 | 0.003 | 0.003 |
| $R^2$ | 0.948 | 0.945 | 0.969 | 0.926 | 0.926 | 0.791 | 0.739 | 0.952 | 0.950 | 0.942 | 0.943 | -0.153 | -0.079 |

(b)

|  | Low-Ca | Int-Ca | High-Ca | High F.CaO |
|---|---|---|---|---|
| α | 0.9793 | 0.9793 | 0.9793 | 0.9793 |
| β | 0.062 | 0.047 | 0.034 | 0.0029 |
| $R^2$ | 0.8937 | 0.9352 | 0.7544 | -0.117 |

Generally, increasing the replacement level of cement with coal fly ashes have decreased the ASR expansions as expected expect for the high free CaO specimens. Moreover, Low-Ca and Int-Ca fly ashes have given the best fitting $R^2$ results since their effect on mitigation of ASR expansions is more compatible with exponential fitting. The only problem is the $R^2$ value of Low-Ca fly ashes which is caused by the fact that even at 15%wt replacement level, the mitigation performance is quite high which makes it difficult to have an exponential fit precisely.

These exponential fits with the α and β values makes it possible to estimate the replacement level requirements for the coal fly ashes used in the experiments. It should be noted that, these formulas are valid only the aggregate type used in this study.

## 4.4. Effect of Oxides on Preventing Alkali Silica Reaction Expansions

In this section of the study, all the constituents of the coal fly ashes are investigated in detail with respect to their effects on the mitigation of the ASR expansions one by one. Each trial is analyzed at a separate graph in order to ensure the intimate observation of the behavior well. Normalized expansion is the ratio of the ASR expansion of the specimen at the specified replacement level, to the ASR expansion of the control specimen. In the next chapter, the combinations of the chemicals and other approaches

are also tried by drawing inspiration from other papers stated in the literature review section.

Since Ye1 and Ye2 fly ash samples do not behave positively on ASR expansions because of their very high free CaO content, they are included in the graphs for every replacement level but excluded from the exponential functions. The free CaO gets into reaction with water and results in CH formation, which leads to huge expansions. These fly ash samples result in even higher expansions than the control experiments which are conducted in the absence of fly ash replacement

### 4.4.1. Oxide Contents of Fly Ash Specimens Inhibiting ASR Expansion

### 4.4.1.1. Silicon Dioxide

As can be seen from Figure 48, when the $SiO_2$ content of the coal fly ash specimens increase, the ASR expansions decrease. This situation holds with the experiments conducted in the literature [40]. The reliance factor $R^2$, which is the reliability factor of the trendline, is nearly 0.8 for 14 days, which is a good value for the suitability of the trendlines for 25% and 15% experiments. The problem with the 50% fly ash replacement level relationships is the fact that most specimens mitigate ASR with a good performance at 50% replacement ratio, the results are close especially for the 14 days experiment, so it is difficult to discriminate samples from each other. At 75 days, the $R^2$ values are between 0.62-0.75, where the best result is determined at 50% replacement level, since the effect becomes visible for this replacement level. Constants for the exponential fits of 14 and 75-day normalized expansion values are summarized at Table 10.

*Table 10. Constants for the exponential fits of 14 and 75-day normalized expansion values - SiO₂ contents for 15%, 25% ve 50% replacement levels*

|  | 14 Days | | | 75 Days | | |
|---|---|---|---|---|---|---|
|  | **15%wt** | **25%wt** | **50%wt** | **15%wt** | **25%wt** | **50%wt** |
| α | 3.7715 | 6.1202 | 0.0972 | 1.5574 | 5.7061 | 1.5354 |
| β | -0.055 | -0.089 | -0.018 | -0.019 | -0.064 | -0.061 |
| $R^2$ | 0.7251 | 0.8443 | 0.1014 | 0.624 | 0.6973 | 0.7478 |
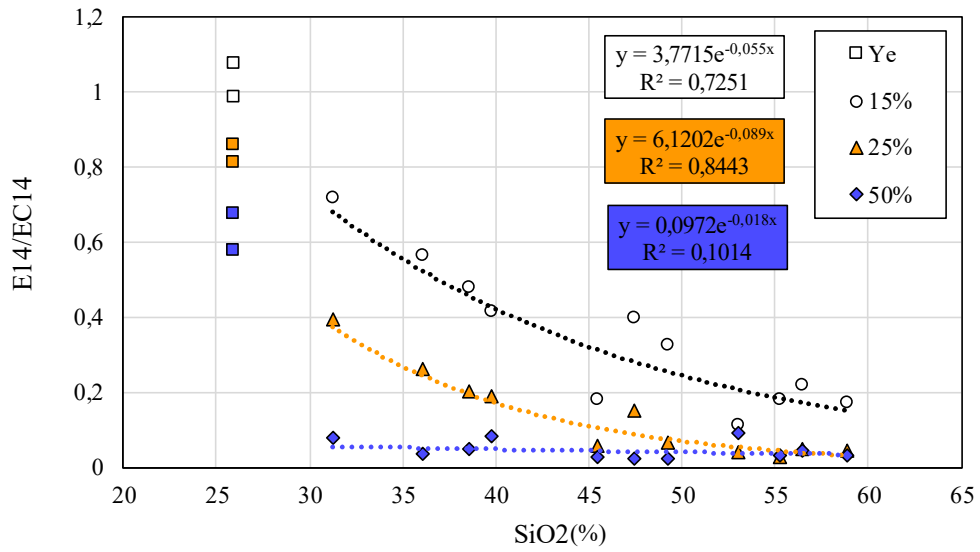
(a)
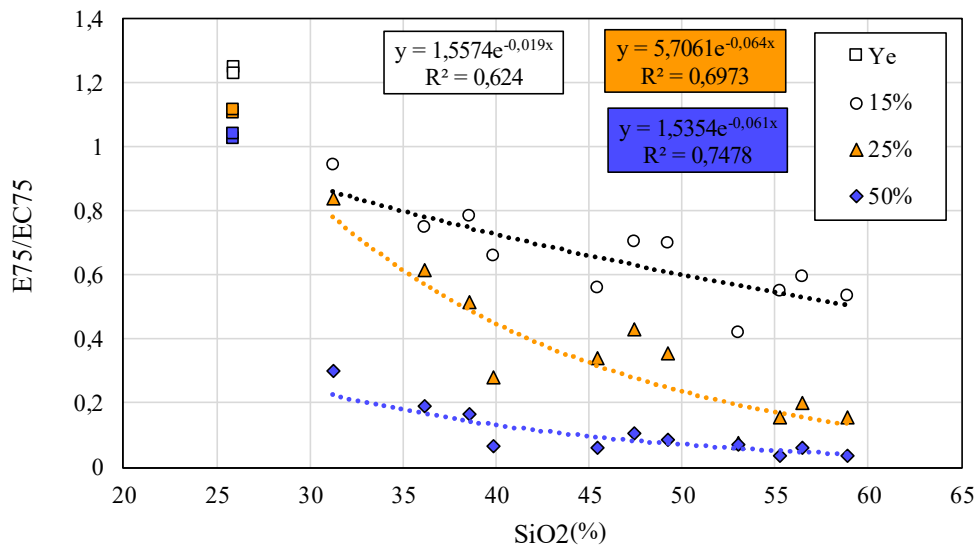


(b)

*Figure 48. (a-b) 14 and 75 days normalized expansion-SiO₂ content graphs for the 50%, 25% and 15% replacement levels respectively*

When the next graphs at Figure 49 are analyzed, it is seen again that as the reactive $SiO_2$ content of the fly ash specimens increase, the ASR expansions decrease just as in the previous graphs for $SiO_2$. This situation is sensible since the R.SiO2 content is proportional to $SiO_2$ content to a large extent in all three ratios. The proportionality can directly be seen when the $SiO_2$ and R.SiO₂ graphs are examined side by side. The problem with 50% replacement level graphs are similar with the case of $SiO_2$ graphs

for 15% replacement level at 14 days duration. Constants for the exponential fits of 14 and 75-day normalized expansion values are summarized at Table 11.

*Table 11. Constants for the exponential fits of 14 and 75-day normalized expansion values – R.SiO₂ contents for 15%, 25% ve 50% replacement levels*

|  | 14 Days | | | 75 Days | | |
|---|---|---|---|---|---|---|
|  | **15%wt** | **25%wt** | **50%wt** | **15%wt** | **25%wt** | **50%wt** |
| α | 6.0824 | 14.177 | 0.0946 | 1.7907 | 8.9905 | 3.2544 |
| β | -0.086 | -0.142 | -0.023 | -0.029 | -0.097 | -0.103 |
| $R^2$ | 0.6756 | 0.8059 | 0.0625 | 0.5525 | 0.6131 | 0.7886 |



(a)
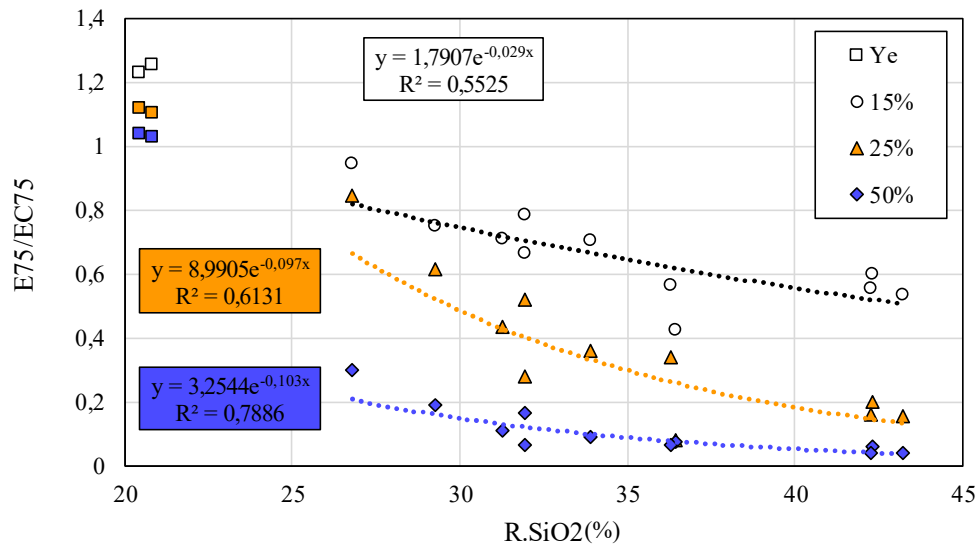


(b)

*Figure 49. (a-b) 14 and 75 days normalized expansion-R.SiO₂ content graphs for the 50%, 25% and 15% replacement levels respectively*

### 4.4.1.2. Aluminum Oxide

It can be seen from the graphs at Figure 50, as $Al_2O_3$ content of the coal fly ash specimens increase, the ASR expansions weakly decrease. This situation also holds with the experiments conducted in the literature [40]. Constants for the exponential fits of 14 and 75-day normalized expansion values are summarized at Table 12.

The reliance factor $R^2$, values which are the reliability factors of the trendline, are not very dependable for the suitability of the trendlines. The relationship of ASR expansions with Al2O3 content is not as strong as the $SiO_2$ content of the fly ash specimens, which also holds with the past experiments conducted [40]. In addition, the closeness of the results of most samples at 50wt% replacement ratio is the other problem.
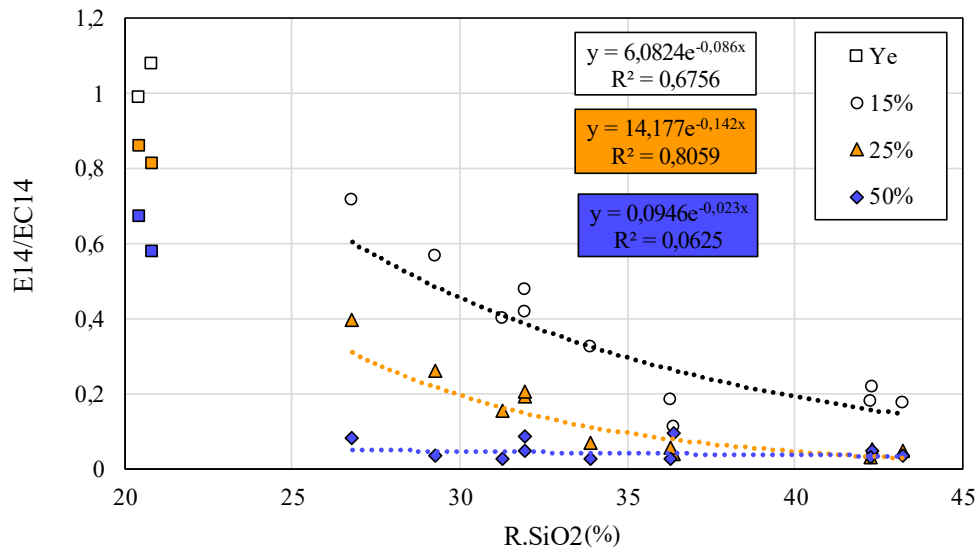
*Table 12. Constants for the exponential fits of 14 and 75-day normalized expansion values – Al$_2$O$_3$ contents for 15%, 25% ve 50% replacement levels*

|  | 14 Days | | | 75 Days | | |
|---|---|---|---|---|---|---|
|  | **15%wt** | **25%wt** | **50%wt** | **15%wt** | **25%wt** | **50%wt** |
| α | 1.9956 | 3.149 | 0.1173 | 1.2074 | 2.452 | 0.5594 |
| β | -0.1 | -0.184 | -0.053 | -0.033 | -0.111 | -0.097 |
| $R^2$ | 0.1757 | 0.2568 | 0.066 | 0.1364 | 0.1533 | 0.1344 |

$$y = 1,9956e^{-0,1x}$$
$$R^2 = 0,1757$$

$$y = 3,149e^{-0,184x}$$
$$R^2 = 0,2568$$

$$y = 0,1173e^{-0,053x}$$
$$R^2 = 0,066$$

(a)



$$y = 1,2074e^{-0,033x}$$
$$R^2 = 0,1364$$

$$y = 2,452e^{-0,111x}$$
$$R^2 = 0,1533$$

$$y = 0,5594e^{-0,097x}$$
$$R^2 = 0,1344$$

(b)

*Figure 50. (a-b) 14 and 75 days normalized expansion-$Al_2O_3$ content graphs for the 50%, 25% and 15% replacement levels respectively*

### 4.4.1.3. Iron Oxide

The following graphs at Figure 51 indicate that, as $Fe_2O_3$ content of the fly ash specimens increase, the ASR expansions decrease just in the case of other oxides discussed so far. This situation holds again with the experiments conducted in the literature [40].

*Table 13. Constants for the exponential fits of 14 and 75-day normalized expansion values – $Fe_2O_3$ contents for 15%, 25% and 50% replacement levels*

|  | 14 Days | | | 75 Days | | |
|---|---|---|---|---|---|---|
|  | **15%wt** | **25%wt** | **50%wt** | **15%wt** | **25%wt** | **50%wt** |
| α | 1.4744 | 0.7373 | 0.0345 | 1.1902 | 1.7426 | 0.2611 |
| β | -0.186 | -0.236 | 0.0251 | -0.071 | -0.205 | -0.125 |
| $R^2$ | 0.5404 | 0.3804 | 0.0133 | 0.5659 | 0.468 | 0.2003 |
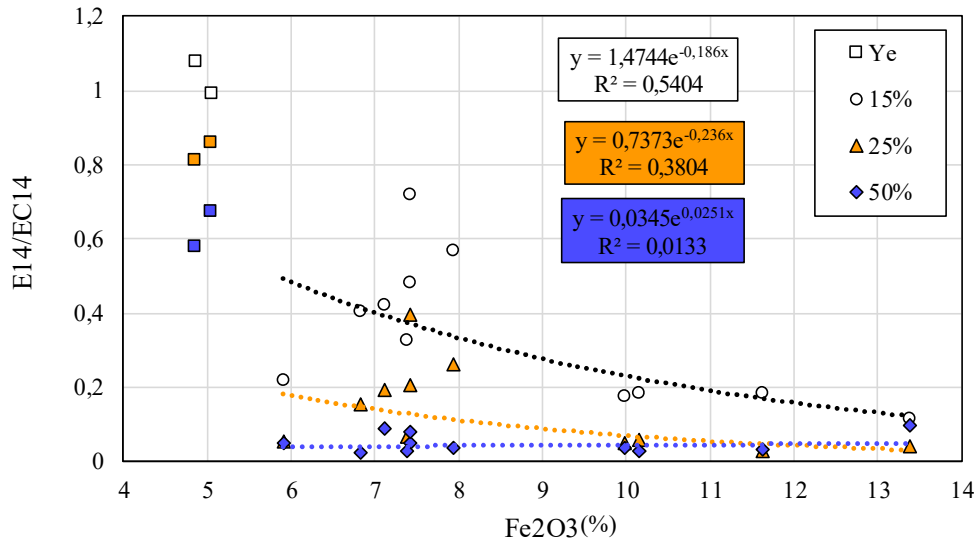


(a)
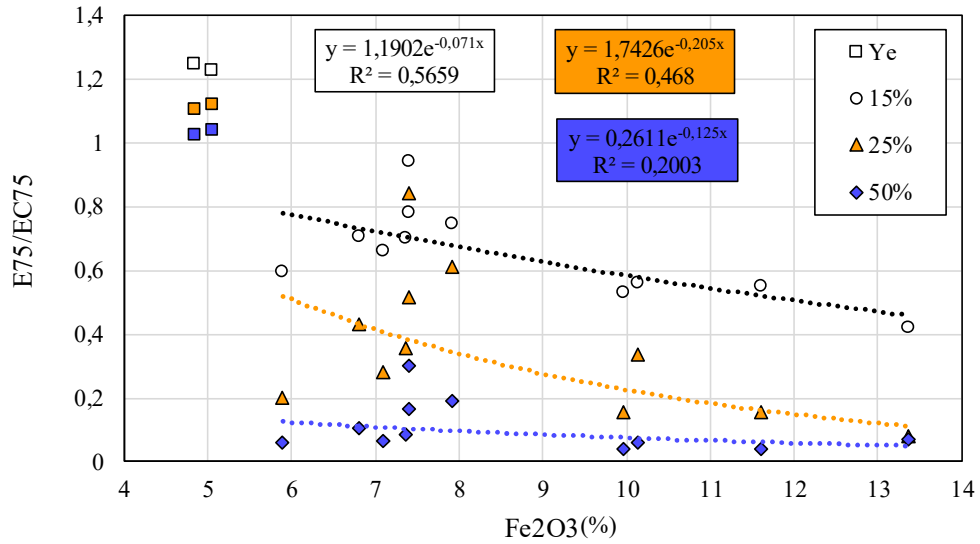


(b)

*Figure 51. (a-b) 14 and 75 days normalized expansion-$Fe_2O_3$ content graphs for the 50%, 25% and 15% replacement levels respectively*
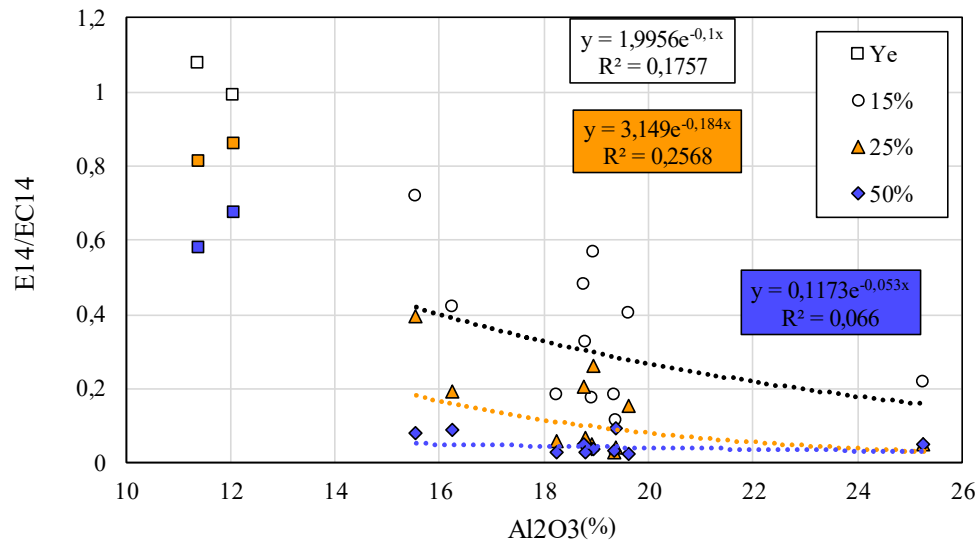
The reliance factor $R^2$, which is the reliability factor of the trendline, is between 0.01-0.54 at 14 days, which is not very dependable for the suitability of the trendlines. Especially, since the mitigation performance of most specimens at 50wt% replacement ratio at 14 days, this situation prevents the relationships at that level. The situation is similar for 75 days graphs, except for the better fitting of 50% replacement level. The fact that relationship of ASR expansions with $Fe_2O3$ content is not as strong as the $SiO_2$ content of the fly ash specimens, also holds with the past experiments conducted [40]. Constants for the exponential fits of 14 and 75-day normalized expansion values are summarized at Table 13.
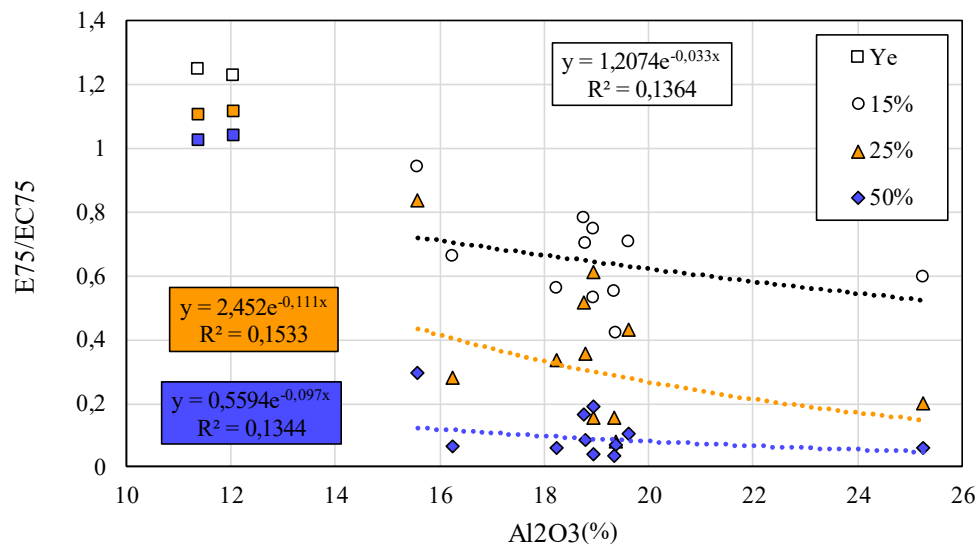
## 4.4.2. Oxide Contents of Fly Ash Specimens Promoting Alkali Silica Reaction Expansion

### 4.4.2.1. Calcium Oxide

It is seen from the following graphs of Figure 52 that the increase of CaO content of the fly ash, which also means the decrease of aluminum oxide and silicon dioxide, definitely results in the scaling up of ASR expansions. Except for the 50wt% replacement ratio of the coal fly ashes, all the graphs have exponential function estimates with reliance factor over 0.85 for 14 days, which means that they are fitting well. The only problem is at the 50wt%, as a result of the fact that all of the specimens have good mitigation of ASR expansions, it is not easy to have a best fit for the equation. At 75 days, the reliance factors are between 0.75-0.84, but 50% replacement level also has good fitting $R^2$ value of 0.75 since the effect becomes visible at this duration. Constants for the exponential fits of 14 and 75-day normalized expansion values are summarized at Table 14.

| | 14 Days | | | 75 Days | | |
|---|---|---|---|---|---|---|
| | **15%wt** | **25%wt** | **50%wt** | **15%wt** | **25%wt** | **50%wt** |
| α | 0.1465 | 0.0322 | 0.0384 | 0.4996 | 0.1299 | 0.043 |
| β | 0.0489 | 0.076 | 0.0078 | 0.0176 | 0.0576 | 0.0506 |
| $R^2$ | 0.8536 | 0.899 | 0.0293 | 0.7827 | 0.8414 | 0.7497 |
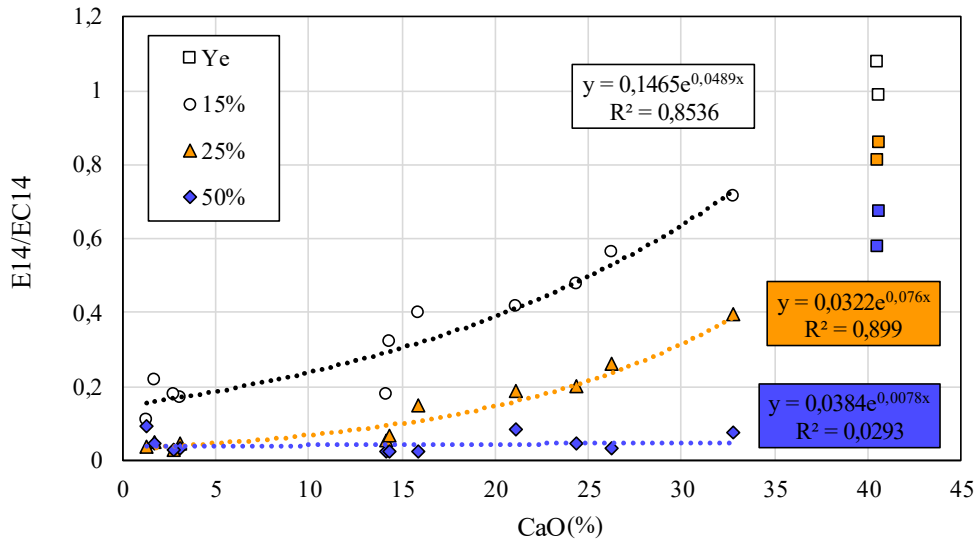


(a)
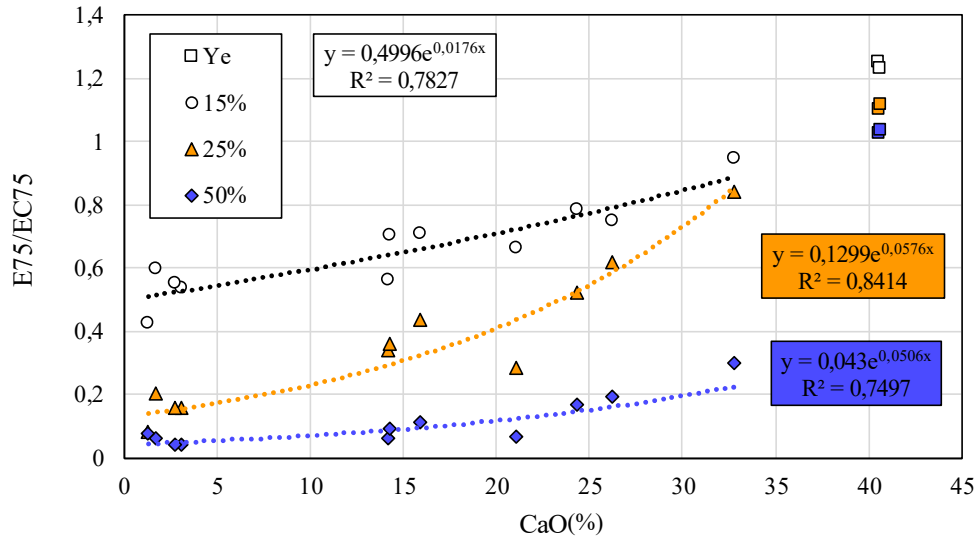


(b)

*Figure 52. (a-b) 14 and 75 days normalized expansion-CaO content graphs for the 50%, 25% and 15% replacement levels respectively*

Just as in the CaO content graphs, graphs at Figure 53 indicate that the increase of R.CaO content of the fly ash definitely results in the scaling up of ASR expansions. This situation is sensible since the R.CaO content is proportional to CaO content to a large extent in all three ratios. The proportionality can directly be seen when the CaO and R.CaO graphs are examined side by side. 50% replacement level graphs are preventing some relationships just in the case of CaO graphs.
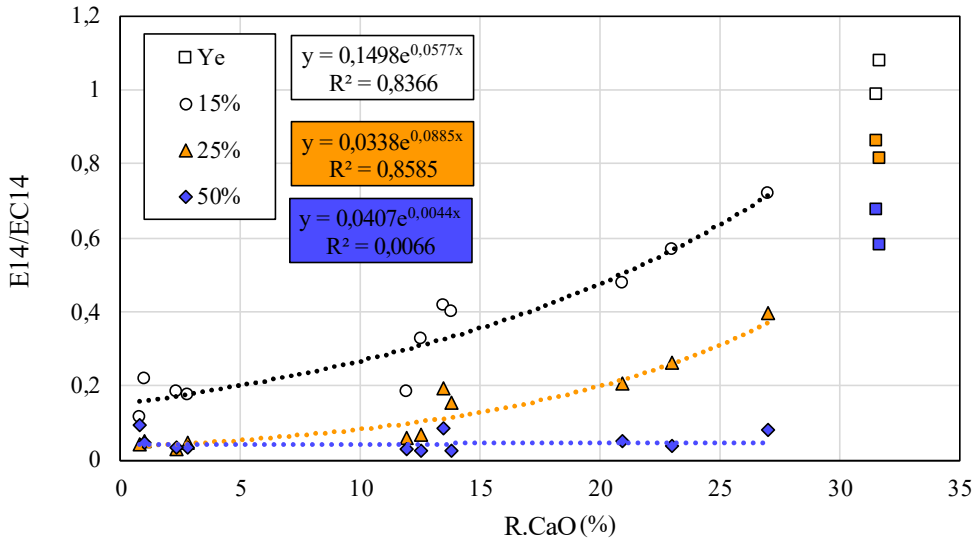


(a)
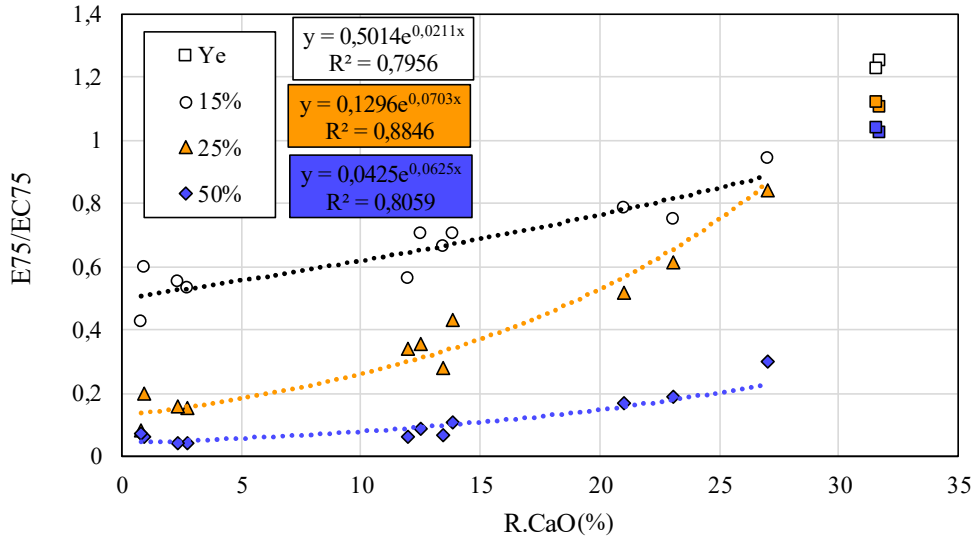


(b)

*Figure 53. (a-b) 14 and 75 days normalized expansion-R.CaO content graphs for the 50%, 25% and 15% replacement levels respectively*

Constants for the exponential fits of 14 and 75-day normalized expansion values are summarized at Table 15.

*Table 15. Constants for the exponential fits of 14 and 75-day normalized expansion values – R.CaO contents for 15%, 25% and 50% replacement levels*

|  | 14 Days | | | 75 Days | | |
|---|---|---|---|---|---|---|
|  | 15%wt | 25%wt | 50%wt | 15%wt | 25%wt | 50%wt |
| $\alpha$ | 0.1498 | 0.0338 | 0.0407 | 0.5014 | 0.1296 | 0.0425 |
| $\beta$ | 0.0577 | 0.0885 | 0.0044 | 0.0211 | 0.0703 | 0.0625 |
| $R^2$ | 0.8366 | 0.8585 | 0.0066 | 0.7956 | 0.8846 | 0.8059 |

## 4.4.2.2. Alkalis

The alkali content of the fly ash specimens didn't show a considerable relationship to ASR expansions as seen on the following graphs at Figure 54. This may be mainly caused by the extreme alkali environment of the test procedure, leading to the alkali content become insignificant. Very low reliance factors also prove this theory. Constants for the exponential fits of 14 and 75-day normalized expansion values are summarized at Table 16.

*Table 16. Constants for the exponential fits of 14 and 75-day normalized expansion values – $Na_2Oeq$ contents for 15%, 25% and 50% replacement levels*

|  | 14 Days | | | 75 Days | | |
|---|---|---|---|---|---|---|
|  | 15%wt | 25%wt | 50%wt | 15%wt | 25%wt | 50%wt |
| $\alpha$ | 0.1947 | 0.0835 | 0.0785 | 0.5173 | 0.1647 | 0.069 |
| $\beta$ | 0.2405 | 0.0803 | -0.347 | 0.125 | 0.3385 | 0.145 |
| $R^2$ | 0.0614 | 0.003 | 0.1733 | 0.1182 | 0.0868 | 0.0184 |
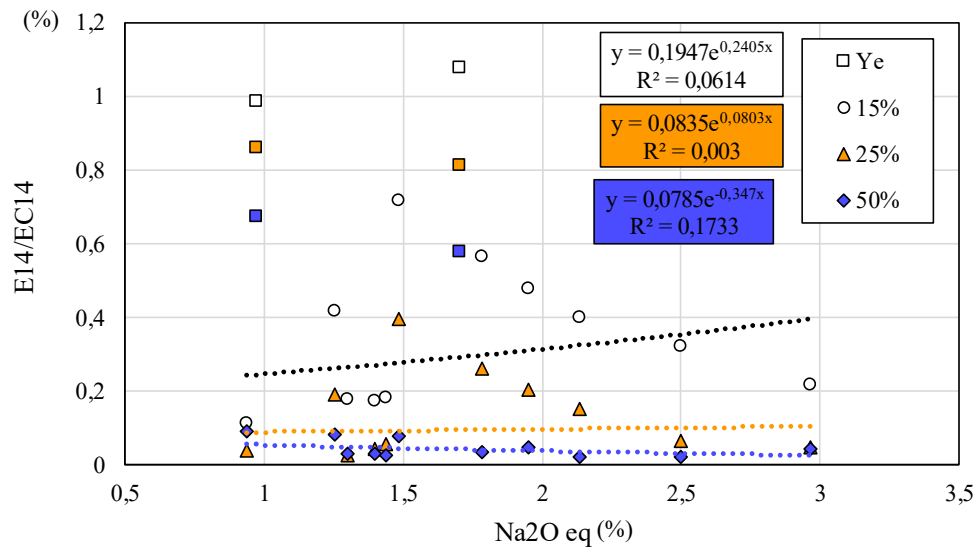
(a)
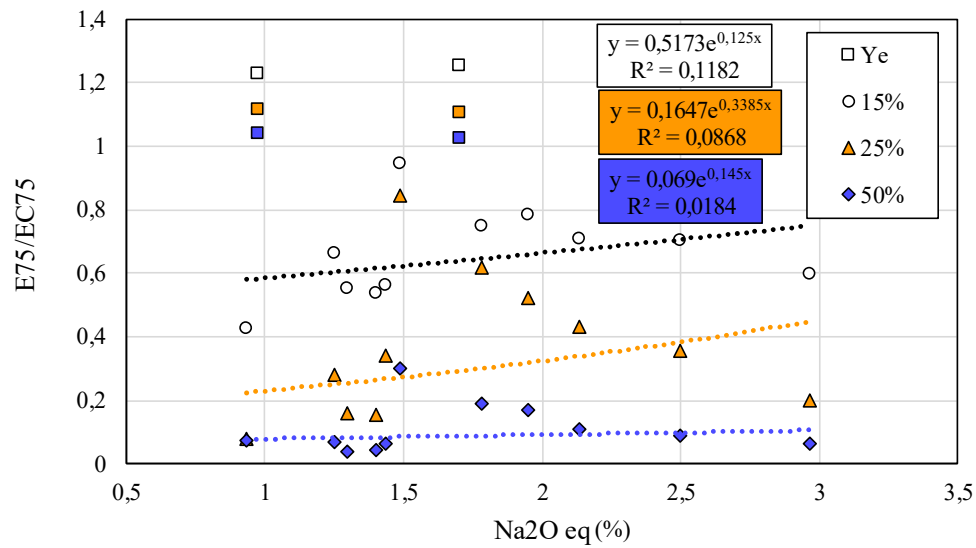


(b)

*Figure 54. (a-b) 14 and 75 days normalized expansion-Na₂O content graphs for the 50%, 25% and 15% replacement levels respectively*

### 4.4.2.3. Magnesium Oxide

There is a fair inverse proportion with the ASR expansions and magnesium oxide content as seen in the following graphs at Figure 55. This result was unexpected since in the literature it is stated that MgO has positive relationship with ASR expansions. The probable reason of this situation is that the other factors influencing ASR

expansions are more effective. Constants for the exponential fits of 14 and 75-day normalized expansion values are summarized at Table 17.

*Table 17. Constants for the exponential fits of 14 and 75-day normalized expansion values – MgO contents for 15%, 25% and 50% replacement levels*

|  | 14 Days | | | 75 Days | | |
|---|---|---|---|---|---|---|
|  | **15%wt** | **25%wt** | **50%wt** | **15%wt** | **25%wt** | **50%wt** |
| α | 0.9017 | 0.5553 | 0.0689 | 0.9487 | 0.8904 | 0.2957 |
| β | -0.349 | -0.549 | -0.148 | -0.122 | -0.344 | -0.376 |
| $R^2$ | 0.5754 | 0.6238 | 0.1412 | 0.4996 | 0.3987 | 0.5514 |
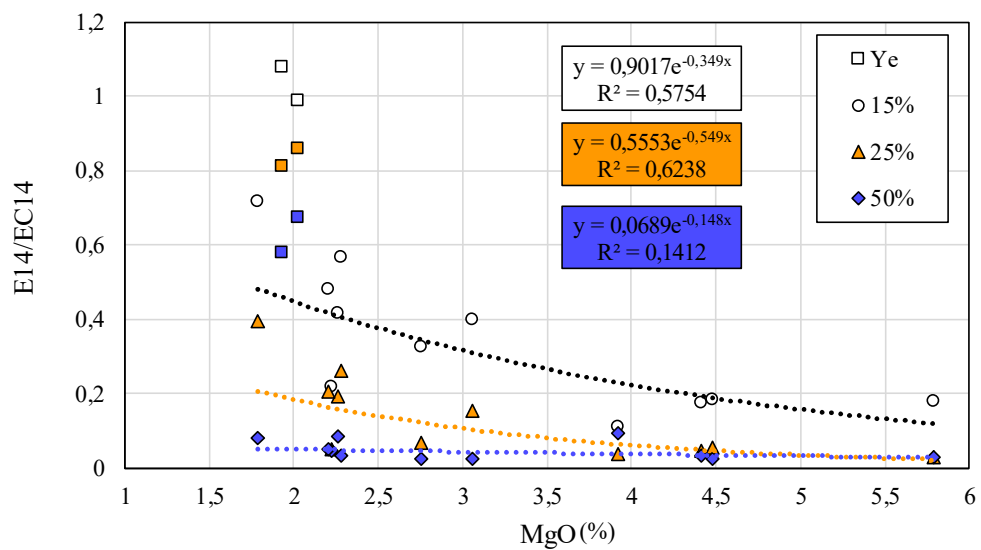


(a)
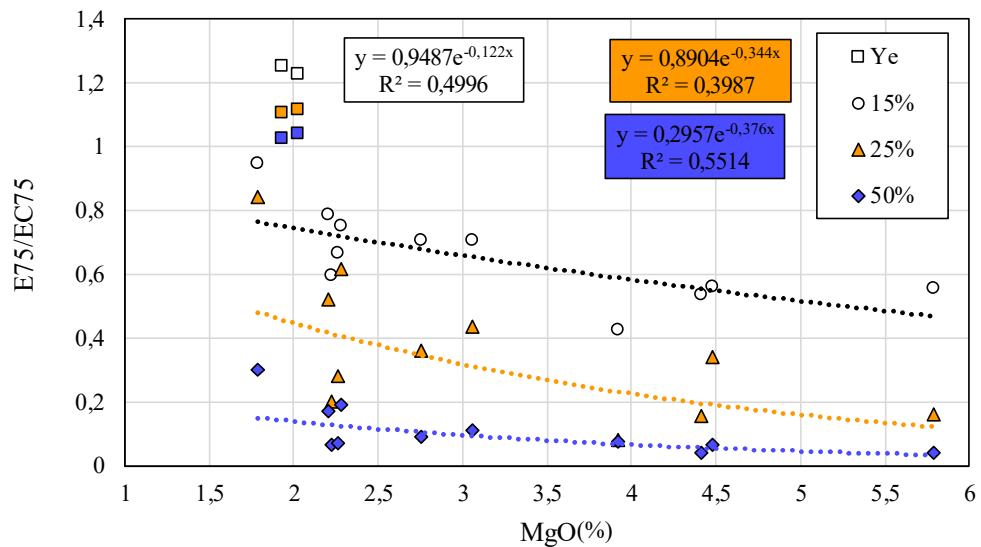


(b)

*Figure 55. (a-b) 14 and 75 days normalized expansion-MgO content graphs for the 50%, 25% and 15% replacement levels respectively*

85

The closeness of the expansion data in the 50wt% replacement ratio is again the problem for 14 days duration which vanishes at 75 days.

### 4.4.2.4. Sulfur Trioxide

There seems to be a reasonable correlation between sulfur trioxide content and the ASR expansion levels (Figure 56). The reliance factors up to 0.75 values also validate this relevance. 50wt% replacement ratio issue also confirms for $SO_3$ - ASR expansion relationships at 14 days duration, as almost all of the specimens have good performance at this replacement level. Although the $R_2$ value is better at 75 days duration, 25% and 15% fitting values are less reliable. Constants for the exponential fits of 14 and 75-day normalized expansion values are summarized at Table 18.

*Table 18. Constants for the exponential fits of 14 and 75-day normalized expansion values – SO₃ contents for 15%, 25% and 50% replacement levels*

|  | 14 Days | | | 75 Days | | |
|---|---|---|---|---|---|---|
|  | **15%wt** | **25%wt** | **50%wt** | **15%wt** | **25%wt** | **50%wt** |
| $\alpha$ | 0.1756 | 0.0406 | 0.0339 | 0.5386 | 0.1688 | 0.0548 |
| $\beta$ | 0.1866 | 0.3079 | 0.0837 | 0.0633 | 0.2018 | 0.1728 |
| $R^2$ | 0.6322 | 0.7519 | 0.1721 | 0.5181 | 0.5268 | 0.4457 |

(a)
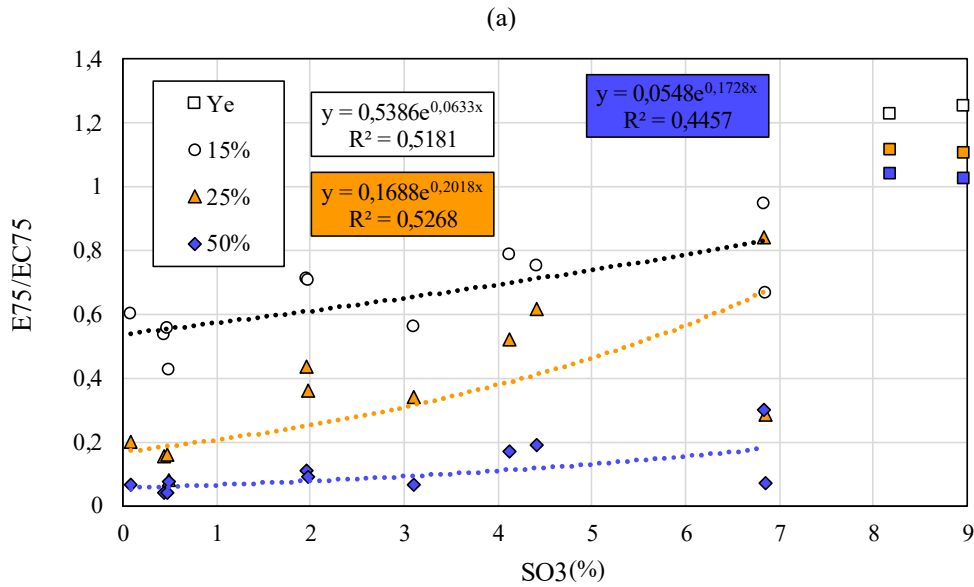


(b)
*Figure 56. (a-b) 14 and 75 days normalized expansion-SO$_3$ content graphs for the 50%, 25% and 15% replacement levels respectively*

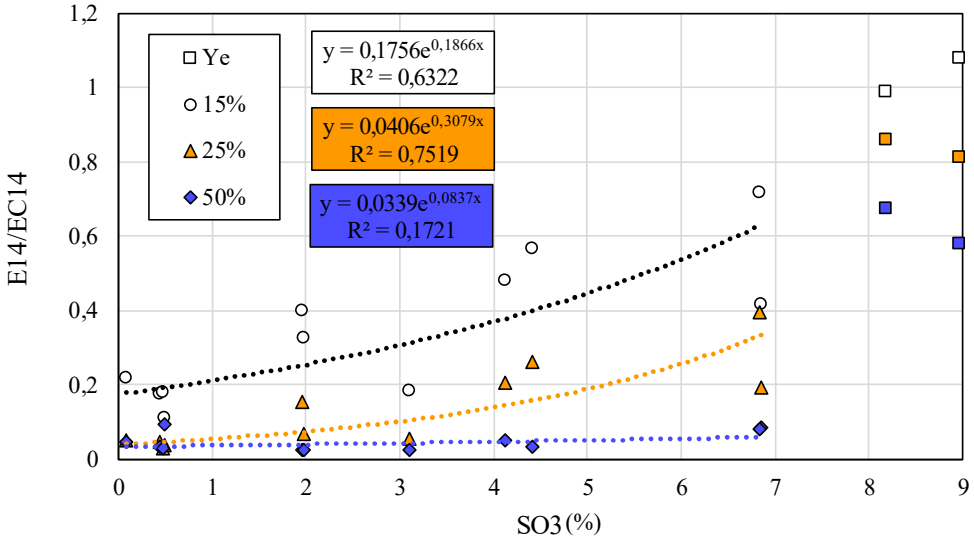These exponential fits with the α and β values makes it possible to estimate the ASR mitigation performance of the coal fly ashes used in the experiments according to their oxide contents. It should be noted that, these formulas are valid only the aggregate type used in this study.

## 4.5. Relationship Between ASR Expansion and Fly Ash Chemistry – Literature Comparisons

A better understanding of the relationship between ASR expansion and fly ash chemistry can be achieved by combining the chemical constituents of the fly ashes with different properties. Ye1 and Ye2 specimens give irrelevant results as a result of their high free CaO content, in every comparison table, thus they are shown in the graphs as seperate points but are not included in the trendlines and best fit formulations. In the literature review, it is seen that the comparable data is within 14 days because of the fact that ASTM C1260 test is originally designed for this duration. Thus, only the 14 days experiment results are used at these studies.

Individual oxide contents' relationship with ASR expansions were discussed in the previous chapter. In the two graphs below (Figure 57), the results of the study of Kizhakkumodom [40] and this study are compared side by side. The general behavior of the specimens with respect to their individual oxide contents inhibiting ASR seem to be similar. The irrelevant attitude of the $Fe_2O_3$ content also holds with this study.
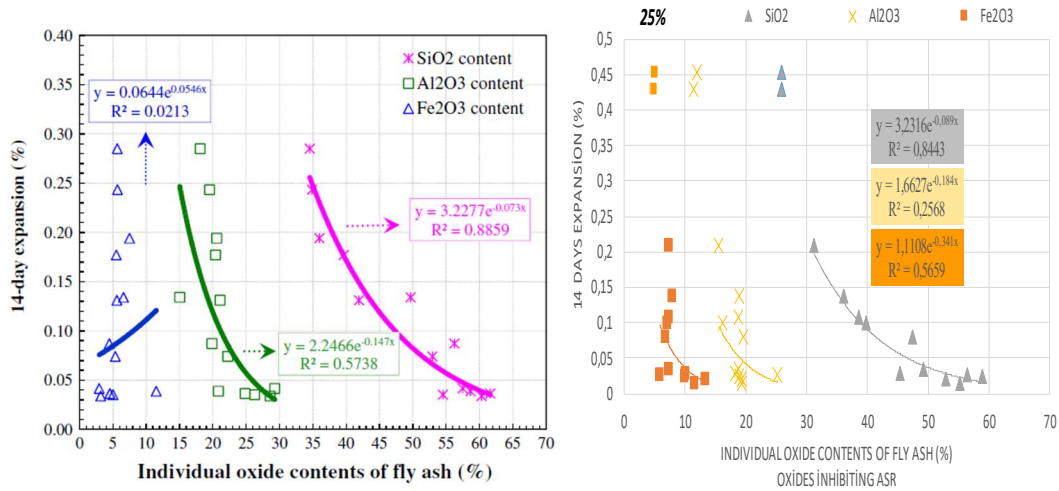


*Figure 57. 14 days expansion% at 25% replacement ratio- Individual oxide contents inhibiting ASR graphs a)*[40] *b) thesis study*

In the next two graphs below (Figure 58), the results of the study of Kizhakkumodom [40] and this study are compared side by side again. The general behavior of the specimens with respect to their individual oxide contents promoting ASR seem to be similar too. The only incompatible data is the MgO content relationship which is not very different in the specimens and also does not seem to have strong relationship in the [40].
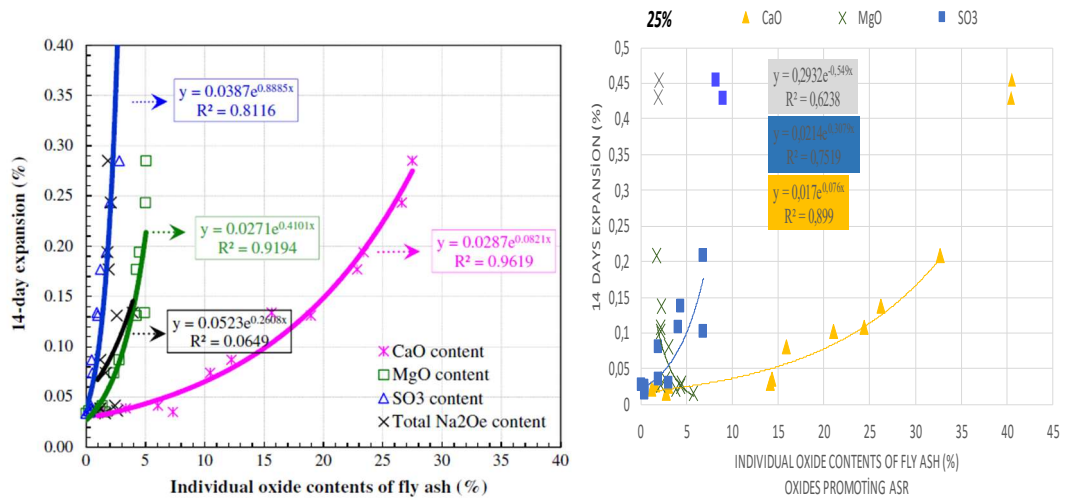
*Figure 58. 14 days expansion% at 25% replacement ratio - Individual oxide contents promoting ASR graphs a)[40] b) thesis study*

As expected, $SiO_2$ equivalent content of fly ashes have direct relationship with ASR expansion levels just as in the case of $SiO_2$ content graphs which were discussed in the previous section. Moreover, the behavior of the results of Kizhakkumodom [40] also holds with the thesis study (Figure 59).
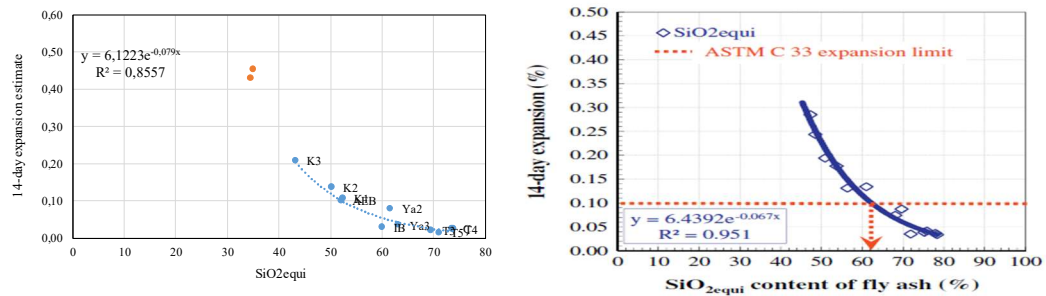


*Figure 59. 14 days expansion %- $SiO_2$ equivalent content graphs of 25% replacement ratio for this study and [40]*

CaO equivalent content of fly ashes have also direct relationship with ASR expansion levels as in the case of CaO content graphs which were discussed in the previous section. The graphs of Kizhakkumodom [40] and this study are similar again (Figure 60).

89
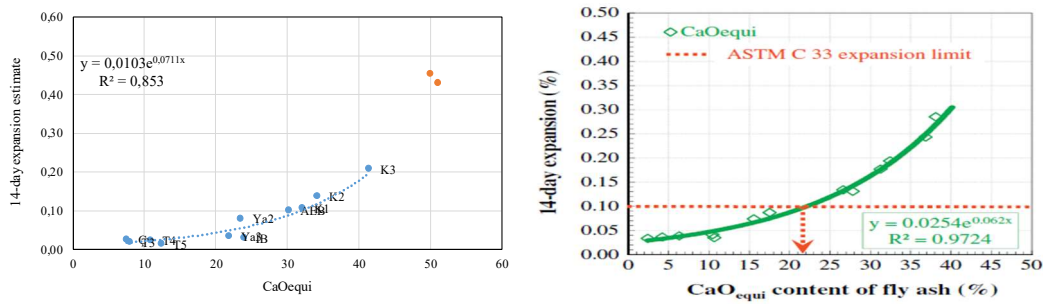
*Figure 60. 14 days expansion %-CaO equivalent content graphs of 25% replacement ratio for this study and* [40]

CaO equivalent content over $SiO_2$ equivalent content ratio of fly ashes have good correlation with ASR expansion levels (Figure 61) at both this study and [40]. In the study of Kizhakkumodom [40], it is offered to have a linear relationship but for the sake of consistency, exponential trendline is used in this study.
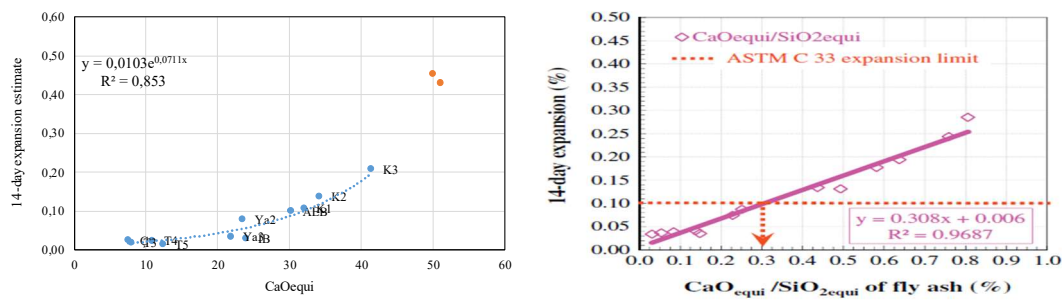


*Figure 61. 14 days expansion %- CaO equivalent/SiO$_2$ equivalent ratio graphs of 25% replacement ratio for this study and* [40]

The S+A+F content (summation of $SiO_2$, $Al_2O_3$ and $Fe_2O_3$ respectively) of the fly ashes give a good reliance with the ASR expansions (Figure 62) . The reliance factor is 0.882 which is a good value. This behavior is very similar at [40].
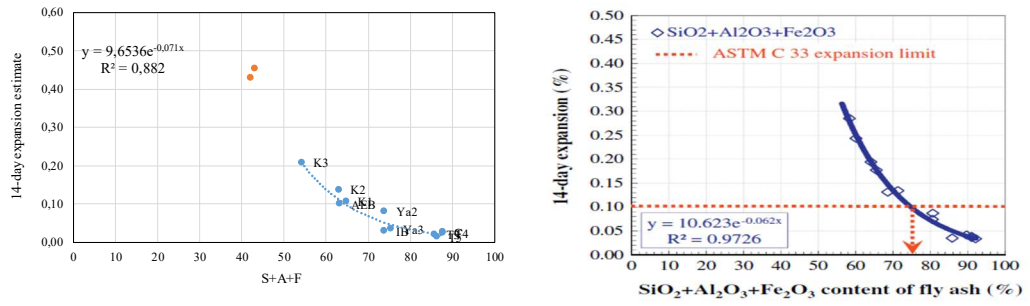
*Figure 62. 14 days expansion %- -S+A+F content graphs of 25% replacement ratio for this study and* [40]

The C+M+S (CaO, MgO and SO$_3$ respectively) content of the fly ashes also have good relationship between ASR expansions (Figure 63), which is similar to study of Kizhakkumodom [40].
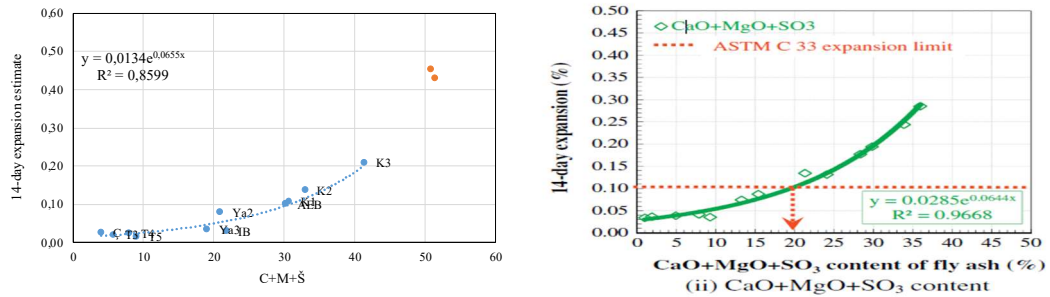


*Figure 63. 14 days expansion%-C+M+S content graphs of 25% replacement ratio for this study and* [40]

C+M+S over S+A+F content of the fly ashes have fair relationship between ASR expansions, as can be seen in Figure 64. In the study of Kizhakkumodom [40], it is offered to have a linear relationship but for the sake of consistency, exponential trendline is used in this study.
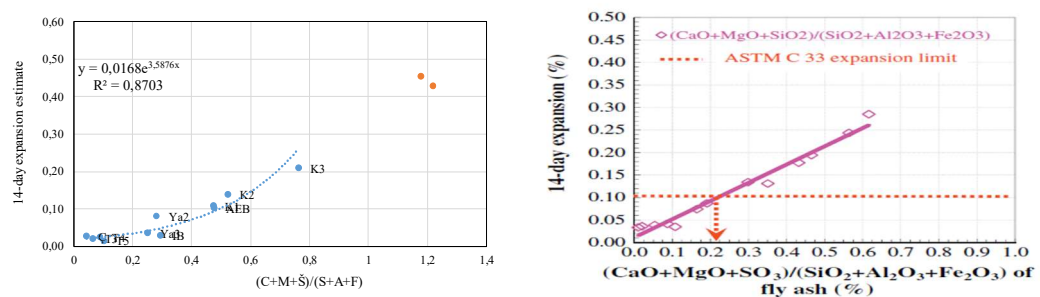


*Figure 64. 14 days expansion%-C+M+S over S+A+F graphs of 25% replacement ratio for this study and* [40]

91

The cementitious CaO contents were discussed in the study of Malvar [41] as stated in the literature review section of this study. Cementitious CaO is the sum of the CaO content of cement and fly ash in their level of participation. The comparison graph of [41] with the data of this study entered in with different colors, is given in Figure 65. As can be seen in this graph, although the cementitious CaO content seems to be higher with a narrow margin, the behavior of the specimens' normalized expansion values with respect to cementitious CaO content seems to be similar in two studies.
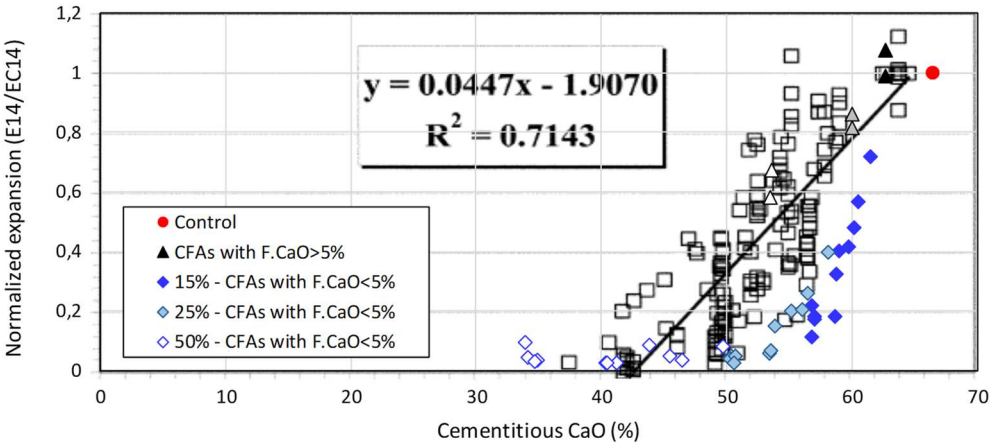


*Figure 65. Combination of* [41] *and the current study, cementitious CaO%-normalized expansion graph*

The cementitious MgO were also discussed in the study of Malvar[41] The results of that study was not supporting the relationships between ASR expansions and MgO content. The situation is similar as can be seen in Figure 66.
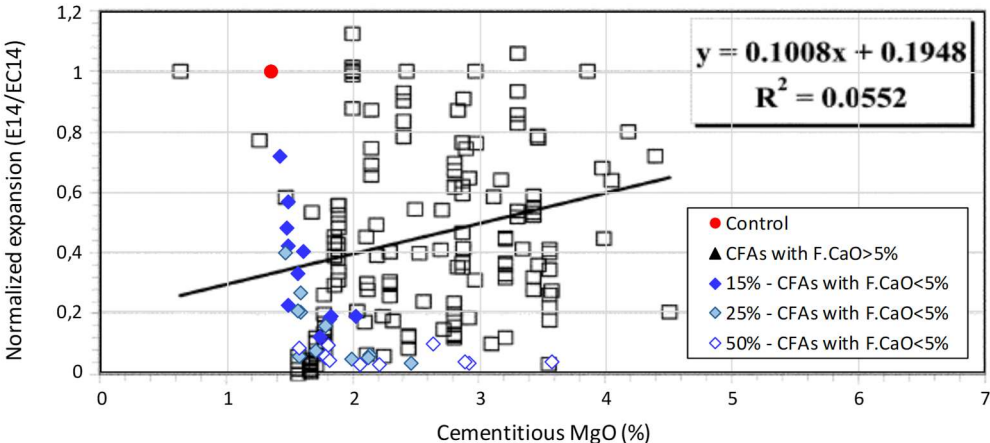


*Figure 66. Combination of* [41] *and the current study, cementitious MgO%-normalized expansion graph*

The cementitious $SiO_2$ contents were also studied in the study of Malvar[41] The comparison of the results current study and [41] is given in Figure 67. The negative correlation is apparent at the results of both studies. The cementitious $SiO_2$ content is slightly smaller than that of Malvar's study but, the behavior of the ASR expansions is similar.
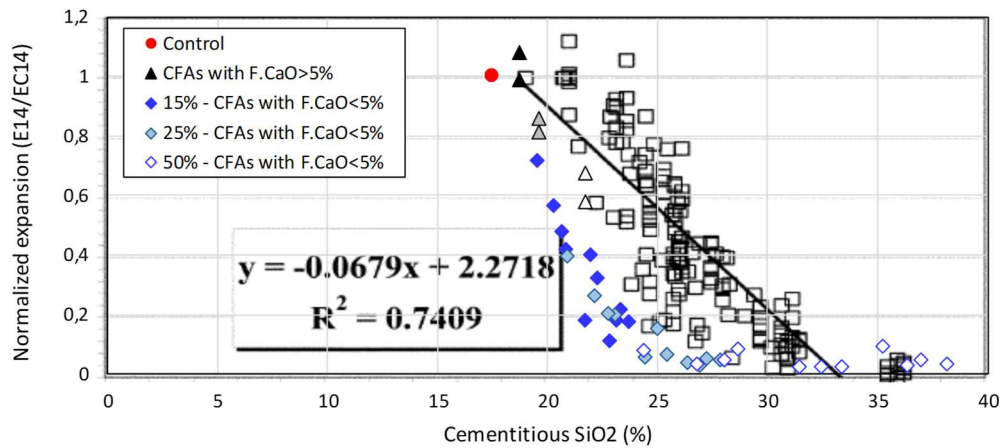


*Figure 67. Combination of* [41] *and the current study, cementitious SiO₂%-normalized expansion graph*

$Fe_2O_3$ content discussion with respect to ASR expansions can be made through the graph given in Figure 68. Both [41] and the current study has analogical results. The $Fe_2O_3$ content does not seem to have a direct relationship with normalized expansion values.
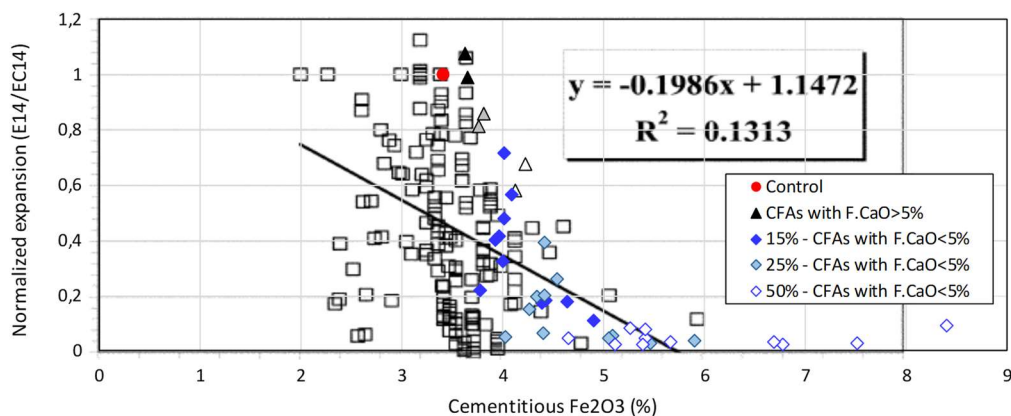


*Figure 68. Combination of* [41] *and the current study, cementitious Fe₂O₃% - normalized expansion graph*

When the result of the comparison between cementitious $SO_3$ content and ASR expansions are analyzed, the result of [41] and the current findings are unlike in the $SO_3$ content section (Figure 69). This difference is probably caused by the different $SO_3$ ratio of the cements used in the experiments. On the other hand, a weak positive correlation between normalized expansion and cementitious $SO_3$ content seems to exist in both studies.
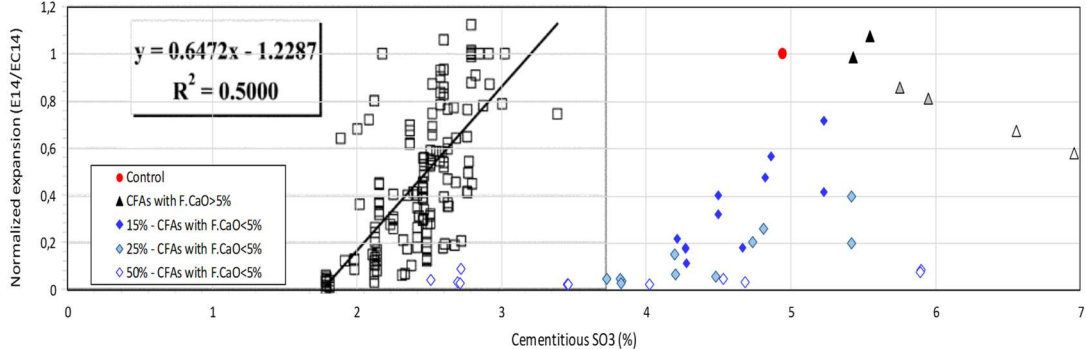


*Figure 69. Combination of* [41] *and the current study, cementitious $SO_3$% - normalized expansion graph*

Cementitious $Al_2O_3$ content versus normalized expansion graphs of [41] and the current study shows resemblance (Figure 70). The negative correlation exists at fair reliance factor for both studies. The $Al_2O_3$ content of this study is slightly lower than that of study of Malvar.
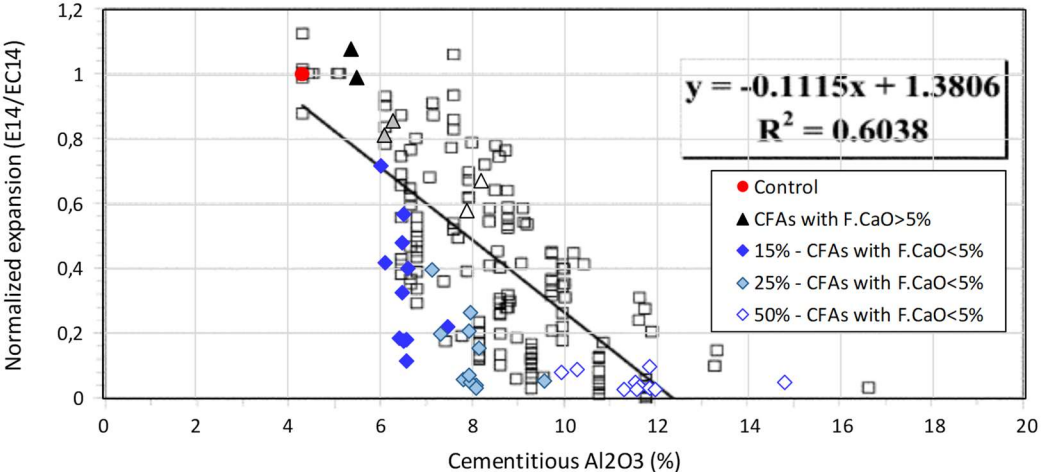


*Figure 70. Combination of* [41] *and the current study, cementitious $Al_2O_3$% - normalized expansion graph*

94

Cementitious CaOeq content – normalized ASR expansion relationships discussed in [41] with the data of this study entered in with different colors, is given in Figure 71. As can be seen in this graph, just like the cementitious CaO content, cementitious CaOeq also seems to be higher with a narrow margin, the behavior of the specimens' normalized expansion values with respect to cementitious CaOeq seems to be similar in two studies.

CaOeq formulation is given in Equation 4.

$$Equation\ 4.\ CaOeq=CaO+0{,}905*Na2O+0{,}595*K_2O+1{,}391*MgO+0{,}7*SO_3$$
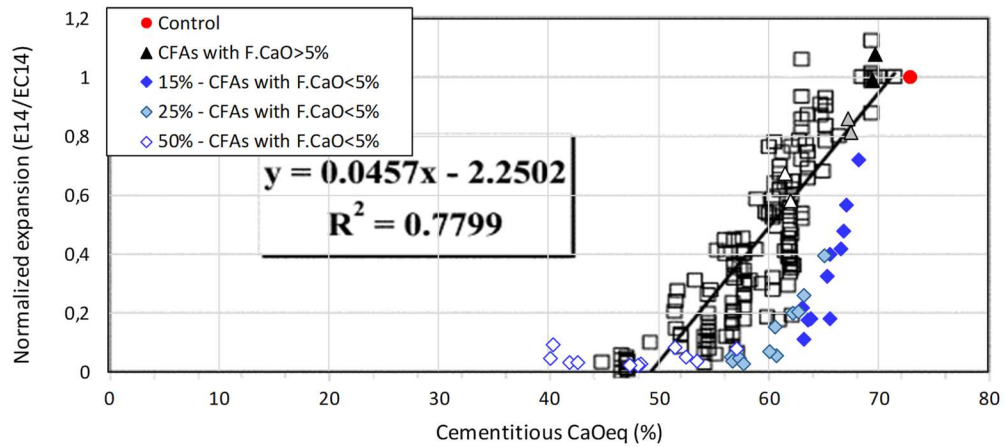


Figure 71. Combination of [41] and the current study, cementitious CaOeq% - normalized expansion graph

The cementitious $SiO_{2eq}$ – normalized ASR expansion relationship was also studied in the study of Malvar[41]. The comparison of the results current study and [41] is given in Figure 72. The negative correlation is obvious at the results of both studies, just as in the case of $SiO_2$ graph. The cementitious $SiO_{2eq}$ content is again smaller than that of Malvar's study but, the behavior of the ASR expansions is similar.

ZiO2eq formulation is given in Equation 5.

$$Equation\ 5.\ SiO_2eq= SiO_2+0{,}589*Al_2O_3+0{,}376*Fe_2O_3$$
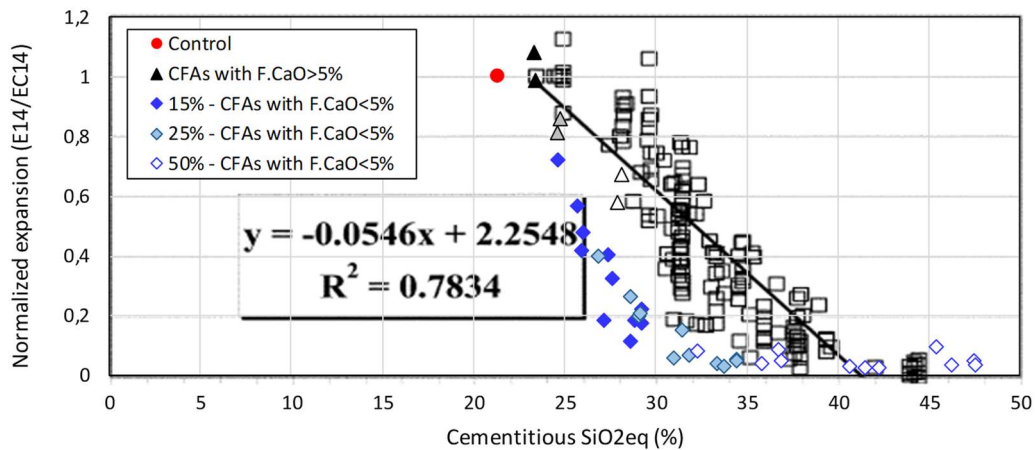
*Figure 72. Combination of* [41] *and the current study, cementitious SiO$_{2eq}$% - normalized expansion graph*

Next, Malvar[41] studied the correlation of normalized cementitious CaOeq/ SiO$_{2eq}$ ratio and the normalized ASR expansion. The comparison graphs is given in Figure 73. In the graph, the data of both studies seem to be consistent. The behavior of the coal fly ash specimens' constituents with respect to their performance on ASR mitigation are quite similar.
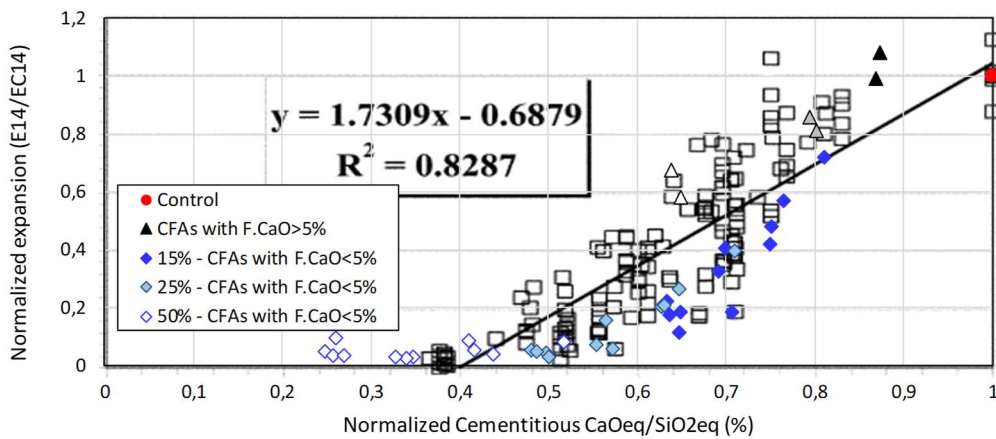


*Figure 73. Combination of* [41] *and the current study, cementitious CaOeq/SiO$_{2eq}$% - normalized expansion graph*

Next, utilization of constituents in cementitious form approach of Malvar [41] and combination of the S-A-F and C-M-S approach of Kizhakkumodom [40] are associated together in the next graphs. As can be seen in Figure 74, summation of

96

cementitious amounts, S+A+F has good relationship with the ASR expansion values for 15% and 25% replacement ratios. The reliance factors between 0.80-0.88 also confirm this relevance. Since almost all of the specimens except Ye1 and Ye2 have good and similar results at 50% replacement level, the right-hand side of the graph which includes the 50% replacement level tests, doesn't seem to follow this relationship.
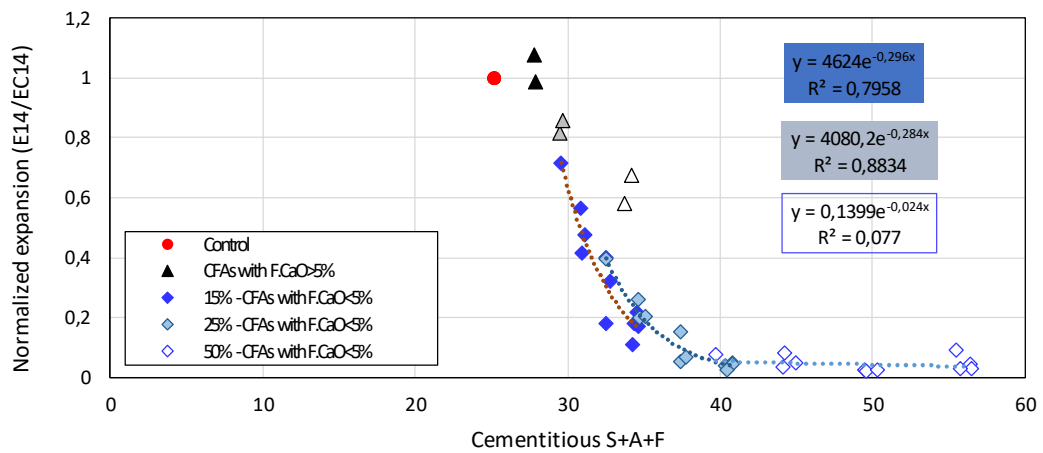


*Figure 74. Cementitious S+A+F - normalized expansion graph*

The behavior is similar for the summation of C+M+S values in cementitious form. ASR expansion values for 15% and 25% replacement ratios are following a scaled attitude (Figure 75). Again, as a result of the fact that almost all of the specimens except Ye1 and Ye2 have good and similar results at 50% replacement level, the left-hand side of the graph doesn't seem to follow this relationship.
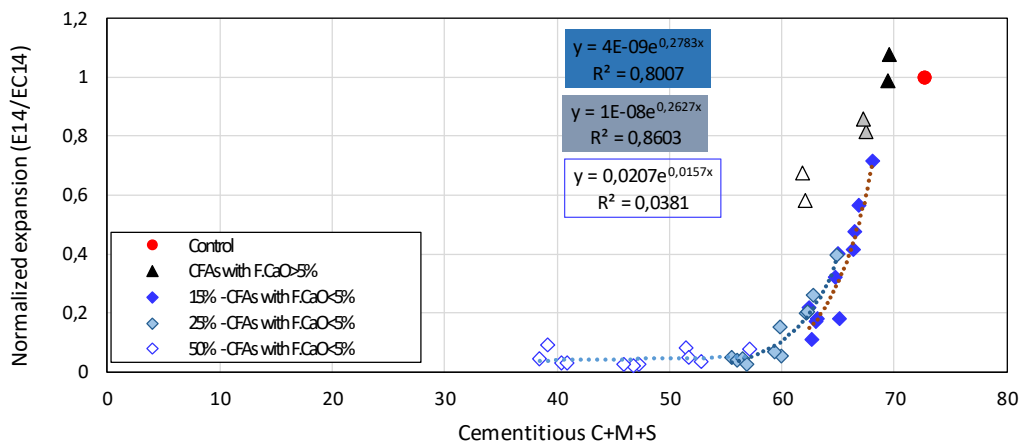


*Figure 75. Cementitious C+M+S - normalized expansion graph*

Finally, the relationship between ratio of the cementitious S+A+F over C+M+S values and the normalized expansions caused by ASR seems to be well for 25% and 50% replacement ratios (Figure 76) with $R^2$ values of 0.80 and 0.87. Again, 50% replacement level experiments does not follow any proportionality because of their closeness to each other, without depending on their chemical constituents substantially.
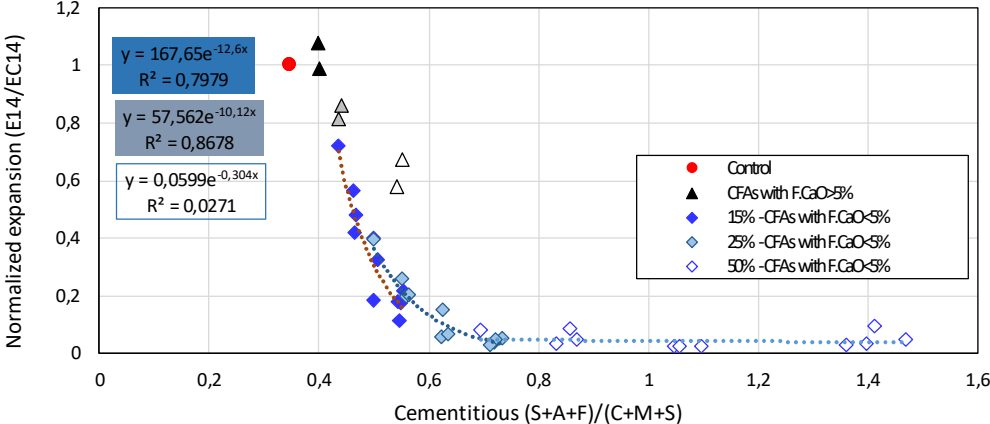


*Figure 76. Cementitious (S+A+F) / (C+M+S) - normalized expansion graph*

## 4.6. Effect of Fly Ash Fineness on Alkali Silica Reaction Performance

14 days expansion estimates – replacement level graphs for 15wt%, 25wt% and 50wt% ratios are given in Figure 77:

– At 15wt% replacement level of the coal fly ash specimens, there seems to be a slight correlation between the D10, D50 and D90 values of the low-Ca and int-Ca specimens and the 14 days expansions. As these gradation values increase which means that the coal fly ash specimens' gradation becomes coarser, the expansions also increase in small quantities. This may be the result of the fact that bigger fly ash particles are not able to go into reaction completely to mitigate ASR thus lead to increase of the expansions. The effect of D10, D50 and D90 values on ASR performance of high-Ca and high free CaO fly ash specimens could not be correlated with the ASR expansions.

*(a) 15 wt% replacement*

*(b) 25 wt% replacement*
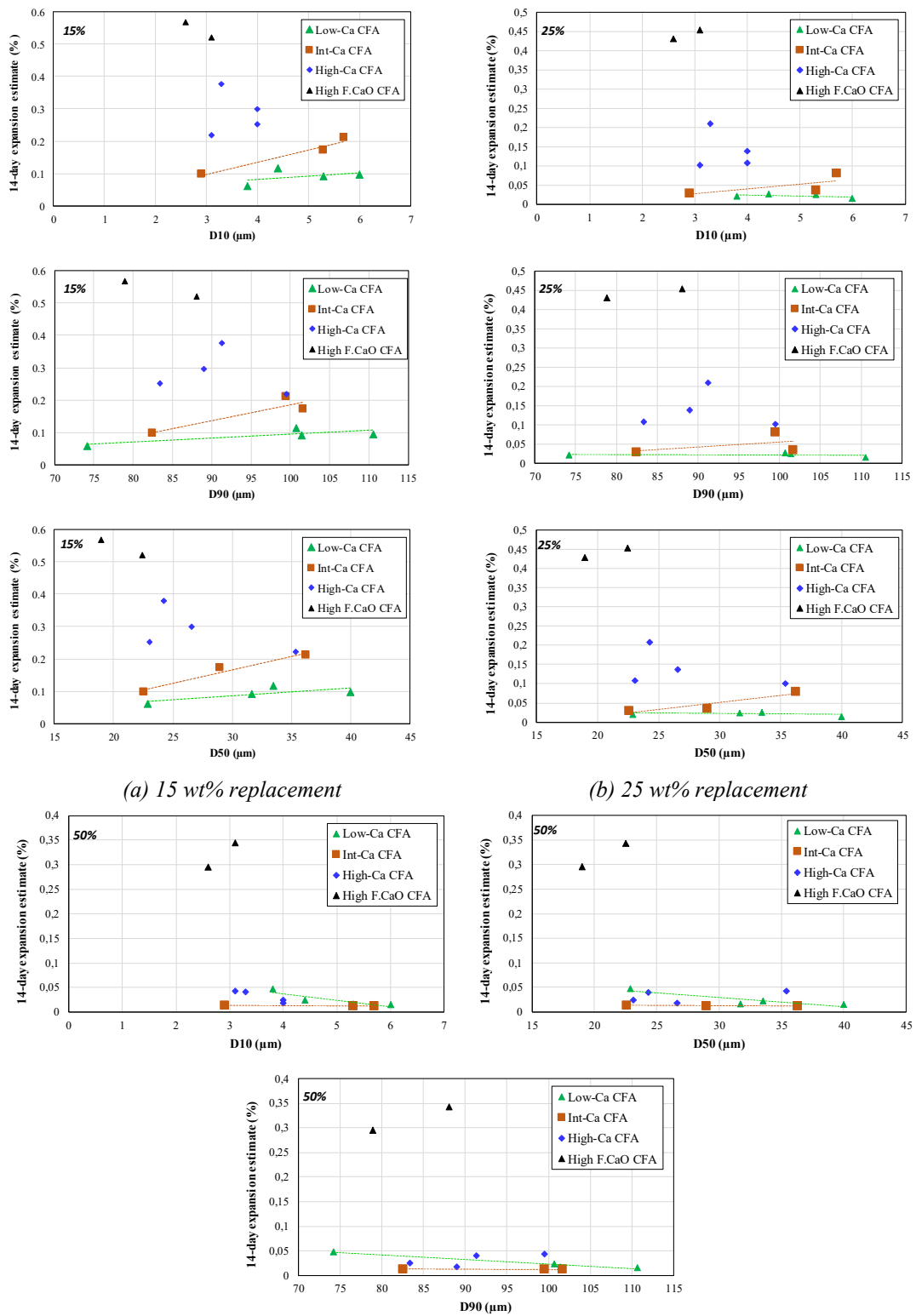
*(c) 50 wt% replacement*

*Figure 77. 14 days expansion estimates – replacement level graphs for (a)15wt%, (b)25wt% and (c)50wt% ratios*

When the replacement ratio of coal fly ash specimens are risen to 25wt%, the correlations determined at the 15wt% ratio could not be observed even for the low-Ca and int-Ca fly ashes which may be caused by the fact that, these specimens had good performance at this replacement rate so the effect of gradation might have become negligible among the other factors such as chemistry. The same situation also holds for the 50wt% replacement level. As a result of possibly same reasons, relevance of the D10, D50 and D90 values with ASR expansions could not be found.

## 4.7. Scanning Electron Microscope Images for Fly Ash – Cement Mortar Specimens

SEM images taken at the Central Laboratory. Those images are both showing the general views from the mortar bars and the ASR gel formation within the mortar. Several magnification levels are used to be able to understand the reactions in detail.

### 4.7.1. Control Mortars

The control mortar has no fly ash, but 100% portland cement as binder. As can be seen from the following SEM images at Figure 78, there have been severe ASR gel formations inside the control group mortar bar. Not only aggregate with ASR gels, but also many aggregates missing significant amount of inside material are also seen. The ASR damaged sections and the channels the ASR gel flow through the aggregate to the matrix can directly be observed at the images, together with the cracks inside aggregates and the cement matrix. Moreover, there are separations between the aggregates and cement paste as a result of the reactions. These images conclude that there has been very severe degradation caused by ASR and the ASTM C1260 experiment results also confirm this outcome.
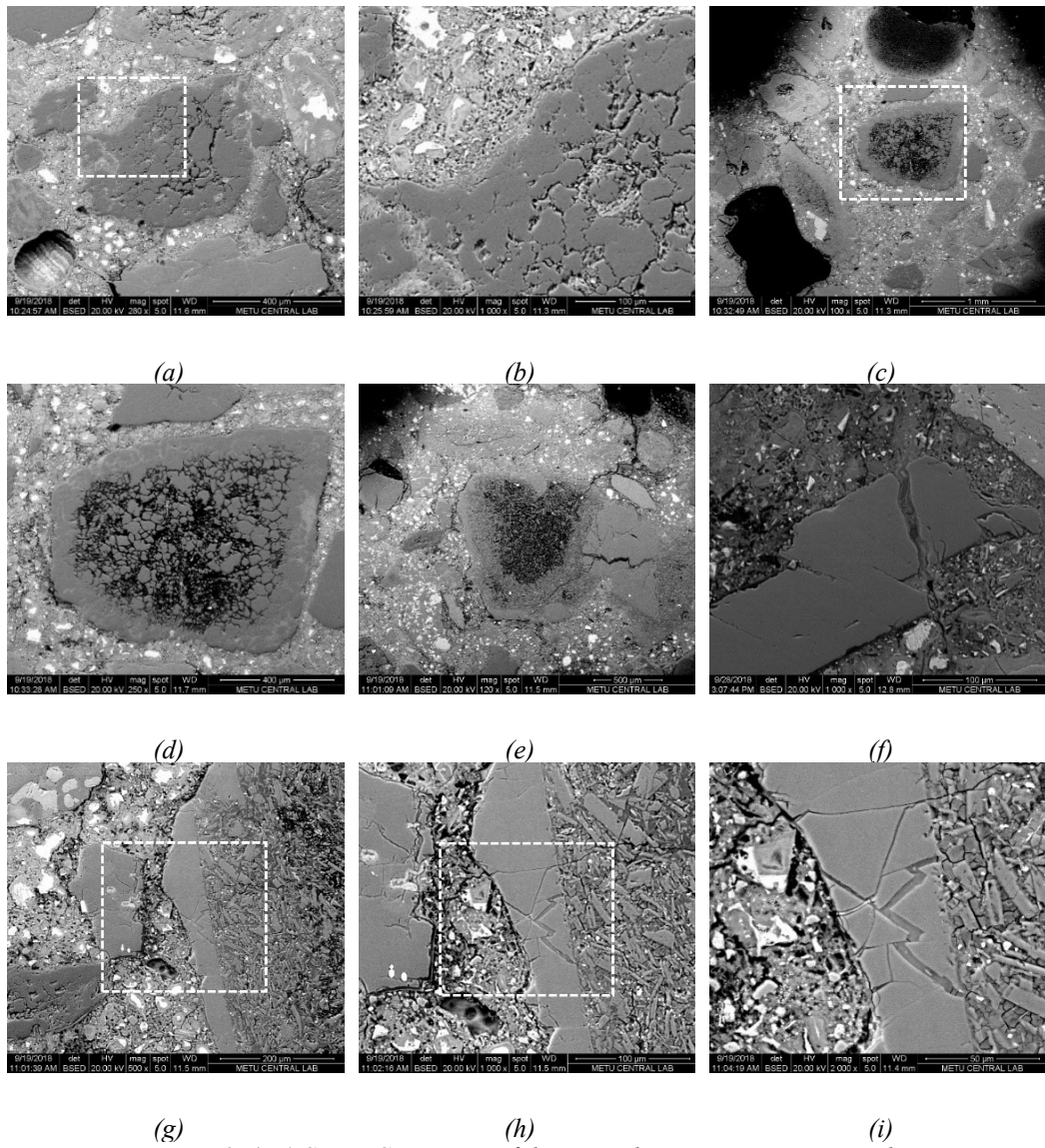
*Figure 78. (a-i) SEM BSE images of the control group, cement mortar bars*

ASR damaged aggregate is subjected to EDX mapping procedure. The images of the elements selected can be seen in Figure 79. SEM BSE images of the same region is given in Figure 80. The high sodium and potassium intensities seem to be attracted to the ASR affected regions. Both images show the elements overlapping with the ASR gel. The other elements tested could not be related with ASR.

*(a) Al*     *(b) Ca*     *(c) C*

*(d) Cl*     *(e) Fe*     *(f) Mg*

*(g) O*     *(h) S*     *(i) Si*

*(j) Na*     *(k) K*
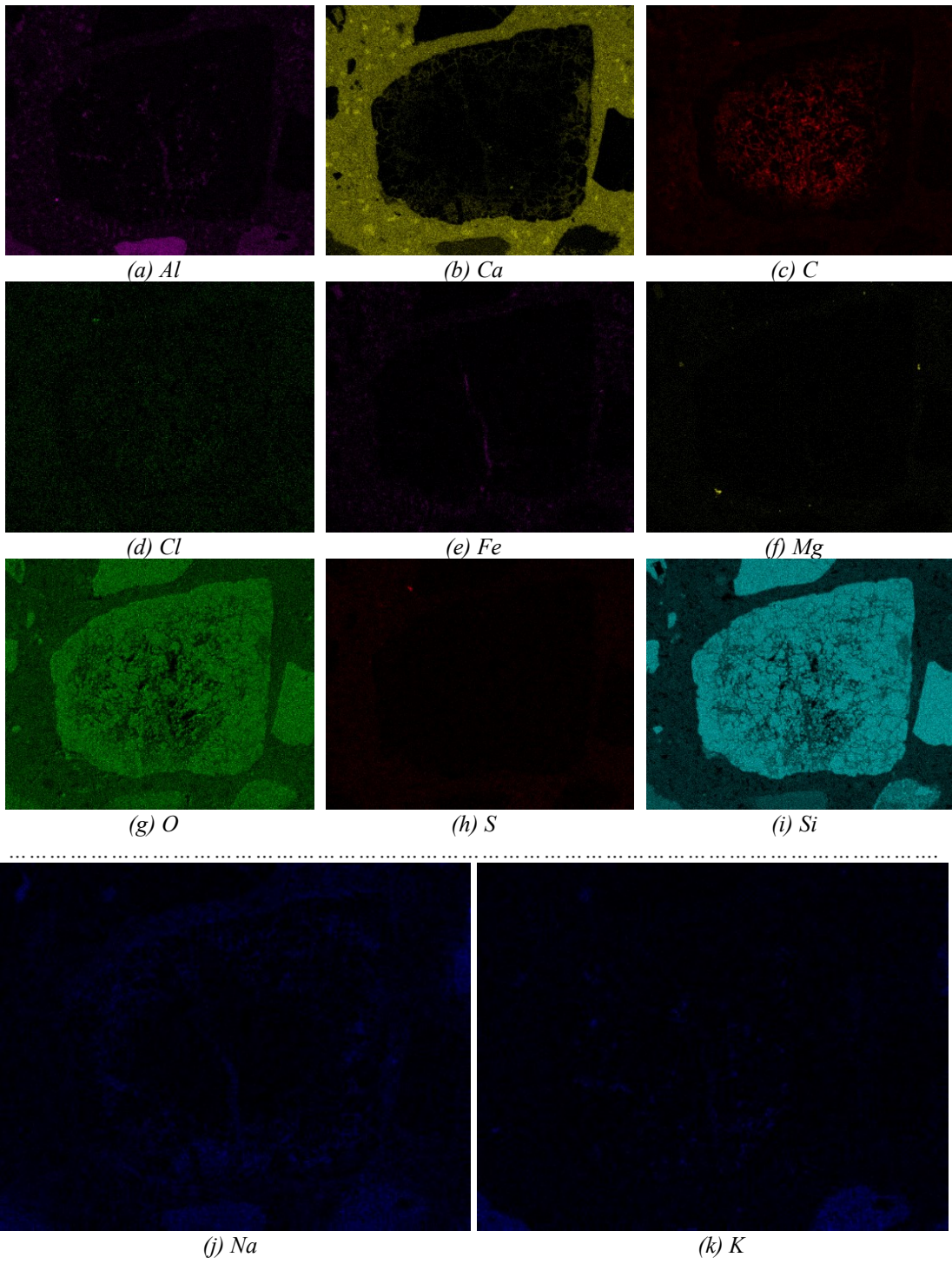
*Figure 79.  (a-k) EDX mapping performed on ASR damaged aggregate*
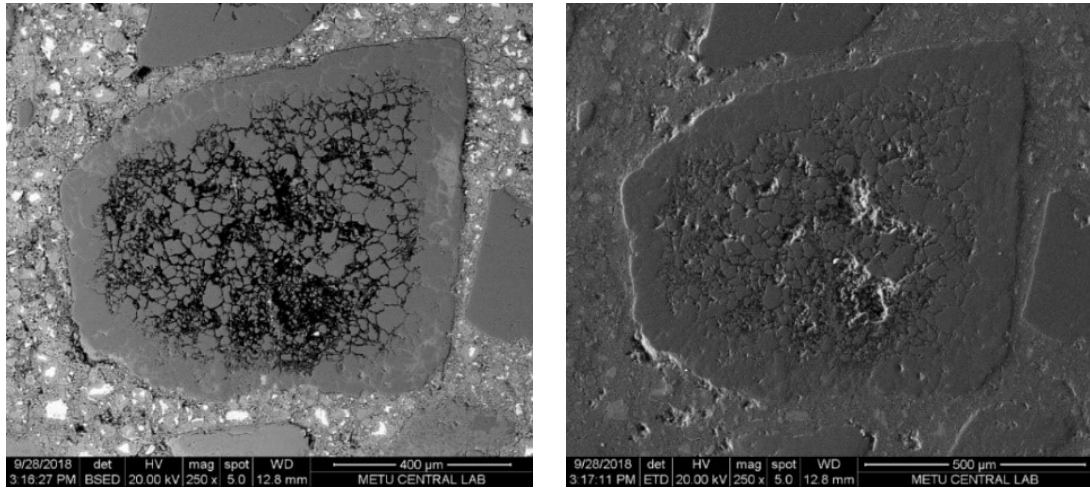
*(a)* *(b)*
*Figure 80. (a-b) SEM BSE images of the ASR damaged aggregate*

### 4.7.2. PC-Ç Mortars

As can be seen from the following SEM images at Figure 81, mitigation of ASR gel formations by the low-Ca Ç fly ash even at 15wt% replacement level is not bad. The remainders of several fly ash particles which are spherical shaped can be clearly observed. There are also cracks inside the matrix and in the transition zone of aggregates and the matrix, but no severe cracks or deterioration caused by ASR is confirmed in the aggregates.

<center>(a)</center>

<center>(b)</center>



<center>(c)</center>

<center>(d)</center>
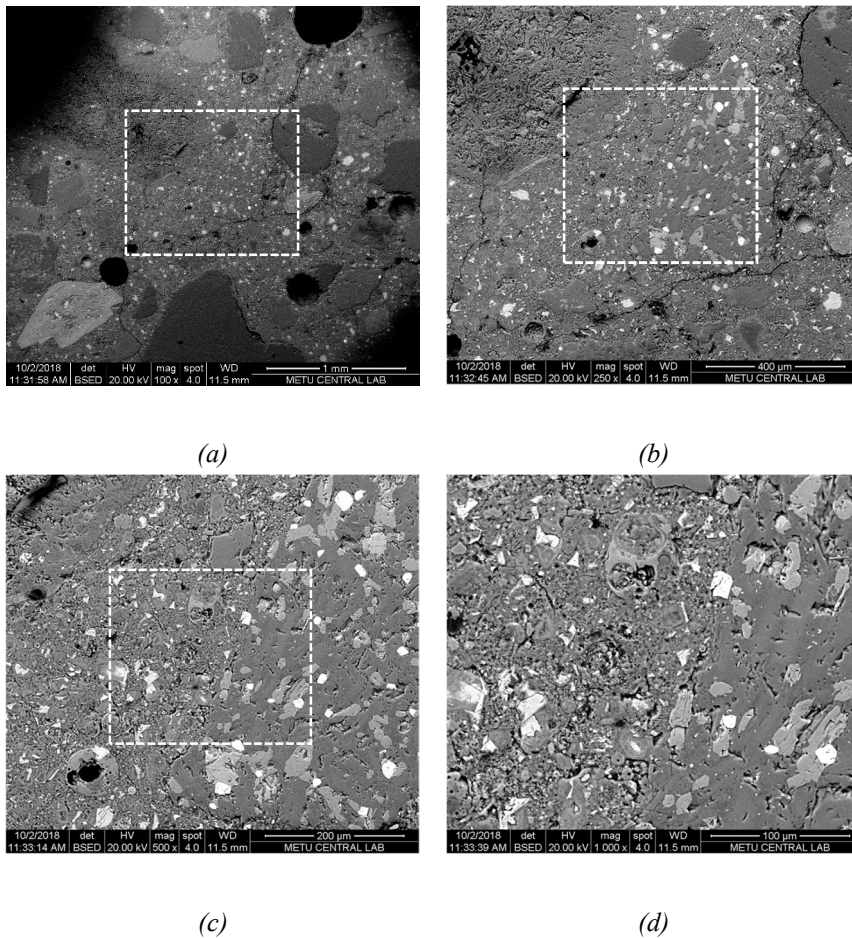
*Figure 81 (a-d) SEM BSE images taken from 15% Replacement, Ç mortar bars*

When the following SEM images at Figure 82 are studied, it is observed that almost all of the ASR gel formations are prevented by the Ç fly ash 25wt% replacement level. No ASR sourced deformation can be determined from the prints. Many coal fly ash particle residuals can be seen in the specimen with spherical shapes. Please note that, the black parts of the image are mostly caused by separation of the aggregate particles at the polishing process of the mortar specimens.

*(a)*                                        *(b)*



*(c)*                                        *(d)*
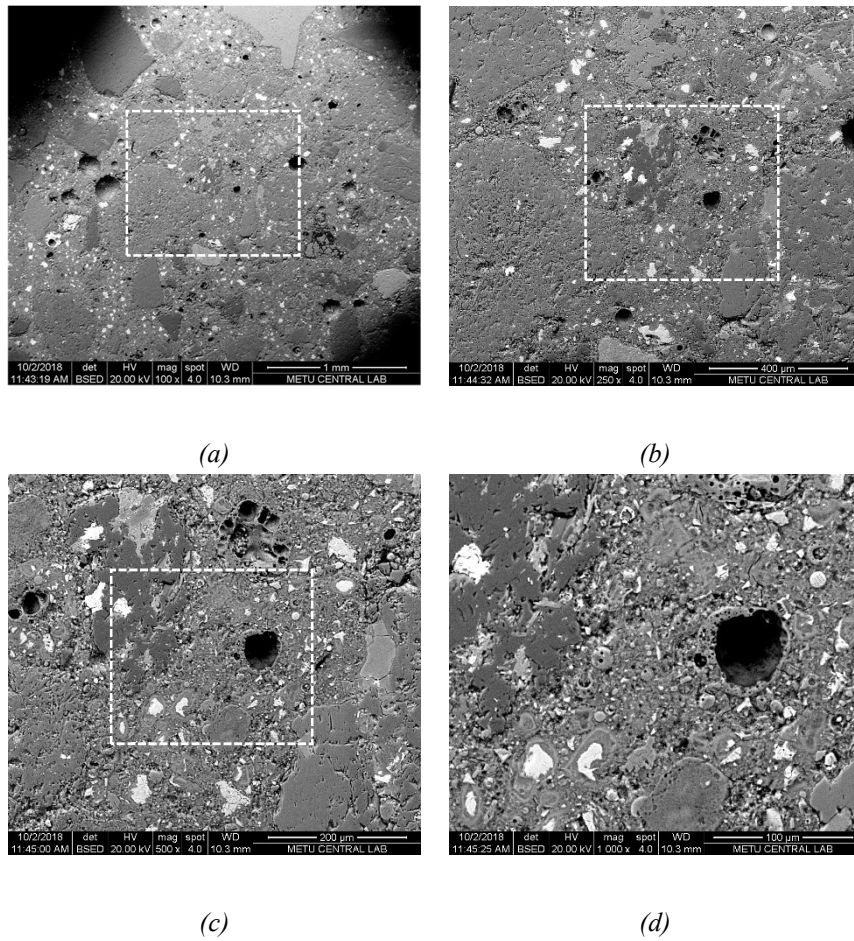
*Figure 82. (a-d) SEM BSE images taken from 25% Replacement, Ç mortar bars*

Next SEM images of Figure 83 signify that ASR is completely vanished from the Ç specimen at 50wt% replacement ratio. Spherical residues of fly ash particles are identifiable. There are black parts caused by separation of some aggregates from the sample at polishing process. Moreover, the surface seems to be very grainy. This is probably caused by the workability issues of this replacement level when the ASTM C1260 directives are used. The water amount is not enough for this coal fly ash usage level.

*(a)*            *(b)*

*(c)*            *(d)*
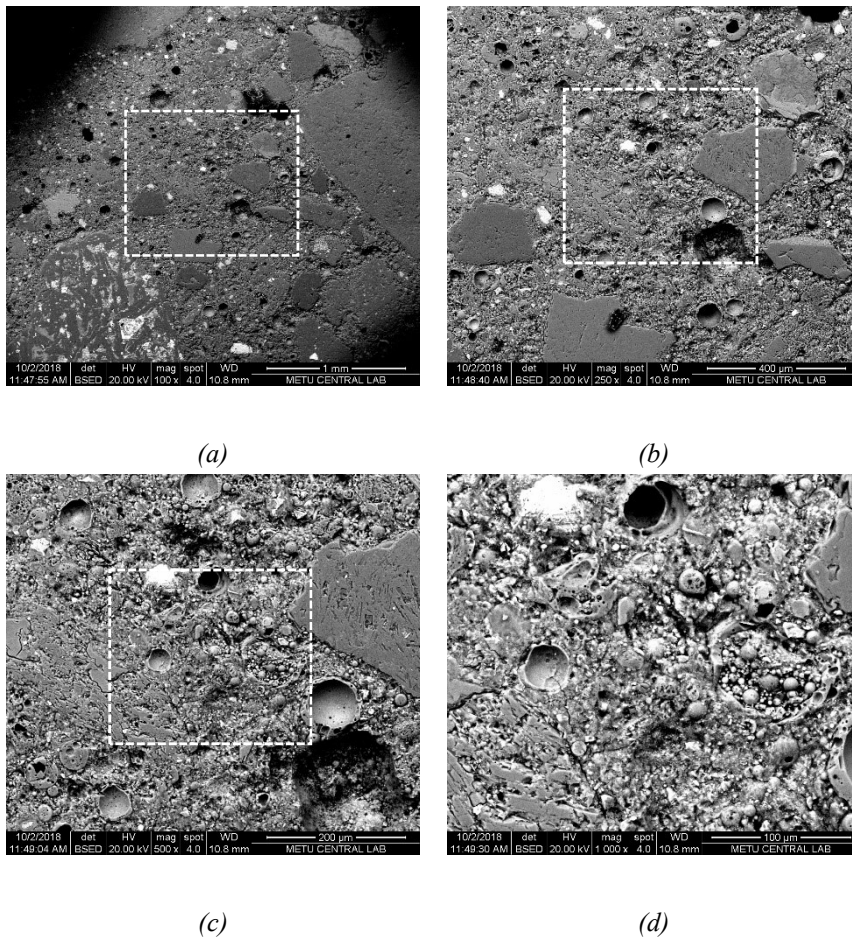
*Figure 83. (a-d) SEM BSE images taken from 50% Replacement, Ç mortar bars*

### 4.7.3. PC-T3 Mortars

As can be seen from the following SEM images of Figure 84, ASR gel formations are mitigated fairly well by the low-Ca T3 coal fly ash 15wt% replacement level just in the case of Ç specimen. There are some cracks observed in the cement matrix and the transition zone between the matrix and aggregates. Fly ash residue spherical particles are also seen but not as much as the Ç specimen.

*(a)*         *(b)*



*(c)*         *(d)*
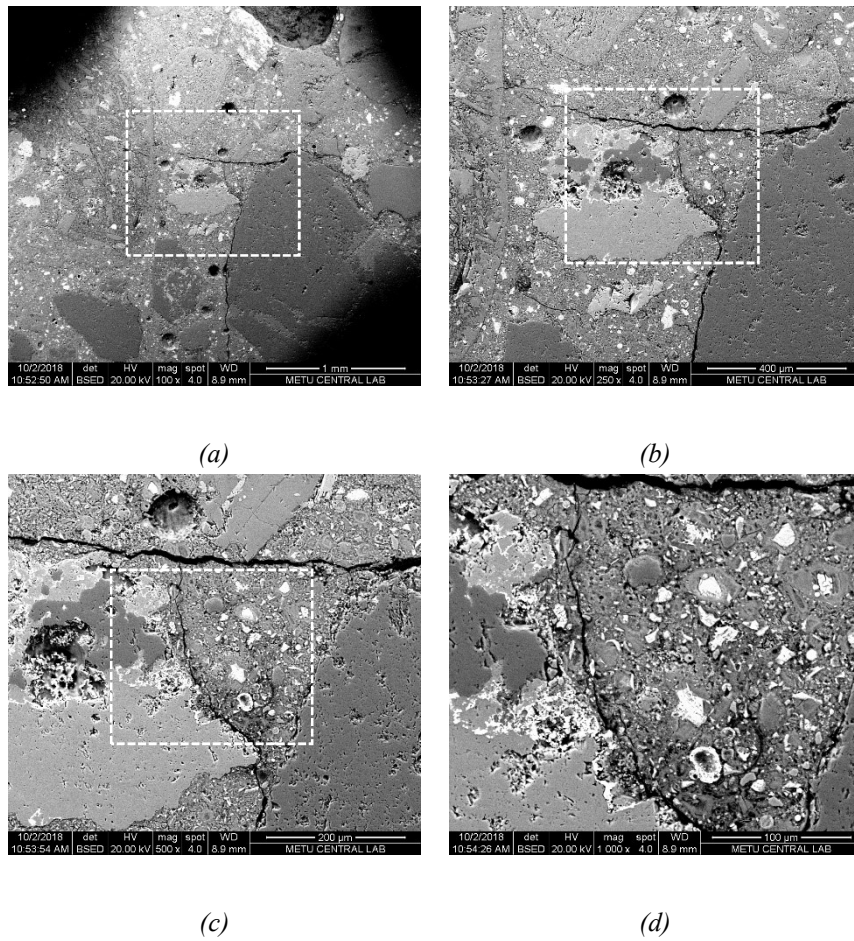
*Figure 84. (a-d) SEM BSE images taken from 15% Replacement, T3 mortar bars*

In the next images (Figure 85), it is determined that T3 specimen at 50wt% replacement level has shown a good performance for mitigation of ASR. Moreover, no cracks are observed in the cement matrix. An aggregate in the right part of the second image seems to be cracked and another one has been separated from the cement matrix but there is no evidence of ASR in these sections. These cases are very probably caused by the cutting or polishing process of the specimen. The spherical fly ash particles are also seen in the images.

*(a)*                                            *(b)*

*(c)*                                            *(d)*
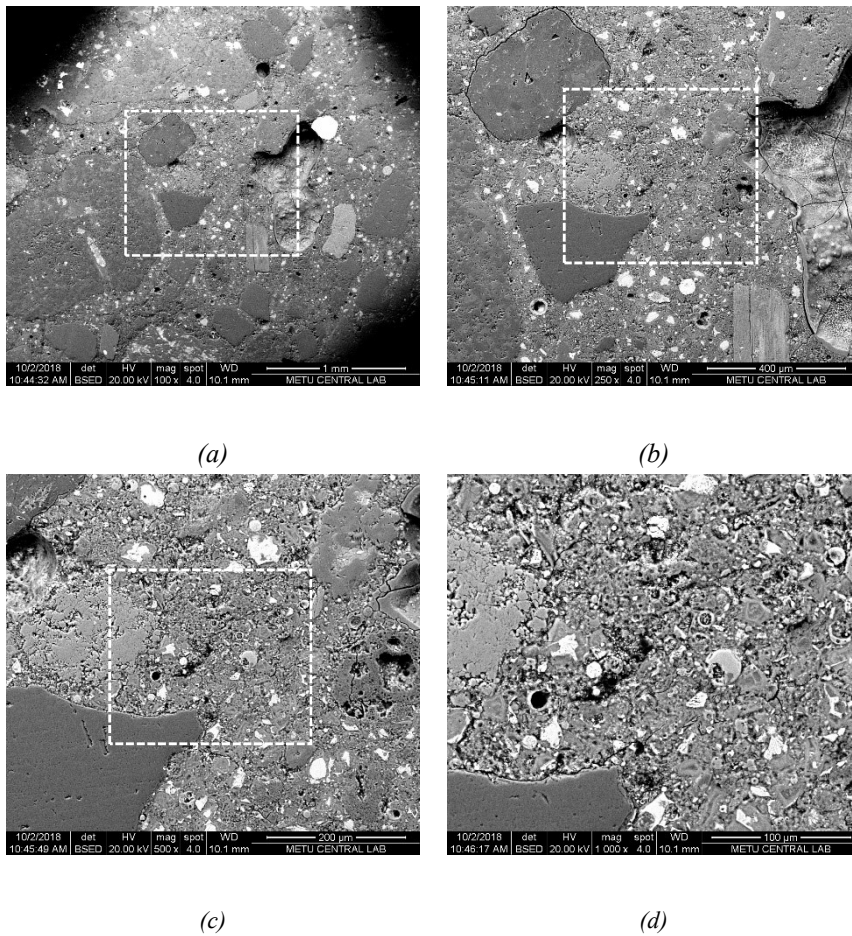
*Figure 85. (a-d) SEM BSE images taken from 25% Replacement, T3 mortar bars*

As can be seen from the following SEM images of Figure 86, almost all ASR gel formations are mitigated by the T3 coal fly ash at 50wt% replacement level. No evidence of ASR can be identified at all. Many spherical fly ash particles can be discriminated from the image. The most important problem of this specimen is, just as in the case of Ç specimen, workability issues and the grainy texture of the matrix with lacking many aggregates. This problem is again caused by low water content of the mixture.

*(a)*                                    *(b)*



*(c)*                                    *(d)*
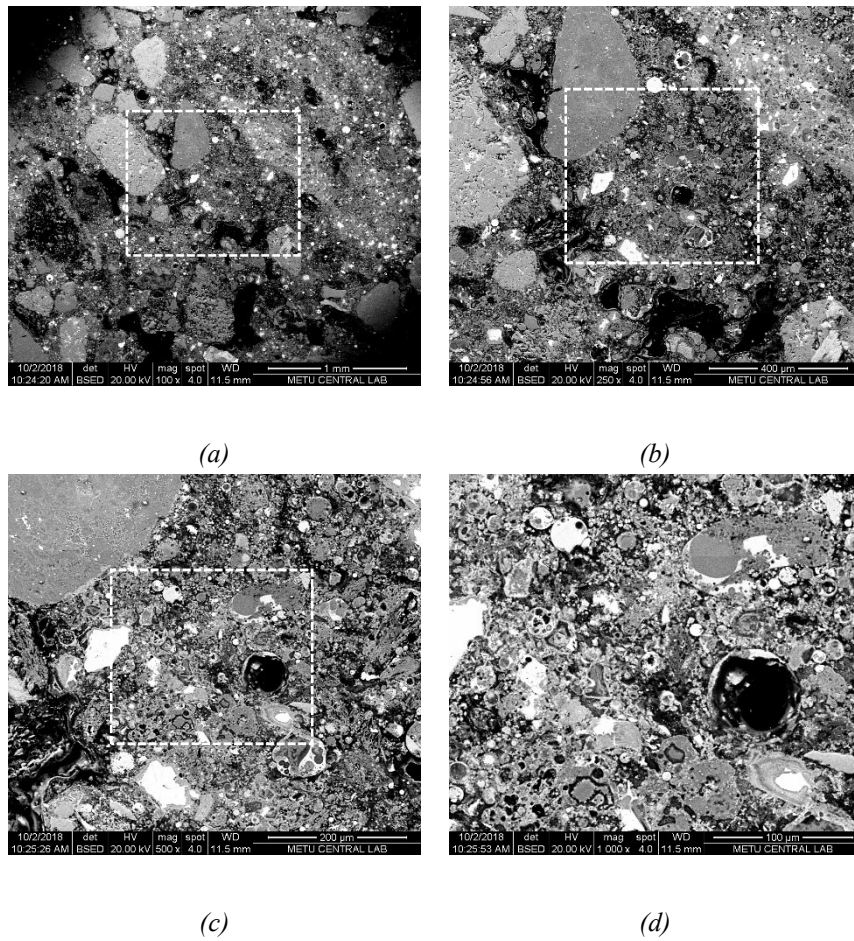
*Figure 86. (a-d) SEM BSE images taken from 50% Replacement, T3 mortar bars*

### 4.7.4. PC-IB Mortars

In figure 87, it is seen that a fair amount of ASR gel formations is mitigated by the 15wt% replaced İB fly ash which is an intermediate-Ca class. Several cracks are observed in the aggregates and cement matrix. Moreover, aggregates have evidence of some deterioration. Remainder fly ash particles are also seen.

*(a)*

*(b)*

*(c)*

*(d)*
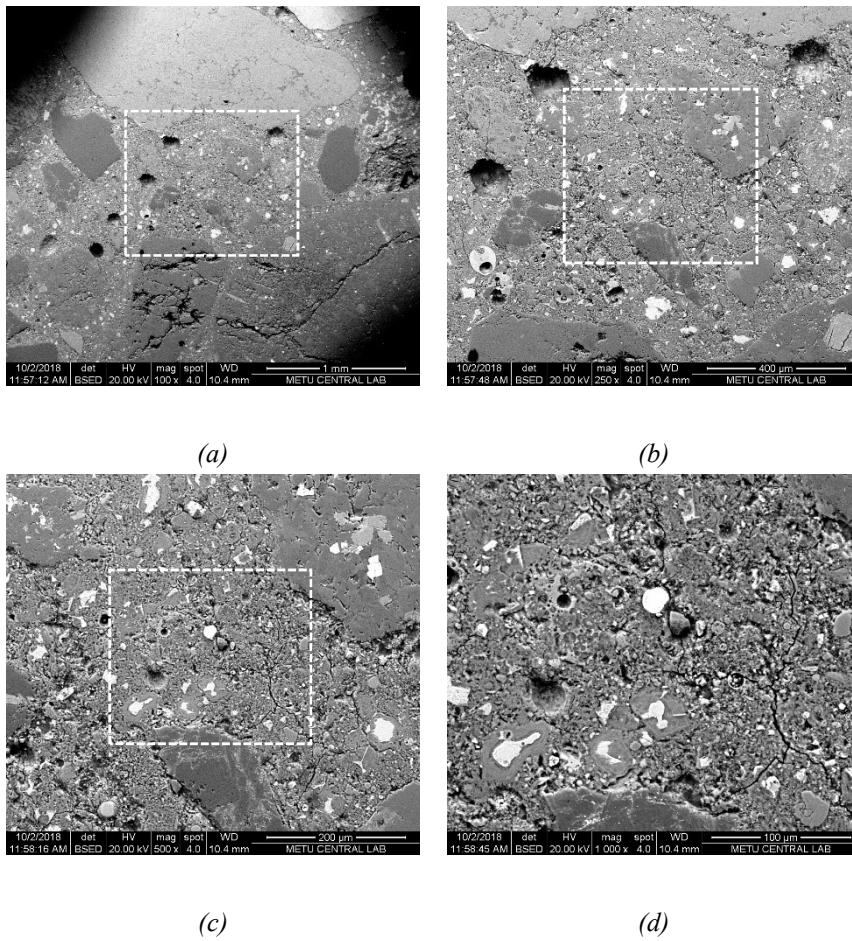
*Figure 87. (a-d) SEM BSE images taken from 15% Replacement, IB mortar bars*

When the images of İB with 25wt% replacement level is analyzed (Figure 88), the mitigation of ASR has increased vastly compared to 15wt% ratio. Inherently, there are more spherical residues of coal fly ash particles and much less evidence of ASR exists. Nearly no cracks are observed in aggregates or cement matrix.

*(a)*　　　　　　　　　　　　　　　*(b)*

*(c)*　　　　　　　　　　　　　　　*(d)*

*Figure 88. (a-d) SEM BSE images taken from 25% Replacement, IB mortar bars*

As can be seen from the following SEM images of Figure 89, some ASR gel formations are mostly mitigated by İB coal fly ash at 50wt% replacement level. Fly ash particles are again discriminable, no evidence of ASR is observed. Just as in the case of T3 and Ç specimens, the most important problem is the grainy texture as a result of the workability problem and lack of water content.

*(a)*                      *(b)*





*(c)*                      *(d)*
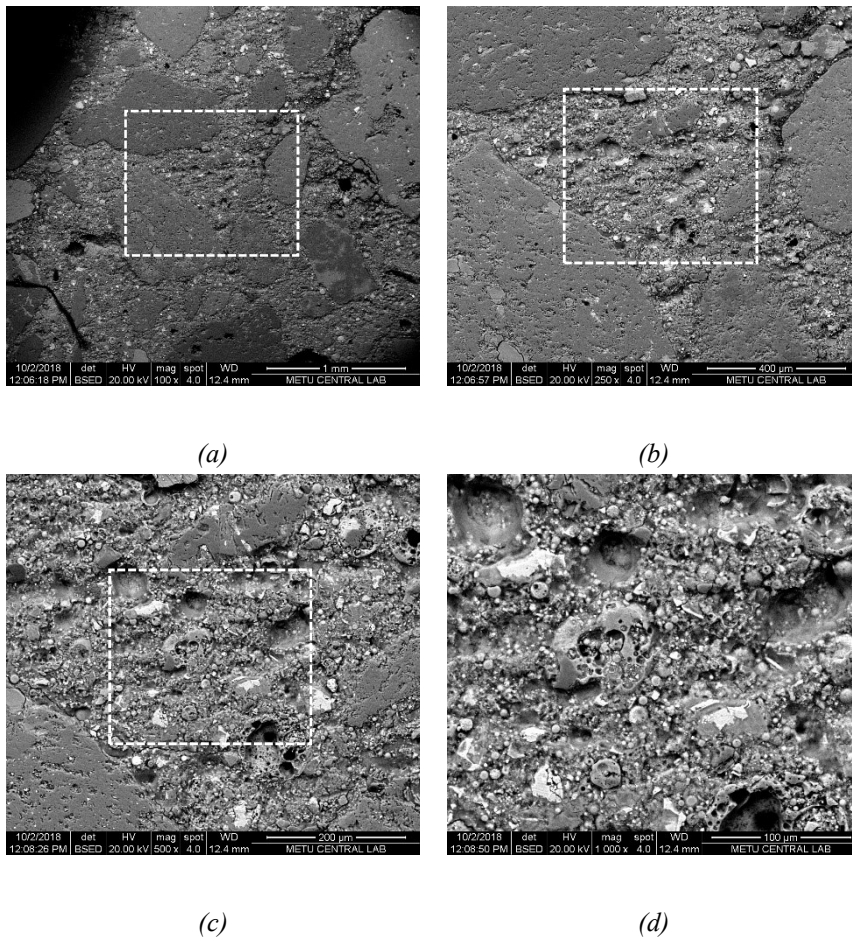
*Figure 89. (a-d) SEM BSE images taken from 50% Replacement, IB mortar bars*

### 4.7.5. PC-K1 Mortars

Following SEM images at Figure 90 show that, at 15wt% replacement level ASR gel formations are reduced at modest level by the K1 coal fly ash specimen which is classified as high-Ca coal fly ash in this study. Some cracks within the aggregates and cement matrix are visible. Moreover, degradation footprints are seen at the aggregates. Some fly ash residues can also be observed.

*(a)*                                                      *(b)*



*(c)*                                                      *(d)*
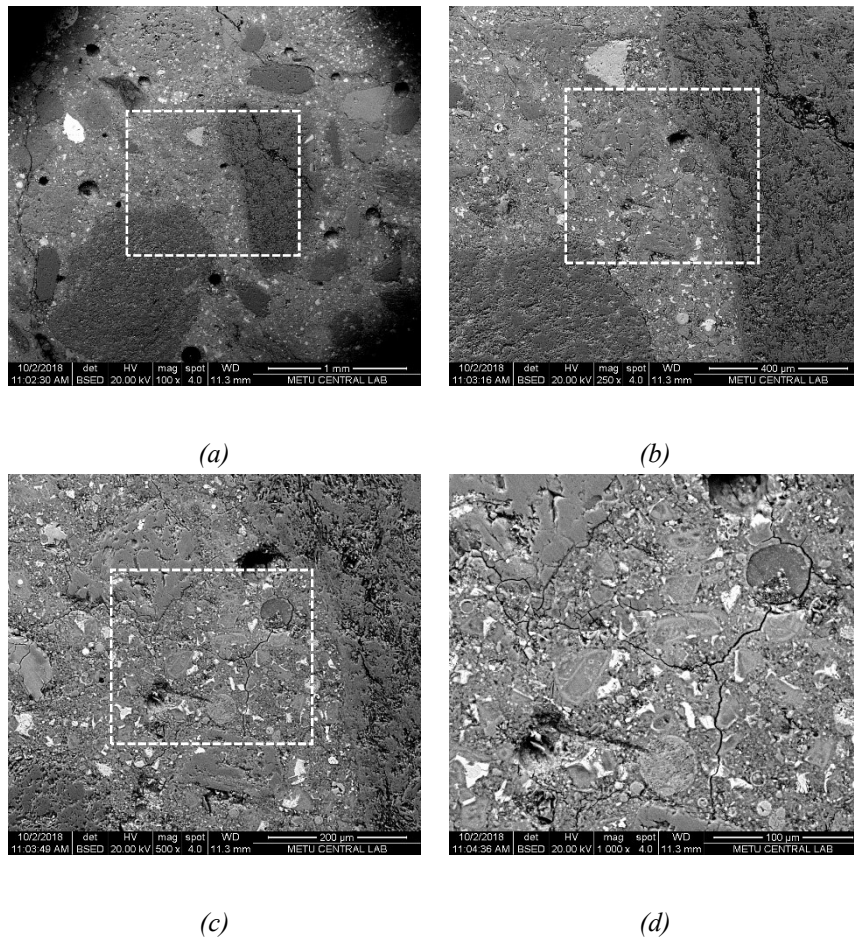
*Figure 90. (a-d) SEM BSE images taken from 15% Replacement, K1 mortar bars*

In the case of 50wt% replacement level for K1 specimen, the mitigation of ASR seems to be much better than 15wt% replacement level of the same specimen (Figure 91). Some microcracks within the cement matrix and in the transition zones are available but not as much as in the case of the former level.

*(a)*                                  *(b)*



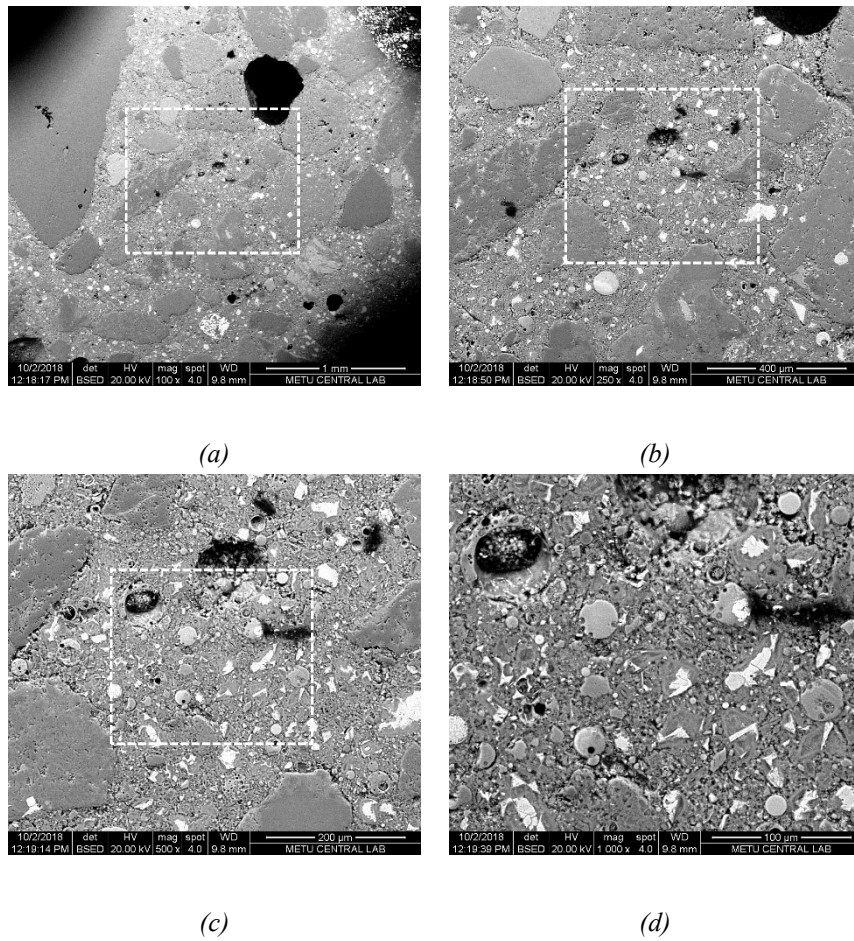*(c)*                                  *(d)*
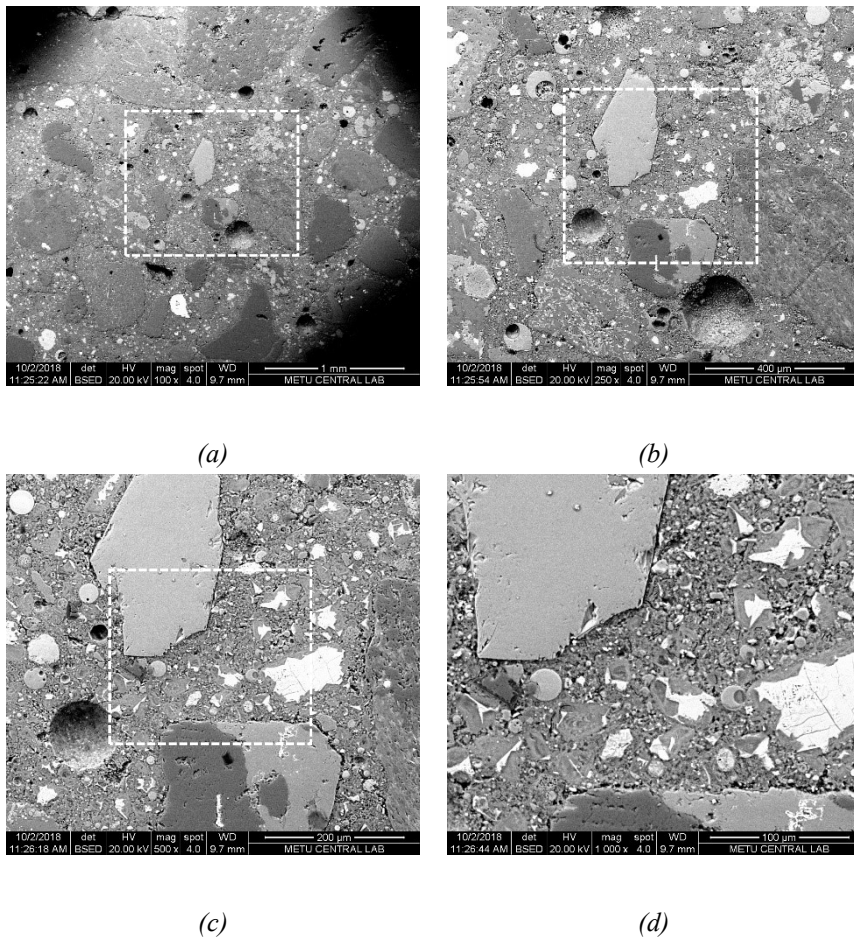
*Figure 91. (a-d) SEM BSE images taken from  25% Replacement, K1 mortar bars*

It can be deduced from the following SEM images of Figure 92 that, ASR is mitigated to a large extent by the 50wt% replacement ratio of K1 specimen. No serious cracks or degradation evidences can be observed. As expected, many spherical fly ash particles exist in the matrix. Although not as much as the Ç, T3, K1 and IB specimens, there is still granular texture caused by workability issues as stated in the other sample comments.
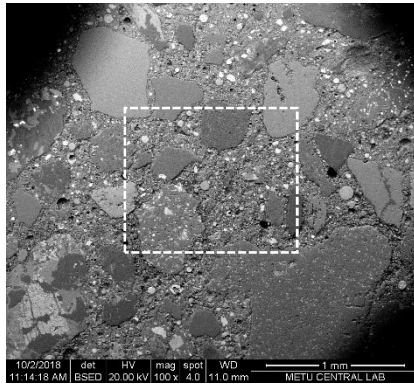
*(a)*
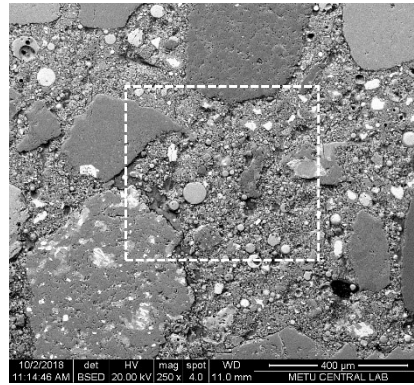
*(b)*
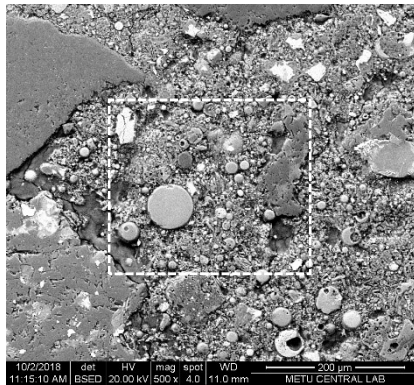
*(c)*
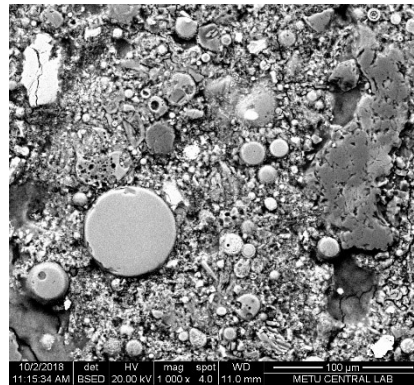
*(d)*

*Figure 92. (a-d) SEM BSE images taken from 50% Replacement, K1 mortar bars*

# CHAPTER 5

## CONCLUSIONS

### 5.1. Concluding Remarks

The results of the experiments conducted in this thesis study holds with the conclusions given in the literature to a large extent.

Low-Ca, intermediate-Ca and High-Ca coal fly ash specimens have mitigated the ASR expansions at every replacement ratio with a variety of performances. 15wt%, 25wt% and 50wt% replacement ratios respectively, are determined to be enough for the mitigation of ASR expansions according to ASTM C1260. These samples had close results at 50wt% replacement level but all of them also had workability issues. The nearness of these values resulted in difficulties to find relationships at his replacement ratio. On the other hand, high free-CaO fly ash specimens, namely Ye1 and Ye2, have resulted in even higher ASR expansions than the control samples. This unfavorable performance was expected since the high free CaO content leads to further CH formation and thus expansions.

The particle size distributions of the specimens have been observed to have very weak relationship to the ASR expansions. This is probably caused by the fact that the other factors such as constituents have more impact on the performance of the specimen.

As expected, the CaO and also R.CaO content of fly ash specimens which are suggested to be promoting ASR expansion, have practically enhanced the reaction and resulted in higher ASR expansion levels. Not surprisingly, $SO_3$ content have also been observed to have proportionality. On the other hand, alkali content of the coal fly ash specimens could not be proportionated to the expansions related to ASR, probably because of the test environment being extremely alkaline. The effect of MgO was unexpected which had negative correlation to the expansions.

On the contrary, $SiO_2$ and R. $SiO_2$ contents of the coal fly ash specimens were determined to have adverse effect on the ASR expansions significantly, which also

holds with the literature review. Moreover, $Al_2O_3$ and $Fe_2O_3$ content are confirmed to have a weak effect on the mitigation of ASR.

More correlations have been studied within the properties of the fly ash specimens, and varied proportions of these properties have given fair results. CaO equivalent and $SiO_2$ equivalent values are determined to have similar proportionalities with CaO content and $SiO_2$ content respectively. The ratio of CaO equivalent over $SiO_2$ equivalent has given good positive correlation to the ASR expansion results. Moreover, summation of $SiO_2$, $Al_2O_3$ and $Fe_2O_3$ has been confirmed to be adversely related to ASR expansion. Likewise, total of CaO, MgO and $SO_3$ is observed to have positive correlation to the expansions. Finally, the ratio of these summations respectively has been approved to have a reliable proportionality to ASR expansions as stated in the [40].

The cementitious contents of the constituents are also studied in the thesis and observed to have similar results with [41]. Some constituents were more or less to a degree as a result of the different constituents of the specimens, but the variance in behaviors were comparable.

In conclusion, the deep investigation of the 13 coal fly ash specimens collected from the leading thermal power plants in Turkey, has been carried out at 15wt%, 25wt% and 50wt% replacement levels and the behavior of the samples have been related to their constituents to a large extend. The relations that are specified in the literature have also been experimented and most of them are observed to be compatible with the result of the experiments conducted on the study.

## 5.2. Limitations, Future Works and Recommendations

As a result of the deadline and financial limitations, this study is restricted by means of experiment type, quantity, duration and specimen variety.

Firstly, since the master studies are limited timewise, the tests are arranged according to this duration. In a study with longer period, the 75 days test duration of the ASTM C1260 AMBT can be extended to several months or even years. In addition, the longer

versions of this test such as ASTM C1293 can be conducted in order to assess the ASR expansions more clearly. Moreover, tests such as SEM analysis and EDX mapping can be applied on more specimens with higher budget. Additionally, nano micro mechanical test device can be used to determine the E-modulus of the ASR products of the mortar bar specimen surfaces with aggressive alkali – silica reactivity which.

The samples studied in this thesis are selected as Tunçbilek reactor 3, 4, 5, Çatalağzı , Afşin Elbistan , İçdaş , Kemerköy reactor 1, 2, 3 , Yatağan reactor 2, 3 and Yeniköy reactor 1, 2 thermal power plants as stated before. As the reactor numbers imply, these power plants have also other reactors to be tested. Moreover, as can be seen from Figure 2, there are several other coal fired thermal power plants whose by product, fly ashes can be tested.

In conclusion, with higher budget and longer time, the experiment numbers, types and periods can be improved and more specimens may be tested for better understanding of the ASR and the performance of fly ash specimens of Turkey.

# CHAPTER 6

# REFERENCES

[1]     K. Ramyar, Betonda Alkali-Silis Reaksiyonu: Bir Derleme, Hazır Bet. (2013) 70–82.

[2]     N.B. Winter, Understanding cement : an introduction to cement production, cement hydration and deleterious processes in concrete, (2012). https//www.understanding-cement.com/alkali-silica.html.

[3]     Ç. Meral, The Study of Disorder in Amorphous Silica, Alkali-Silica Reaction Gel and Fly Ash, University of California, Berkeley, 2012. doi:http://dx.doi.org/10.1016/j.physbeh.2008.04.026.

[4]     S.W. Forster, R.L. Boone, M.S. Hammer, J.F. Lamond, D.S. Lane, R.E. Miller, S.E. Parker, A. Pergalsky, J.S. Pierce, M.Q. Robert, J.W. Schmitt, R.E. Tobin, State-of-the-Art Report on Alkali-Aggregate Reactivity Reported by ACI Committee 221, ACI Comm. 221. 98 (1998) 1–31.

[5]     Sika Group, Alkali-Silica-Reaction Resistant Concrete | Sika AG, (2019). https://www.sika.com/content/corp/main/en/solutions_products/construction-markets/sika-concrete-technology/concrete-handbook-2013/concrete-types/alkali-silica-reaction-resistant-concrete.html.

[6]     M.D.A. Thomas, B. Fournier, K.J. Folliard, Y.A. Resendez, Alkali-Silica Reactivity Field Identification Handbook, Fed. Highw. Adm. Publ. FHWA-HRT-04-113 Techbr. FHWA-HRT-06-071. (2011) 69. https://www.fhwa.dot.gov/pavement/concrete/asr/pubs/hif12022.pdf.

[7]     Federal Highway Administration Research and Technology, Chapter 2 - Alkali-Silica Reaction , Publication Number: FHWA-RD-03-047, (2003). https://www.fhwa.dot.gov/publications/research/infrastructure/pavements/pccp/03047/02.cfm.

[8]     M.H. Shehata, M.D.A. Thomas, Use of ternary blends containing silica fume and fly ash to suppress expansion due to alkali-silica reaction in concrete, Cem. Concr. Res. 32 (2002) 341–349. doi:10.1016/S0008-8846(01)00680-9.

[9]     L.S. Dent Glasser, N. Kataoka, The chemistry of alkali-aggregate reaction, Cem. Concr. Res. 11 (1981) 1–9.

[10]    M. Thomas, The effect of supplementary cementing materials on alkali-silica reaction: A review, Cem. Concr. Res. 41 (2011) 1224–1231. doi:10.1016/j.cemconres.2010.11.003.

[11]    A.J. Jasso, Characterization of Fly Ash for Evaluating the Alkali-Silica Reaction Resistance of Concrete, 2012.

[12] R. Pignatelli, Modeling of degradation induced by alkali-silica reaction in concrete structures, Politecnico Di Milano, 2012.

[13] RJ Lee Group, Alkali-Silica Reaction, (2019). https://www.rjlg.com/materials-insights/alkali-silica-reactions/.

[14] S.( Pleau, R., Berube, M. A., Pigeon, M., Fournier, B., and Raphael, Engineering properties of concrete affected by alkali-silica reaction", in: Roceedings 8th Int. Conf. Alkali-Aggregate React., Kyoto, 1989: pp. 721–726.

[15] K. Inoue, S., Fuji, M., Kobayashi, K., and Nakano, No Title, in: Struct. Behav. Reinf. Concr. Beams Affect. by Alkali-Silica React., International Conference on Alkali- Aggregate Reaction, Kyoto, 1989: pp. 727–732.

[16] M.M. Swamy, R. N. and Al-Asali, Engineering properties of concrete affected by alkali-silica reaction, ACI Mater. J. (1988) 367–374.

[17] J. Siemes, T., Han, N., and Visser, Unexpectedly low tensile strength in concrete structures, Heron. 47(2) (2002) 111–124.

[18] H. Asai, H., Maeno, H., Morishita, N., and Nakamura, Study on creep of pc beams damaged by asr., in: Creep, Shrinkage Durab. Mech. Concr. Concr. Struct. Proc. Concreep 8 Conf., Ise-Shima, 2009: pp. 1147–1153.

[19] A. Murazumi, Y., Matzumoto, N., Takiguchi, K., Hosokawa, T., Mitsugi, S., Y. Masuda, Study on the influence of alkali-silica reaction on mechanical properties of reinforced concrete members., in: 18th Int. Conf. Struct. Mech. React. Technol. (Smirt 18), 18th International Conference on Structural Mechanics in Reactor Technology (Smirt 18), Beijing, 2005.

[20] R.A. Deschenes, Mitigation of Alkali-Silica Reaction ( ASR ) in an Interstate Median Barrier, University of Arkansas, 2014.

[21] W.J. Phillips, Alkali Silica Reaction Mitigation Using High Volume Class C Fly Ash, Cl (2015).

[22] ASTM Committee C09.26, ASTM C1260-14 Standard Test Method for Potential Alkali Reactivity of Aggregates ( Mortar-Bar Method), 2014. doi:10.1520/C1260-14.2.

[23] M.A.B. and J. Duchesne, Evaluation of Testing Methods Used for Assessing the Effectiveness of Mineral Admixtures in Suppressing Expansion due to Alkali-Aggregate Reaction, Spec. Publ. (1992) 549–576.

[24] ASTM, ASTM C305/2014 - Standard Practice for, Astm. (2015) 1–3. doi:10.1520/C0305-14.2.

[25] S. Stark, D. C.; Morgan, B.; Okamoto, P.; and Diamond, Eliminating or Minimizing Alkali-Silica Reactivity, Strategic Highway Research Program, National Research Council, Washington D.C., 1993.

[26] A.E. Kosmatka, S. H., and Fiorato, Detecting and Avoiding Alkali-Aggregate Reactivity, Concr. Technol. Today Portl. Cem. Assoc. 12 (1991).

[27] B. Mather, How to Avoid Excessive Expansion of Concrete Due to Alkali-Aggregate Reaction, in: Second Int. Conf. Alkali-Aggregate React.

Hydroelectr. Plants Dams, U. S. Committee on Large Dams, Denver, 1995: pp. 421–439.

[28]   D.C. Stark, The Moisture Condition of Field Concrete Exhibiting Alkali-Aggregate Reactivity 221.1R-31 Alkali-Silica Reactivity, Am. Concr. Inst. (1991) 973–987.

[29]   H. Durand, B., and Chen, Preventive Measures Against AlkaliAggregate Reactivitytle, 1991.

[30]   M. Berube, M. A.; Chouinard, D.; Boisvert, L.; Frenette, J.; and Pigeon, Influence of Wetting-Drying and Freezing-Thawing Cycles, and Effectiveness of Sealers on ASR, in: Tenth Int. Conf. AAR Concr., Melbourne, 1996: pp. 1056–1063.

[31]   E.R. Latifee, State-of-the-Art Report on Alkali Silica Reactivity Mitigation Effectiveness Using Different Types of Fly Ashes, J. Mater. 2016 (2016) 1–7. doi:10.1155/2016/7871206.

[32]   Astm, ASTM C 150 - 07 Standard Specification for Portland Cement, 552 (2007).

[33]   ASTM, ASTM C 618-08a, Standard Specification for Coal Fly Ash and Raw or Calcined Natural Pozzolan for Use in Concrete, (2009) 8–10.

[34]   M.H. Shehata, M.D.A. Thomas, Effect of fly ash composition on the expansion of concrete due to alkali-silica reaction, Cem. Concr. Res. 30 (2000) 1063–1072. doi:10.1016/S0008-8846(00)00283-0.

[35]   R. Detwiler, The Role of Fly Ash Composition in Reducing Alkali-Silica Reaction, PCA R&D Serial No. 2092, 1-33, Porl. Cem. Assoc. (1997) 1–33. doi:PCA R&D Serial No. 2092.

[36]   R.F. Bleszynski, M.D. a Thomas, Microstructural Studies of Alkali-Silica Reaction in Fly Ash Concrete Immersed in Alkaline Solutions, Adv. Cem. Based Mater. 7 (1998) 66–78. doi:10.1016/S1065-7355(97)00030-8.

[37]   A.K. Saha, M.N.N. Khan, P.K. Sarker, F.A. Shaikh, A. Pramanik, The ASR mechanism of reactive aggregates in concrete and its mitigation by fly ash: A critical review, Constr. Build. Mater. 171 (2018) 743–758. doi:10.1016/j.conbuildmat.2018.03.183.

[38]   Y. Kawabata, K. Yamada, The mechanism of limited inhibition by fly ash on expansion due to alkali–silica reaction at the pessimum proportion, Cem. Concr. Res. 92 (2017) 1–15. doi:10.1016/j.cemconres.2016.11.002.

[39]   F. Rajabipour, E. Giannini, C. Dunant, J.H. Ideker, M.D.A. Thomas, Alkali-silica reaction: Current understanding of the reaction mechanisms and the knowledge gaps, Cem. Concr. Res. 76 (2015) 130–146. doi:10.1016/j.cemconres.2015.05.024.

[40]   H. Kizhakkumodom Venkatanarayanan, P.R. Rangaraju, Decoupling the effects of chemical composition and fineness of fly ash in mitigating alkali-silica reaction, Cem. Concr. Compos. 43 (2013) 54–68. doi:10.1016/j.cemconcomp.2013.06.009.

[41]   L.J. Malvar, L.R. Lenke, Efficiency of fly ash in mitigating alkali-silica reaction based on chemical composition, ACI Mater. J. 103 (2006) 319–326.

[42]   M. Mahyar, S.T. Erdoğan, M. Tokyay, Extension of the chemical index model for estimating Alkali-Silica reaction mitigation efficiency to slags and natural pozzolans, Constr. Build. Mater. 179 (2018) 587–597. doi:10.1016/j.conbuildmat.2018.05.217.

[43]   Ç. Meral Akgül, S. Yoncacı, Fly ashes from coal fired thermal power plants in Turkey, Ankara, 2019.

[44]   M. Ryzak, A. Bieganowski, Methodological aspects of determining soil particle-size distribution using the laser diffraction method, J. Plant Nutr. Soil Sci. 174 (2011) 624–633. doi:10.1002/jpln.201000255.